SWITCHABLE ANTENNAS AND THEIR APPLICATION IN DIELECTRIC PROPERTIES DETERMINATION

THUNYAWAT LIMPITI

A THESIS SUBMITTED IN PARTIAL FULLFILLMENT
OF THE REQUIREMENT FOR THE DEGREE OF
DOCTOR OF ENGINEERING IN ELECTRICAL ENGINEERING
FACULTY OF ENGINEERING
KING MONGKUT'S INSTITUTE OF TECHNOLOGY LADKRABANG
2013

KMITL-2013- EN-D-018-156

หัวข้อวิทยานิพนธ์	สายอากาศสวิตช์และการประยุกต์ใช้งานในการหาค่าคุณสมบัติไดอิเล็กตริก
นักศึกษา	นายธัญวัฒน์ ลิมปิติ
รหัสประจำตัว	51060011
ปริญญา	วิศวกรรมศาสตรดุษฎีบัณฑิต
สาขาวิชา	วิศวกรรมไฟฟ้า
พ.ศ.	2556
อาจารย์ที่ปรึกษาวิทยานิพนธ์	ศ. ดร. โมไนย ไกรฤกษ์

บทคัดย่อ

วิทยานิพนธ์นี้นำเสนอสายอากาศสวิตช์และการประยุกต์ใช้งาน โดยนำเสนอผ่านตัวอย่างการประยุกต์ใช้งานที่มีประโยชน์ต่อการพัฒนาประเทศในด้านเกษตรกรรม และการออกแบบเพื่อนำไปประยุกต์ใช้ในด้านอุตสาหกรรม สายอากาศที่นำเสนอมีโครงสร้างเป็นรูปกากบาทและมีสวิตช์ทำหน้าที่ปรับเปลี่ยนรูปแบบการจัดวาง ในการประยุกต์ใช้ด้านเกษตรกรรมสายอากาศสวิตช์ทำหน้าที่เป็นเซ็นเซอร์วัดความชื้นข้าวเปลือกในระบบการลดความชื้นแบบปิด ด้วยการนำเสนอเทคนิคใหม่ที่วัดเฉพาะขนาดของการเชื่อมต่อร่วมของสายอากาศ อาศัยการสวิตช์รูปแบบการจัดวางระหว่างขนานและตั้งฉากแทนที่การวัดเฟสเพื่อหาค่าคุณสมบัติไดอิเล็กตริก ขนาดของการเชื่อมต่อร่วมที่ได้จากการวัดถูกนำมาพลอตบนกราฟเชิงพื้นผิวที่ได้จากการคำนวณด้วยสูตรสำเร็จที่นำเสนอใหม่ ซึ่งในวิทยานิพนธ์นี้จะเน้นเฉพาะกรณีรูปแบบการจัดวางแบบตั้งฉาก เปรียบเทียบค่าคุณสมบัติไดอิเล็กตริกของข้าวเปลือกที่ได้จากเทคนิคที่นำเสนอกับงานวิจัยที่มีมาก่อน พบว่าค่าคงที่ไดอิเล็กตริกค่อนข้างแม่นยำ มีความเบี่ยงเบนมาตรฐานสูงสุดเท่ากับ ± 0.19 แต่ค่าตัวประกอบการสูญเสียไดอิเล็กตริกมีความแตกต่าง ซึ่งความเบี่ยงเบนมาตรฐานสูงสุดเท่ากับ ± 0.36 เนื่องจากธรรมชาติของเทคนิคที่นำเสนอ ดังนั้นได้นำเสนอการชดเชยการสูญเสียและการแก้ไขความผิดพลาด ซึ่งความเบี่ยงเบนมาตรฐานสูงสุดของค่าคงที่ไดอิเล็กตริกและค่าตัวประกอบการสูญเสียไดอิเล็กตริกเท่ากับ ± 0.18 และ ± 0.29 ตามลำดับ จากนั้นสร้างระบบลดความชื้นแบบปิดขนาดย่อม

เพื่อศึกษาความเป็นไปได้ของการใช้งานเซ็นเซอร์ร่วมกับระบบลดความชื้นแบบปิด ผลที่ได้จากการทดลองยืนยันว่าเซ็นเซอร์ทำงานได้แม่นยำ และมีข้อดีที่ราคาถูกและสามารถทำงานได้ตามเวลาจริง ถัดมาได้นำเสนอการพัฒนาสายอากาศโครงสร้างเดิมด้วยเทคโนโลยีการสร้างท่อนำคลื่นเสมือน ในตัวกลางของแผ่นวงจรพิมพ์ที่ความถี่ 24 กิกะเฮิรตซ์ ร่วมกับหลักการปรับเปลี่ยนแบบรูปการแพร่กระจายคลื่นโดยใช้ไดโอดพินในการสวิตซ์ สายอากาศที่ออกแบบสามารถปรับเลือกทิศทางได้ 4 ทิศทางรอบตัว เพื่อให้เหมาะสำหรับการนำไปประยุกต์ใช้งานด้านอุตสาหกรรม เช่น เซ็นเซอร์สำหรับรถยนต์ การรักษาความปลอดภัย หรือ ระบบการสื่อสาร เป็นต้น

Thesis Title	Switchable Antennas and Their Application in Dielectric Properties Determination
Student	Mr. Thunyawat Limpiti
Student ID.	51060011
Degree	Doctor of Engineering
Program	Electrical Engineering
Year	2013
Thesis Advisor	Prof. Dr. Monai Krairiksh

ABSTRACT

This dissertation presents a switchable antenna and its applications via an exemplification which will be beneficial to the agricultural development of the Kingdom, and the design of an antenna for the use in industrial applications. The designed antenna structure is like a cross configuration whose elements are attached with RF switches to function in switching configuration. For the agricultural application, the switchable antenna is employed as a moisture content sensor for paddy (rough rice) in a closed-loop drying system based on the new proposed aspect in characterizing the dielectric properties of material by means of measuring only the magnitude of mutual coupling and omitting the measurement of phase by switching configurations between parallel and perpendicular instead. The measured magnitudes of mutual coupling are plotted on a surface curve of mutual coupling magnitudes, which is obtained by a novel presented of closed-form solution, to obtain the dielectric properties of paddy. Only the case of perpendicular configuration is focused in this dissertation. The dielectric properties of paddy provided by the surface curve of mutual coupling magnitudes are compared with the work in literature and found that the dielectric constants are slightly different, but the dielectric loss factors are quite different due to the inherent behavior of this technique. The maximum standard deviations of them are respectively equal to ± 0.19 and ± 0.36.

Thus, the loss compensation and the error correction are presented. The compensated results show that the maximum standard deviations of the dielectric constant and the dielectric loss factor decrease to ± 0.18 and ± 0.29, respectively. Then, a model system of the closed-loop drying system was set up to validate the feasibility of exploiting this sensor with this system. The results confirm that the sensor is able to accurately perform with its advantages of low cost and real-time monitoring. In addition, this antenna with the same structure of a cross configuration is further developed by means of the substrate integrated waveguide (SIW) technique combined with the concept of reconfigurable antenna. The antenna is designed on a single printed circuit board (PCB) to operate at the frequency of 24 GHz and its radiation patterns steered to 4 directions around its structure by using PIN diodes. Consequently, it is suitable for industrial applications, i.e., automotive sensor, security application, communication system, and others.

ACKNOWLEDGEMENTS

This dissertation would not be completed without the assistance of many persons. I would like to express my appreciation to whom I owe many thanks for helping throughout my Ph.D. course.

First of all, I am deeply grateful to my advisor, Professor Monai Krairiksh, who has been giving many ideas, suggestions, and helpful guidance not only in research, but also in living.

I also would like to thank to Associate Professor Sompol Kosulvit and Associate Professor Chuwong Phongcharoenpanich for their helpful discussions.

I would like to thank Associate Professor Panmanas Sirisomboon for her helpful suggestions and support in the moisture content testing of paddy.

I also would like to express my deep gratitude to Professor Ian D. Robertson for his suggestions and guidance in SIW technique and all support throughout my research at Institute of Microwave and Photonics, University of Leeds, United Kingdom, during my visiting scholar program.

I would like to thank Mr.Vichit Lohprapan for his kind suggestions, discussion, and support in English proof.

I wish to thank all colleagues in Wireless Communication Laboratory: Dr.Jhirat Mearnchu, Assistant Professor Duang-arthit Srimoon, Dr.Suwan Janin, Dr.Akkarat Boonpoonga, Mr.Paiboon Yoiyod, Mr.Tanawut Tantisopharak, Mr.Prapan Leekul, Mr.Pobsook Sooksumrarn, and Mr.Chainarong Kittiyanpanya for their kind supports and providing a friendly atmosphere during the work.

Many thanks also go to Dr.Thanya Parametthanuwat, Mr.Noraset Wichaipanich, Mr.Parinya Soontornwong, and Ms.Siraporn Sakphrom for their helpful suggestions and kind support.

I am grateful to the Thailand Research Fund which provides financial support through the Royal Golden Jubilee Ph.D. Program (Grant No. PHD/0284/2549) throughout the Ph.D. program.

Special thanks go to Ms.Pattawan Butrug for her patience, understanding, and cheerfulness during a long period of my Ph.D. course.

Finally, I wish to express my gratitude to my parents for their excessively love, understanding, and encouragement throughout my entire life.

Thunyawat Limpiti

TABLE OF CONTENTS

TABLE OF CONTENTS (CONTINUE)

Page

TABLE OF CONTENTS (CONTINUE)

Page

LIST OF FIGURES

Figure Page

LIST OF FIGURES (CONTINUE)

Figure Page

LIST OF FIGURES (CONTINUE)

Figure Page

LIST OF FIGURES (CONTINUE)

Figure Page

LIST OF FIGURES (CONTINUE)

Figure Page

LIST OF TABLES

Table Page

CHAPTER 1

INTRODUCTION

1.1 Motivation and Objective

Due to the tremendous development of wireless communication technology, new applications, and the rapid increase in a number of wireless devices, the current allocated frequency spectrum is being immediately occupied. Various methods have been studied to enhance the channel capacity or the system reliability, e.g., multiple-input multiple-output (MIMO) technique, ultra-wideband (UWB) technique, and diversity techniques. Among these techniques, they concern the use of multiple antennas and antennas with multi-band or wideband performance which also have drawback on unwanted interference that affects signal-to-noise ratio. However, the technique of antenna diversity is an interesting one that is classified into three types: spatial, pattern, and polarization diversities. The diversity technique in particular polarization is much attractive since its structure combines pairs of antennas with orthogonal polarization arrangement, i.e., horizontal/vertical polarization, $\pm 45^{\circ}$ inclined polarization, left-hand/right-hand circular polarization, etc. With the arrangement of orthogonal polarization, an idea of switching it to each polarization will be useful to employ in a lot of applications.

The advantages of applying such a switchable antenna will be exemplified with an application based on attribution of Thailand since the Kingdom has been a developing country whose economy is mainly comprised of an agricultural sector and an industrial sector. On focusing the agricultural sector, it is applied for a sensor to measure the moisture content of paddy (rough rice) since rice is one of the most important agricultural products not only in local, but also worldwide as shown in Fig. 1.1. It is consumed and exported in huge amounts each year; thus, its quality control is essential. Normally, rice is stored in the form of paddy which is prone to attack by a multitude of insects adapted to the relatively dry environment of a mill. Infesting insects flourish at grain moisture content of 10%-14% whereas at 14% up to 18% moisture content, fungal growth is critical. Hence, paddy is optimally stored at a narrow range of around 14% moisture content [1]. In actual practice, it is hard to maintain paddy at this suitable condition since

moisture content is always changing. In order to maintain proper moisture content level, various published drying methods have been utilized:

- Fluidized bed paddy drying by super-heated steam with hot air temperature 100-150°C. [2]-[5],
- A combination of microwave with hot air drying as a fluidized bed microwave heating method [6]-[8],
- A continuous fluidized bed microwave paddy drying system [9].

However, this system operated in an open loop, so the quality of the paddy was not guaranteed. Therefore, a moisture content sensor is desirable for implementing a closed-loop drying system. In this system, the sensor is immersed in the stored paddy to monitor the moisture content level while the drying system is in operation.

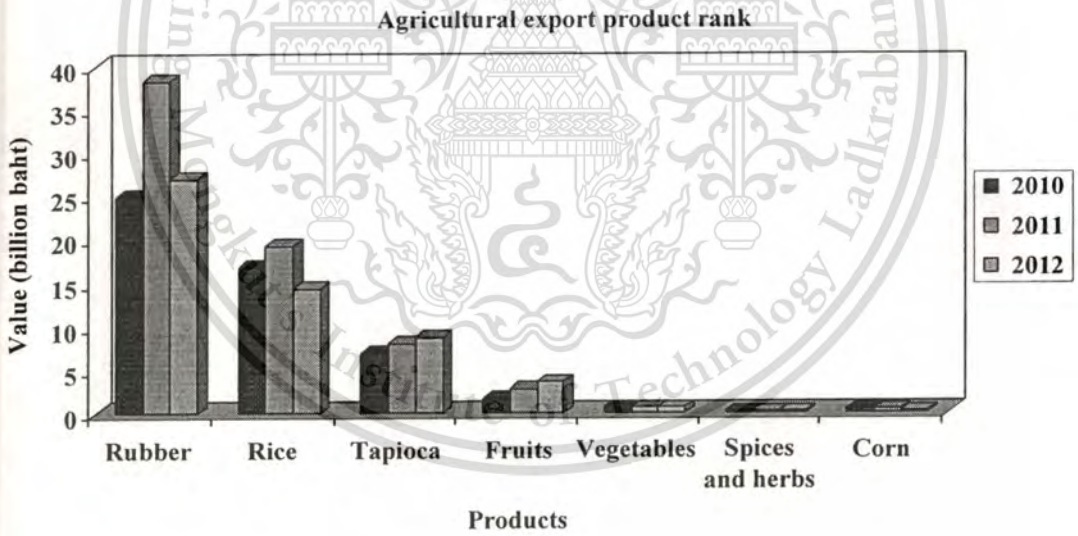

Source : Department of Foreign Trade, Ministry of Comerce.

Figure 1.1 Top 7 ranking of agricultural export products.

For the industrial sector, further development of the sensor structure will be designed and investigated its performance for applying it as an industrial sensor at the frequency of 24 GHz. The frequency band at 24 GHz is the license free for industrial,

scientific and medical (ISM) band which has been identified as a potential host for future short range wireless systems and various applications such as Doppler sensor in automotive and industrial applications, security applications, and communication applications.

According to aforementioned, it is further designed with a reconfigurable technique and a substrate integrated waveguide (SIW) to be a candidate for industrial applications. The reconfigurable technique is categorized into three types: resonant frequency, polarization, and radiation pattern. Its performance provides radiation pattern more than one or different frequencies or polarizations that is a potential alternative approach for many systems. In general, the pattern reconfigurable has much been paid attention than others because of its capability of noise avoidance by steering beam toward the direction of desired signal [10]. Moreover, it is also utilized to increase functionality, e.g., beam steering, radar, control, and direction finding for a confined volume to enhance a greater burden on nowadays systems. With a great deal of applications [11] that this technique performs as illustrated in Fig. 1.3, it is thus applied by means of the switch-configuration antenna and SIW to use as sensors in industrial applications.

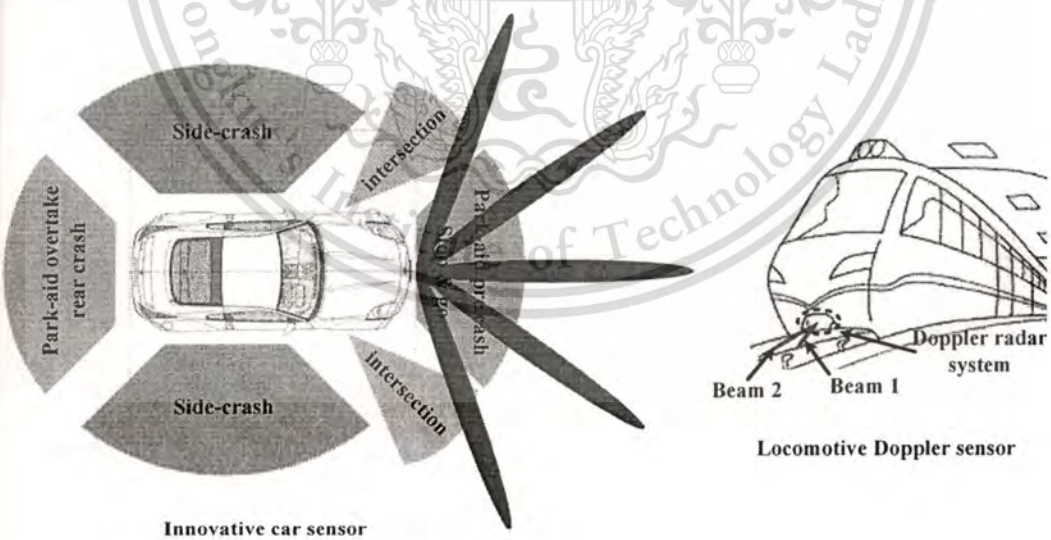

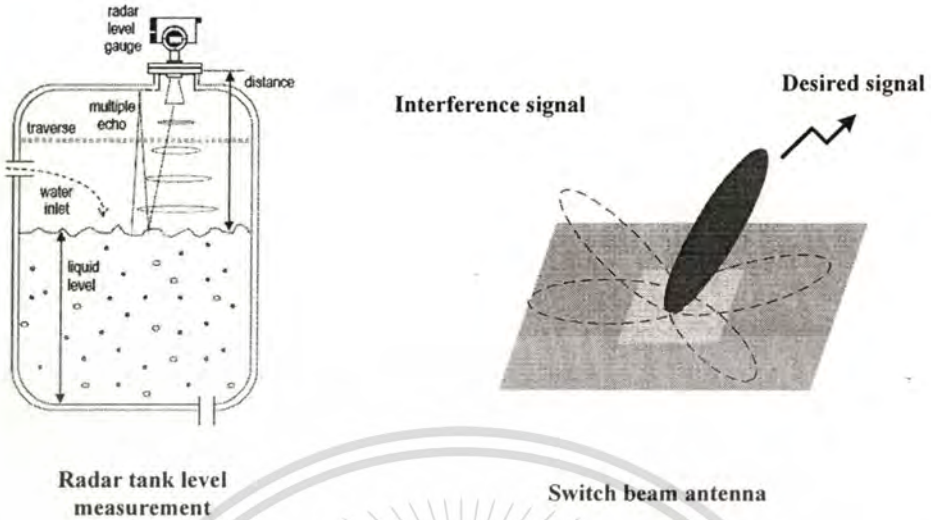

Figure 1.2 24 GHz microwave sensors for industrial applications [11].

Consequently, the objective of this dissertation is to present the use of switchable antenna as the moisture content sensor for a closed-loop drying system of paddy as illustrated in Fig. 1.4. Three aspects of the sensor development are presented: a new closed-form calculation of mutual impedance of perpendicular polarization dipole antenna, a novel design of an antenna, and an investigation of performance enhancement. The procedure to obtain the first of which is explained step by step; then the obtained mutual coupling magnitude is utilized with mutual coupling magnitude of parallel polarization to form a surface curves which exhibits as a solution to get the dielectric constant and the dielectric loss factor of paddy. These dielectric properties are correlated with the moisture content by a standard method of American Society of Agricultural and Biological Engineers (ASAE) [12]. While the design of sensor employs a printed cross-dipole antenna structure with a pair of single-pole double-throw (SPDT) switches to switch polarizations between perpendicular and parallel polarizations. In addition, analysis is conducted to compensate loss caused by the non-ideal RF switch and coupled elements in the vicinity, including feeding systems. The designed sensor is then fabricated to validate by using it in the moisture content of paddy determination. To further develop the concept of switch-polarization antenna with the same structure as the moisture content sensor for being a sensor in industrial applications, it is designed with the pattern reconfigurable technique and SIW.

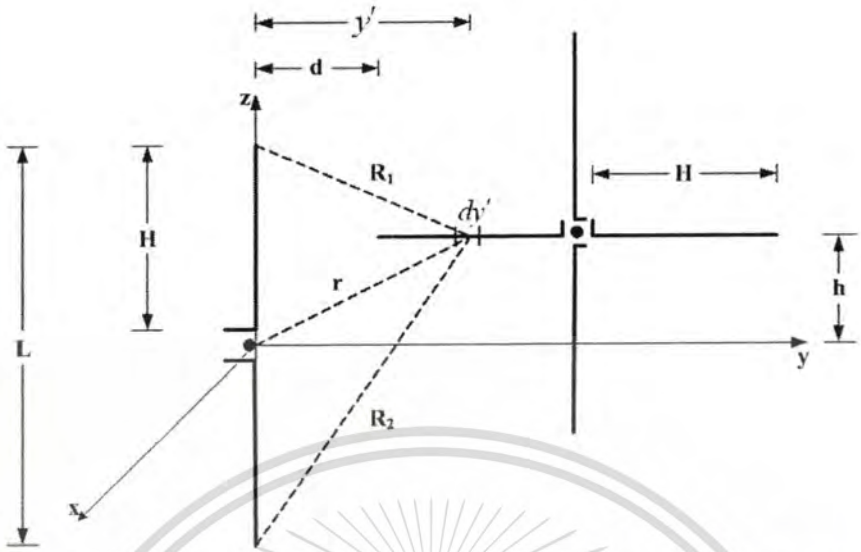

Figure 1.3 Switchable antenna between perpendicular and parallel configurations.

1.2 Outline of the Dissertation

The problems of interest which lead to the objective and motivation of this dissertation are described in this chapter. The remaining chapters are briefly detailed as follows:

Chapter 2 presents literature reviews of the dielectric properties determination techniques, a mutual impedance analysis of perpendicular dipole antenna in lossy medium and a novel technique of using magnitudes of mutual coupling between perpendicular and parallel dipole antenna in determining the dielectric properties.

Chapter 3 presents design of a printed cross-dipole antenna with the performance of switching configuration. The subsections consist of one dipole antenna design, details of switch-configuration dipole antenna structure, and compensation loss caused by: parasitic elements from different polarizations and RF switches.

Chapter 4 presents validation of the designed and fabricated switchable antenna for the dielectric properties of paddy. The obtained dielectric properties are correlated with the moisture content by a standard method of American Society of Agricultural and Biological Engineers (ASAE). In order to show the accuracy of the proposed sensor, the results are compared with those from the conventional method, the transmission line

technique in the previous work [13]. In addition, the usefulness of applying it to control the quality of paddy in a closed-loop drying system is illustrated.

Chapter 5 presents further development of the cross-dipole structure with a pattern reconfigurable technique and substrate integrated waveguide (SIW). The cross structure employs slot antennas mounted with PIN diodes to exhibit as the driven element. While the states "ON" or "OFF" of PIN diodes is set to switch polarization of slots that causes the radiation patterns reconfigurable. The whole structure is designed on a single printed circuit board (PCB) by means of SIW. Effect of parameters: length of antenna elements, spacing between director and driven elements, and spacing between reflector and driven elements to S-parameters and radiation patterns are investigated by a commercial electromagnetic simulation program.

Chapter 6 concludes all presentations in this dissertation and discusses the remark for future work.

CHAPTER 2

MUTUAL IMPEDANCE OF PERPENDICULAR DIPOLE ANALYSIS AND THE USE OF MUTUAL COUPLING MAGNITUDE IN THE DIELECTRIC PROPERTIES DETERMINATION

2.1 Introduction

In this chapter, literatures review of the dielectric properties determination techniques including the advantage and disadvantage of each method are briefly detailed. A novel technique exploiting mutual coupling magnitudes of perpendicular and parallel polarizations of dipole antennas to determine the dielectric properties is presented. To obtain the mutual coupling magnitudes, an analysis of mutual impedance related to the dielectric constants and the dielectric loss factors variation is expressed especially in the case of perpendicular polarization. The expressions are in closed form and applicable to lossy medium. Their advantage is using less processing time compared to other methods in previous works and other commercial electromagnetic simulation programs.

2.2 Brief Details of the Dielectric Properties Determination Techniques

In this dissertation, the application for moisture content of agricultural products is on focused especially paddy (rough rice). Normally, standard methods for moisture content determination utilize oven drying with specific time periods and temperatures, but they are much tedious, time consuming, and expensive [13]. Most of the practical moisture content sensors concern with sensing the electrical characteristics of the paddy. The dc electrical resistance of paddy was correlated with the moisture content [14]. For the ac measurement, the studies of changes in the capacitance of sample holding capacitors were published [15]. Later, a moisture content sensor measuring capacitance and phase angle of a parallel-plate system was presented. It provides accurate results due

to the closed boundary [16], but the need to fill the sample to the full volume limits its use in on-line monitoring and closed-loop system.

The presented moisture content sensor applies the principle of dielectric property determination of a material. Many techniques to characterize the dielectric properties of materials at microwave frequencies have been intensively developed for over decades [17]. These techniques generally fall into resonant and non-resonant methods. The methods of non-resonant are often utilized over a frequency range whereas the resonant methods are suitable for a single frequency or several discrete frequencies. Both methods are sometimes able to be used in combination. Non-resonant methods are fundamentally deduced from their impedance and velocity of wave in materials; mainly include reflection methods and transmission/reflection methods. The well-known techniques of the non-resonant methods are transmission line, open-ended probe, and free space. Resonant methods such as cavity resonator technique or cavity perturbation technique are the methods that calculate the change of resonant properties of the resonant structure caused by the introduction of the material which serve as a resonator or a key part of a resonator [18]. Each technique has its advantages and constraints hence providing it to the suitable application will get the more accurate results. The accuracy of each technique also depends on its natural property of materials: physical property, electrical property, and operating frequency. The advantages and constraints of each technique are detailed as follow:

2.2.1 Transmission Line Technique

This technique concerns filling the material under test inside an enclosed transmission line. A portion of the contained material in the line is usually a section of rectangular waveguide or air-filled coaxial as shown in Fig. 2.1. The dielectric properties are calculated from the measurement of the reflected signal (S_{11}) and the transmitted signal (S_{21}). To obtain an accurate result, the adequate thickness of material sample is much essential [19]-[20]. The constraints of this technique are:

- Material surfaces must be smooth, flat and perpendicular to transmission line.
- Materials must be homogeneous medium.

- No air gaps or any bubbles between material and container.

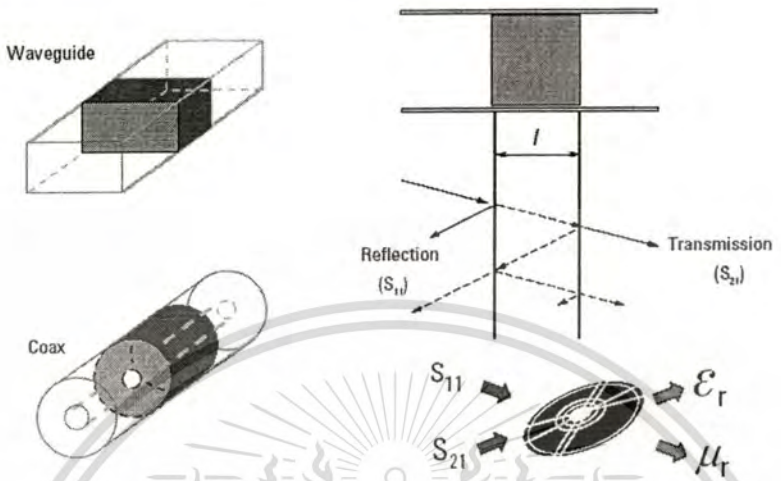

Figure 2.1 Transmission line technique: waveguide and coaxial line [21].

2.2.2 Free-Space Technique

This technique is one of the non-destructive evaluation (NDE) approaches. NDE is the examination of a material with technology that does not affect the future usefulness of the material [22]. The method of free space measures the attenuation amplitude and phase shift of the signal from a material which is placed between a transmitting antenna and a receiving antenna [23]. Thus, the measurement setup is quite complicated since it needs to measure both the magnitude and phase [24]. However, the advantage of this technique is that it is capable of dynamic measurement since it can measure instantaneously, nondestructively, and is contactless. It is also able to use in special conditions such as high temperature. The limitations of this technique are:

- Materials shape should be large and flat.
- Materials must be placed parallel to the wavefront of transmitting antennas.

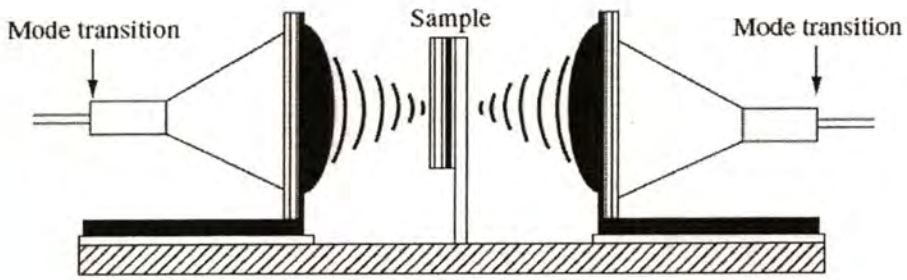

Figure 2.2 Setup for free-space technique measurement [18].

2.2.3 Cavity Resonator Technique

This technique is a high-Q structure that resonates at certain frequencies. It requires a small sample of material such that the field in the cavity is slightly disturbed to shift the resonant frequency and Q of the cavity. The changes of the resonant frequency and Q are used to calculate for the dielectric properties. The advantages of this technique are high accuracy and sensitivity, and its flexibility in sample preparation. The constraints of this technique are:

- Measurement can be done at only one or a few frequencies.
- Only well-suited for low-loss bulk materials, small-size sample of materials [25], and irregular shape of samples.

$$\varepsilon_r' = \frac{V_c(f_c - f_s)}{2V_s f_s} + 1$$

$$\varepsilon_r'' = \frac{V_c}{4V_s}\left(\frac{1}{Q_s} - \frac{1}{Q_c}\right)$$

V is the volume

index c is for the empty cavity,

index s is for the sample loaded

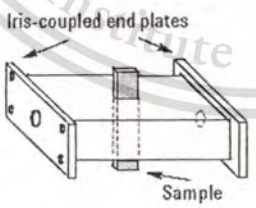

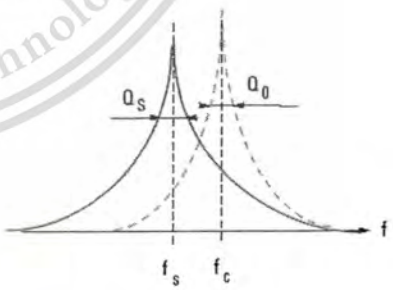

Figure 2.3 Resonant cavity technique [21].

2.2.4 Open-ended Probe

An open-ended probe technique which has been successfully commercialized can measure over a wide frequency range with moderate accuracy. It is a cut-off section of transmission line which concerns measuring the reflected signal (S_{11}) of materials by immersing the probe into the sample (liquid materials) or touching it on the flat surface of sample (solid materials). The limitations of this technique are:

- Materials must be non-magnetic, isotropic, and homogeneous.
- Materials surface should be flat.
- Materials must be sufficiently thick.
- No air gaps or any bubbles between probe and material [26]-[29].
- Standoff distance extremely affects the sensitivity of measurement [22].

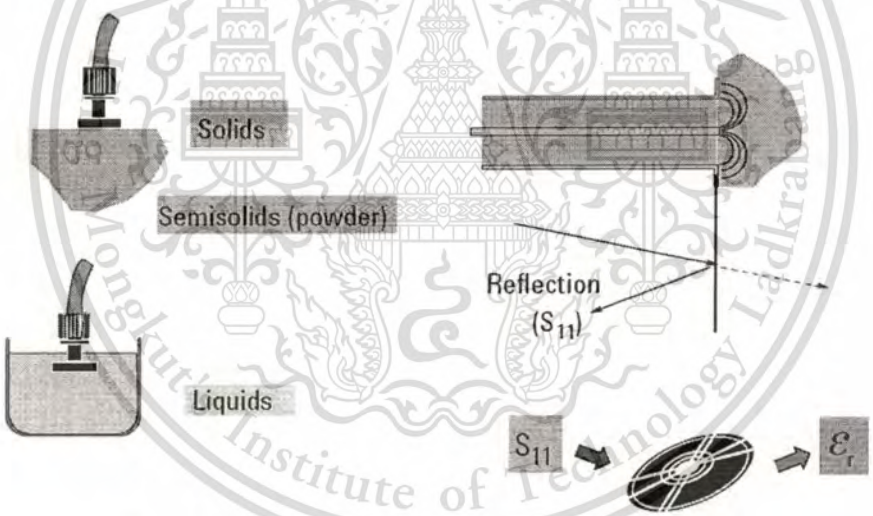

Figure 2.4 Open-ended probe technique [21].

According to the exemplified techniques of the dielectric properties at microwave frequencies, the advantages and constraints of each technique which depend on material under test, operating frequency, material size, material preparation, and the need of accuracy are summarized and compared as illustrated in Table. 1.

Table 1. Comparison of the dielectric properties determination techniques

Factors	Transmission Line	Free-space	Cavity Resonant	Open-ended Probe
Frequency	Fraction	Fraction	Single	Wideband
Material Size	Moderate	Large	Small	Small
Temperature Control	Hard	Very Easy	Very Easy	Easy
Accuracy				
Low-Loss Material	Moderate	Moderate	High	Low
High-Loss Material	Moderate	Moderate	Not suitable	High
Material Preparation	Hard	Easy	Very Hard	Easy
Suitable Condition	Solid	Large & Flat	Solid & Liquid	Solid & Liquid
Measurement Type	Destructive	Nondestructive	Destructive	Nondestructive

Note that the free-space technique is one of the most interesting approaches to correlate the dielectric properties with agricultural applications, e.g., ripeness of fruits, moisture content, and mixture intensity since it is able to measure materials which need contactless and non-destructiveness. In spite of the quite complicated of measurement setup, many attempts to reduce it have been published. An interesting approach is to omit phase measurement and measure reflection and transmission coefficients instead [30], [31]. Subsequently, a coupled-dipole sensor using the magnitude of S_{11} and S_{21} was developed [32]. However, it was not suitable to apply in a closed-loop drying system

since it could only measure at the surface of the bulk material. Consequently, a technique using the magnitude of mutual coupling between parallel and perpendicular polarized dipole antenna was proposed [33], [34]. This technique overcomes the complication of the free-space technique by means of considering only the magnitude and switching polarization instead of measuring the magnitude of S_{11}. Furthermore, it can function at any depth inside the bulk material.

This dissertation presents an *in-situ* moisture content sensor to use in a closed-loop drying system for paddy [35]. The solution to carry out the dielectric properties of paddy is the surface curves of mutual coupling magnitudes ($|S_{21}|$) between perpendicular and parallel configurations of dipole antennas, which is obtained by transforming the expressions of mutual impedance (Z_{21}) calculation in lossy medium. In the case of parallel configuration, the calculation is modified from [36] whereas the perpendicular configuration is newly derived. Although, there have been many publications on mutual coupling analysis [37]-[39], all those proposed expressions were not in closed form and not applicable to lossy medium. The derived closed-form expressions are desirable since they use low processing time compared to other methods in previous works and other commercial electromagnetic simulations.

2.3 Mutual Impedance Expressions of Perpendicular Dipole Antenna

The characteristic of an antenna surrounded by a medium is a function of the constitutive parameters which is provided in mutual impedance measurement. For nonmagnetic material, the constitutive parameters are conductivity (σ) and relative permittivity ($\varepsilon_r = \varepsilon_r' - j\varepsilon_r''$) which are the dielectric constant and the dielectric loss factor, real and imaginary parts, respectively. The dielectric constant indicates the energy storage capability of a material subjected to an electric field whereas the dielectric loss factor specifies electric energy dissipation. Obtaining the accurate evaluation of both parameters is essential for providing a unique electrical signature.

2.3.1 Near-Field Region of Dipole Antenna

In order to obtain the mutual coupling of an antenna, the antenna is considered in a near-field region assumed that it is a thin center-fed dipole with the length L. The

electromagnetic fields at a point P which is at an arbitrary distance from the antenna as illustrate in Fig. 2.5 can be calculated by assuming the sinusoidal current distribution on the antenna is

$$\bar{I}(z') = \begin{cases} \hat{a}_z I_m \sin\left[k\left(H - z'\right)\right], & 0 \le z' \le H \\ \hat{a}_z I_m \sin\left[k\left(H + z'\right)\right], & -H \le z' \le 0 \end{cases} \tag{2.1}$$

when I_m and k are respectively the maximum current and the phase constant. H represents a half-wavelength of dipole and the length of dipole antenna is L.

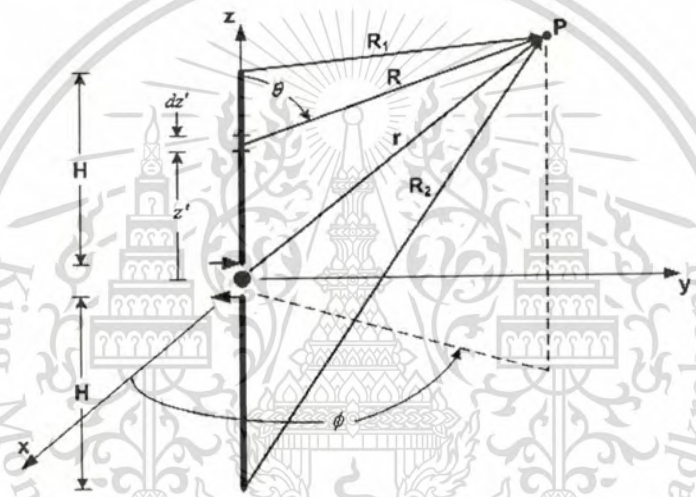

Figure 2.5 Configuration of near-field region calculation.

From the shown geometry in fig. 2.5, the relations between the distance and the observation point P are as follow:

$$R = \sqrt{\left[\left(z - z'\right)^2 + y^2\right]} \tag{2.2a}$$

$$R_1 = \sqrt{\left[\left(z - H\right)^2 + y^2\right]} \tag{2.2b}$$

$$R_2 = \sqrt{\left[\left(z + H\right)^2 + y^2\right]} \tag{2.2c}$$

$$r = \sqrt{\left(z^2 + y^2\right)}. \tag{2.2d}$$

Vector potential at the point P is

$$A_z = \frac{\mu I_m}{4\pi}\left(\int_0^H \frac{\sin\left[k\left(H-z'\right)\right]\exp\left(-jkR\right)}{R}dz' + \int_{-H}^0 \frac{\sin\left[k\left(H+z'\right)\exp\left(-jkR\right)\right]}{R}dz'\right)$$

$$= \frac{\mu I_m}{8\pi j}\left(\exp(jkH)\int_0^H \frac{\exp\left[-jk(R+z')\right]}{R}dz' - \exp\left(-jkH\right)\int_0^H \frac{\exp\left[-jk(R-z')\right]}{R}dz'\right.$$

$$\left. + \exp\left(jkH\right)\int_{-H}^0 \frac{\exp\left[-jk\left(R-z'\right)\right]}{R}dz' - \exp\left(-jkH\right)\int_{-H}^0 \frac{\exp\left[-jk\left(R+z'\right)\right]}{R}dz'\right). \quad (2.3)$$

In cylindrical coordinates, the magnetic field at the point P is given by

$$\bar{H} = \hat{a}_\phi H_\phi \quad (2.4)$$

where

$$H_\phi = -\frac{1}{\mu}\frac{\partial A_z}{\partial \rho} \quad (2.5)$$

and μ is the permeability.

Due to the symmetry of the z-axis, the point P can be shown in the y-z plane without loss of generality. In this case,

$$H_\phi = -H_x = -\frac{1}{\mu}\frac{\partial A_z}{\partial y}. \quad (2.6)$$

Substitute equation (2.3) into equation (2.6) results in the expression

$$H_\phi = -\frac{I_m}{8\pi j}\left[\exp(jkH)Q_1 - \exp(-jkH)Q_2 + \exp(jkH)Q_3 - \exp(-jkH)Q_4\right] \quad (2.7)$$

where

$$Q_1 = \frac{\partial}{\partial y}\int_0^H \frac{\exp\left[-jk\left(R+z'\right)\right]}{R}dz' \quad (2.8a)$$

$$Q_2 = \frac{\partial}{\partial y}\int_0^H \frac{\exp\left[-jk\left(R-z'\right)\right]}{R}dz' \quad (2.8b)$$

$$Q_3 = \frac{\partial}{\partial y}\int_{-H}^{0} \frac{\exp\left[-jk\left(R-z'\right)\right]}{R}dz' \tag{2.8c}$$

$$Q_4 = \frac{\partial}{\partial y}\int_{-H}^{0} \frac{\exp\left[-jk\left(R+z'\right)\right]}{R}dz' . \tag{2.8d}$$

Substitute equations (2.8a)-(2.8d) into equation (2.7) and simplify; then obtain

$$H_\phi = -\frac{I_m}{4\pi jy}\left[\exp\left(-jkR_1\right)+\exp\left(-jkR_2\right)-2\cos\left(kH\right)\exp\left(-jkr\right)\right]. \tag{2.9}$$

From Maxwell's equations, the electric field is given by

$$\bar{E} = \frac{1}{j\omega\varepsilon}\nabla\times\bar{H} . \tag{2.10}$$

Thus, the radiated electric field from the dipole antenna is

$$\bar{E} = \hat{a}_\rho E_\rho + \hat{a}_z E_z = -\hat{a}_\rho \frac{1}{j\omega\varepsilon}\frac{\partial H_\phi}{\partial z} + \hat{a}_z \frac{1}{j\omega\varepsilon}\frac{1}{\rho}\frac{\partial}{\partial\rho}\left(\rho H_\phi\right) \tag{2.11}$$

where

$$E_z = -j\frac{\eta I_m}{4\pi}\left(\frac{\exp\left(-jkR_1\right)}{R_1}+\frac{\exp\left(-jkR_2\right)}{R_2}-2\cos\left(kH\right)\frac{\exp\left(-jkr\right)}{r}\right) \tag{2.12}$$

$$E_y = j\frac{\eta I_m}{4\pi y}\left(\frac{z-H}{R_1}\exp\left(-jkR_1\right)+\frac{z+H}{R_2}\exp\left(-jkR_2\right)-\frac{2z\cos\left(kH\right)}{r}\exp\left(-jkr\right)\right) \tag{2.13}$$

and η is an intrinsic impedance.

2.3.2 Mutual Impedance of Linear Dipole Antennas

In the previous subsection, the observation point P was derived when a linear dipole antenna radiated into an unbound medium. When P is on the presence of an obstacle or on another antenna, it is able to alter the current distribution, the radiated field, and the impedance of the antenna. The input impedance of the antenna in the presence of the other elements or obstacles, which will be referred to as driving-point impedance, depends on the self-impedance and the mutual impedance between the driven

element and the other obstacles or elements [40]. The driving-point impedance is given by

$$Z_{1d} = \frac{V_1}{I_1} = Z_{11} + Z_{12}\left(\frac{I_2}{I_1}\right) \tag{2.14a}$$

$$Z_{2d} = \frac{V_2}{I_2} = Z_{22} + Z_{21}\left(\frac{I_1}{I_2}\right) \tag{2.14b}$$

where Z_{1d} and Z_{2d} are respectively the input impedance of antennas 1 and 2 considered in two ports network. Each driving-point impedance depends on the current ratio (I_1/I_2), the mutual impedance, and the self-impedance.

To calculate the mutual impedance Z_{21}, consider antenna number 2 to be in the electromagnetic field of antenna number 1 which both antennas are in close vicinity. Let the distance from an elements dz' on antenna number 2 to the feed center is equal to z' and the incident electric field parallel to the element dz' is E_{z21}. The induced electric field at dz' will be $E_{zi} = -E_{z21}$ since the total field must add up to zero for a perfect conductor. The induced electromotive force (EMF) in dz' is thus equal to $-E_{z21}dz'$. When the center terminal is shorted circuit, the EMF will cause a current flow across this terminals denoted by dI_{sc} as shown in Fig. 2.6.

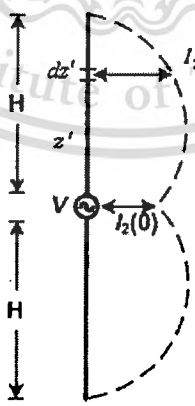

Figure 2.6 Current distribution on a dipole antenna [41].

According to Fig. 2.6, the relation is given by

$$\frac{-E_{z21}dz'}{dI_{sc}} = \frac{V}{I_2(z')}$$

or

$$dI_{sc} = -\frac{E_{z21}dz'}{V} I_2(z'). \tag{2.15}$$

The total short-circuit current I_{sc} is the contributions of all the EMF along the entire antenna as given by

$$I_{sc} = -\frac{1}{V}\int E_{z21} I_2(z')\,dz'. \tag{2.16}$$

The open-circuit voltage V_{21} is equal to the shorted-circuit current I_{sc} multiplied by the antenna impedance z_2:

$$V_{21} = I_{sc}Z_2 = -\frac{Z_2}{V}\int E_{z21} I_2(z')\,dz'. \tag{2.17}$$

Since $Z_2 = V / I_2(0)$, gets

$$V_{21} = -\frac{1}{I_2(0)}\int E_{z21} I_2(z')\,dz'. \tag{2.18}$$

Substitute equation (2.18) in the relation of $Z_{21} = \left.\frac{V_2}{I_1}\right|_{I_2=0}$, yields

$$Z_{21} = -\frac{1}{I_1(0) I_2(0)}\int E_{z21} I_2(z')\,dz'. \tag{2.19}$$

Equation (2.19) expresses the mutual coupling in terms of an integral of the product of the component of the incident electric field parallel to the antenna E_{z21} and the current distribution along the antenna $I_2(z')$. When $I_1(0)$ and $I_2(0)$ are respectively the current at the center terminal of antennas number 1 and number 2.

2.3.3 Mutual Impedance Analysis of Perpendicular Dipole Antennas in Lossless Medium

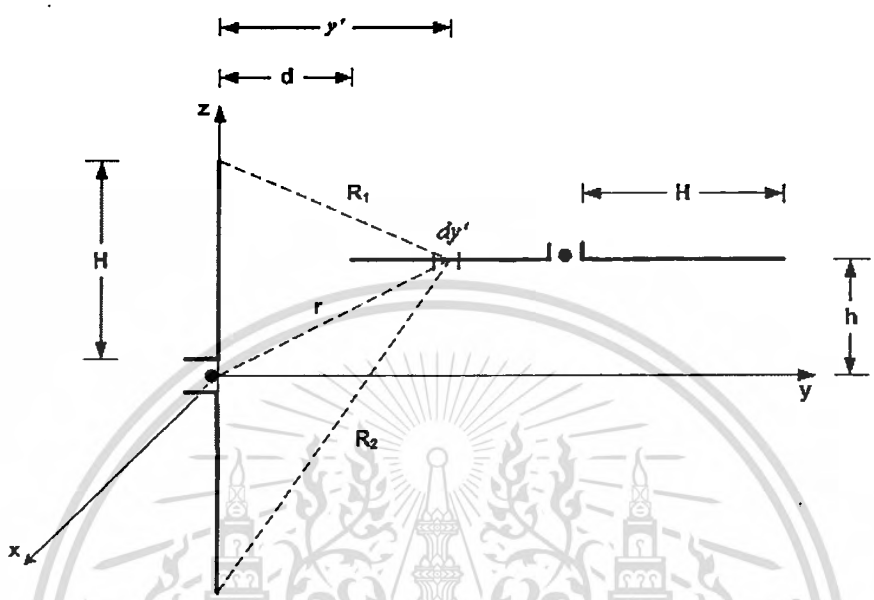

Figure 2.7 Perpendicular dipole antennas configuration.

The mutual impedance of perpendicular dipole antennas is initially analyzed in the case of lossless medium [42] to compare the accuracy of results obtained from the derived expressions with those from the commercial electromagnetic simulation program [43]. The analysis will be exhaustively detailed with step-by-step procedure.

Figure 2.7 shows that two center-feed dipole antennas with the length L, which the primary antenna is placed along the z-axis and its feed terminal assumed to have infinitesimal spacing is located at the origin of a Cartesian coordinate system, is separated from the secondary antenna with the same configuration by a distance d and h along y and z axis, respectively. Mutual impedance of both antennas is calculated by

$$Z_{21} = -\frac{1}{I_1(0)I_2(0)}\int E_{21}I_2(y')dy'. \tag{2.20}$$

The current distribution on the secondary antenna $I_2(y')$ is assumed to be sinusoidal and given by

$$I_2(y') = \begin{cases} I_m \sin\left[k(y'-d)\right] & ; \quad d<y'<H+d \\ I_m \sin\left[k(2H+d-y')\right] & ; H+d<y'<2H+d \end{cases}. \tag{2.21}$$

Substitute equations (2.21) and (2.13) into equation (2.20), yields

$$Z_{21} = -j\frac{\eta I_{1m} I_{2m}}{4\pi I_1(0) I_2(0)}\left[\int_d^{H+d}\left\{\left(\frac{z-H}{y}\frac{\exp(-jkR_1)}{R_1}+\frac{z+H}{y}\frac{\exp(-jkR_2)}{R_2}-\frac{2z\cos(kH)}{y}\frac{\exp(-jkr)}{r}\right)\times\sin\left[k(y'-d)\right]\right\}dy'\right.$$

$$\left.+\int_{H+d}^{2H+d}\left\{\left(\frac{z-H}{y}\frac{\exp(-jkR_1)}{R_1}+\frac{z+H}{y}\frac{\exp(-jkR_2)}{R_2}-\frac{2z\cos(kH)}{y}\frac{\exp(-jkr)}{r}\right)\times\sin\left[k(2H+d-y')\right]\right\}dy'\right]. \tag{2.22}$$

To simplify equation (2.22), transforms $\sin\left[k(y'-d)\right]$ and $\sin\left[k(2H+d-y')\right]$ in the form of exponential function; then gets

$$\sin\left[k(y'-d)\right] = \frac{1}{2j}\left\{\exp\left[jk(y'-d)\right]-\exp\left[-jk(y'-d)\right]\right\} \tag{2.23}$$

$$\sin\left[k(2H+d-y')\right] = \frac{1}{2j}\left\{\exp\left[jk(2H+d-y')\right]-\exp\left[-jk(2H+d-y')\right]\right\}. \tag{2.24}$$

Equation (2.22) can be rewritten as

$$Z_{21} = -j\frac{\eta I_{1m} I_{2m}}{4\pi I_1(0) I_2(0)}\times\frac{1}{2j}\left[\int_d^{H+d}\left\{\left(\frac{z-H}{y}\frac{\exp(-jkR_1)}{R_1}+\frac{z+H}{y}\frac{\exp(-jkR_2)}{R_2}-\frac{2z\cos(kH)}{y}\frac{\exp(-jkr)}{r}\right)\times\right.\right.$$

$$\left.\left(\exp\left[jk(y'-d)\right]-\exp\left[-jk(y'-d)\right]\right)\right\}dy'+\int_{H+d}^{2H+d}\left\{\left(\exp\left[jk(2H+d-y')\right]-\exp\left[-jk(2H+d-y')\right]\right)\times\right.$$

$$\left.\left.\left(\frac{z-H}{y}\frac{\exp(-jkR_1)}{R_1}+\frac{z+H}{y}\frac{\exp(-jkR_2)}{R_2}-\frac{2z\cos(kH)}{y}\frac{\exp(-jkr)}{r}\right)\right\}dy'\right]. \tag{2.25}$$

Integrate equation (2.25) will get 12-term expressions. The first of which is exemplified here. Let the first term expression be A_1 which is calculated from

$$A_1 = \int_d^{H+d}\left\{\left(\frac{z-H}{y}\frac{\exp(-jkR_1)}{R_1}\right)\times\left(\exp\left[jk(y'-d)\right]\right)\right\}dy'. \tag{2.26}$$

Substitute H, $z=h$, and $y=d$ in equation (2.26), yields

$$A_1 = \frac{h-H}{d}\int_{d}^{H+d}\frac{\exp\left[-jk\left(R_1 - y' + d\right)\right]}{R_1}dy' . \tag{2.27}$$

Define u to simplify the integration as

$$u = k\left(y' - R_1\right)$$

$$\frac{du}{dy'} = k\left(1 - \frac{dR_1}{dy'}\right)$$

and substitute $R_1 = \sqrt{\left(H-h\right)^2 + y'^2}$, gets

$$\frac{du}{dy'} = k\left(\frac{R_1 - y'}{R_1}\right)$$

or

$$dy' = \frac{-R_1}{u}du .$$

Substitute dy' in equation (2.27), yields

$$A_1 = \frac{h-H}{d}\int_{u_1}^{u_0}\frac{\exp\left[-j\left(kd-u\right)\right]}{R_1}\times\left(\frac{-R_1}{u}\right)du \tag{2.28}$$

when

$$u_0 = k\left[\left(H+d\right) - \sqrt{\left(H-h\right)^2 + \left(H+d\right)^2}\right]$$

$$u_1 = k\left[d - \sqrt{\left(H-h\right)^2 + d^2}\right].$$

With the relation of $\exp\left(-ju\right) = \cos u - j\sin u$, equation (2.28) can be rewritten as

$$A_1 = -\left(\frac{h-H}{d}\right)\left[\int_{u_1}^{u_0}\frac{\cos(kd-u)}{u}du - j\int_{u_1}^{u_0}\frac{\sin(kd-u)}{u}du\right]. \tag{2.29}$$

According with the relation of

$$\cos(A-B) = \cos A \cos B + \sin A \sin B$$

$$\sin(A-B) = \sin A \cos B - \cos A \sin B$$

then equation (2.29) can be rearranged as

$$A_1 = -\left(\frac{h-H}{d}\right)\left[\int_{u_1}^{u_0}\frac{\cos(kd)\cos(u)}{u}du+\int_{u_1}^{u_0}\frac{\sin(kd)\sin(u)}{u}du-j\int_{u_1}^{u_0}\frac{\sin(kd)\cos(u)}{u}du+j\int_{u_1}^{u_0}\frac{\cos(kd)\sin(u)}{u}du\right]. \tag{2.30}$$

Integrate equation (2.3) and arrange in the form of Cosine and Sine integrals, then gets

$$A_1 = -\left(\frac{h-H}{d}\right)\left[\cos(kd)\int_{u_1}^{u_0}\frac{\cos(u)}{u}du+\sin(kd)\int_{u_1}^{u_0}\frac{\sin(u)}{u}du-j\sin(kd)\int_{u_1}^{u_0}\frac{\cos(u)}{u}du+j\cos(kd)\int_{u_1}^{u_0}\frac{\sin(u)}{u}du\right]$$

$$A_1 = -\left(\frac{h-H}{d}\right)\left[\cos(kd)\left\{\int_{u_1}^{\alpha}\frac{\cos(u)}{u}du-\int_{u_0}^{\alpha}\frac{\cos(u)}{u}du\right\}+\sin(kd)\left\{\int_{0}^{u_0}\frac{\sin(u)}{u}du-\int_{0}^{u_1}\frac{\sin(u)}{u}du\right\}\right.$$

$$\left.-j\sin(kd)\left\{\int_{u_1}^{\alpha}\frac{\cos(u)}{u}du-\int_{u_0}^{\alpha}\frac{\cos(u)}{u}du\right\}+j\cos(kd)\left\{\int_{0}^{u_0}\frac{\sin(u)}{u}du-\int_{0}^{u_1}\frac{\sin(u)}{u}du\right\}\right]$$

$$= -\left(\frac{h-H}{d}\right)\left[\cos(kd)\{Ci(u_0)-Ci(u_1)\}+\sin(kd)\{Si(u_0)-Si(u_1)\}-j\sin(kd)\{Ci(u_0)-Ci(u_1)\}\right.$$

$$\left.+j\cos(kd)\{Si(u_0)-Si(u_1)\}\right] \tag{2.31}$$

when the definition of Cosine and Sine integrals are

$$Si(x) = \int_0^x \frac{\sin(\tau)}{\tau}d\tau$$

$$Ci(x) = -\int_x^{\alpha}\frac{\cos(\tau)}{\tau}d\tau = \int_{\alpha}^{x}\frac{\cos(\tau)}{\tau}d\tau.$$

With the same analysis procedure as aforementioned, the others 11 terms are shown as follow:

$$A_2 = -\left(\frac{h+H}{d}\right)\Big[\cos(kd)\left\{Ci(u_3)-Ci(u_2)\right\}+\sin(kd)\left\{Si(u_3)-Si(u_2)\right\}$$
$$-j\sin(kd)\left\{Ci(u_3)-Ci(u_2)\right\}+j\cos(kd)\left\{Si(u_3)-Si(u_2)\right\}\Big] \quad (2.32)$$

$$A_3 = \frac{2h}{d}\cos(kH)\Big[\cos(kd)\left\{Ci(u_5)-Ci(u_4)\right\}+\sin(kd)\left\{Si(u_5)-Si(u_4)\right\}$$
$$-j\sin(kd)\left\{Ci(u_5)-Ci(u_4)\right\}+j\cos(kd)\left\{Si(u_5)-Si(u_4)\right\}\Big] \quad (2.33)$$

$$A_4 = -\left(\frac{h-H}{d}\right)\Big[\cos(kd)\left\{Ci(v_0)-Ci(v_1)\right\}+\sin(kd)\left\{Si(v_0)-Si(v_1)\right\}$$
$$-j\cos(kd)\left\{Si(v_0)-Si(v_1)\right\}+j\sin(kd)\left\{Ci(v_0)-Ci(v_1)\right\}\Big] \quad (2.34)$$

$$A_5 = -\left(\frac{h+H}{d}\right)\Big[\cos(kd)\left\{Ci(v_3)-Ci(v_2)\right\}+\sin(kd)\left\{Si(v_3)-Si(v_2)\right\}$$
$$-j\cos(kd)\left\{Si(v_3)-Si(v_2)\right\}+j\sin(kd)\left\{Ci(v_3)-Ci(v_2)\right\}\Big] \quad (2.35)$$

$$A_6 = \frac{2h}{d}\cos(kH)\Big[\cos(kd)\left\{Ci(v_5)-Ci(v_4)\right\}+\sin(kd)\left\{Si(v_5)-Si(v_4)\right\}$$
$$-j\cos(kd)\left\{Si(v_5)-Si(v_4)\right\}+j\sin(kd)\left\{Ci(v_5)-Ci(v_4)\right\}\Big] \quad (2.36)$$

$$A_7 = \left(\frac{h-H}{d}\right)\Big[\cos\left[k(2H+d)\right]\left\{Ci(m_1)-Ci(v_0)\right\}+\sin\left[k(2H+d)\right]\left\{Si(m_1)-Si(v_0)\right\}$$
$$-j\cos\left[k(2H+d)\right]\left\{Si(m_1)-Si(v_0)\right\}+j\sin\left[k(2H+d)\right]\left\{Ci(m_1)-Ci(v_0)\right\}\Big] \quad (2.37)$$

$$A_8 = \left(\frac{h+H}{d}\right)\Big[\cos\left[k(2H+d)\right]\left\{Ci(m_2)-Ci(v_3)\right\}+\sin\left[k(2H+d)\right]\left\{Si(m_2)-Si(v_3)\right\}$$
$$-j\cos\left[k(2H+d)\right]\left\{Si(m_2)-Si(v_3)\right\}+j\sin\left[k(2H+d)\right]\left\{Ci(m_2)-Ci(v_3)\right\}\Big] \quad (2.38)$$

$$A_9 = -\frac{2h}{d}\cos(kH)\Big[\cos\big[k(2H+d)\big]\Big\{Ci\big(m_3\big)-Ci\big(v_5\big)\Big\}+\sin\big[k(2H+d)\big]\Big\{Si\big(m_3\big)-Si\big(v_5\big)\Big\}$$
$$-j\cos\big[k(2H+d)\big]\Big\{Si\big(m_3\big)-Si\big(v_5\big)\Big\}+j\sin\big[k(2H+d)\big]\Big\{Ci\big(m_3\big)-Ci\big(v_5\big)\Big\}\Big] \quad (2.39)$$

$$A_{10} = \left(\frac{h-H}{d}\right)\Big[\cos\big[k(2H+d)\big]\Big\{Ci\big(m_4\big)-Ci\big(u_0\big)\Big\}+\sin\big[k(2H+d)\big]\Big\{Si\big(m_4\big)-Si\big(u_0\big)\Big\}$$
$$-j\sin\big[k(2H+d)\big]\Big\{Ci\big(m_4\big)-Ci\big(u_0\big)\Big\}+j\cos\big[k(2H+d)\big]\Big\{Si\big(m_4\big)-Si\big(u_0\big)\Big\}\Big] \quad (2.40)$$

$$A_{11} = \left(\frac{h+H}{d}\right)\Big[\cos\big[k(2H+d)\big]\Big\{Ci\big(m_5\big)-Ci\big(u_3\big)\Big\}+\sin\big[k(2H+d)\big]\Big\{Si\big(m_5\big)-Si\big(u_3\big)\Big\}$$
$$-j\sin\big[k(2H+d)\big]\Big\{Ci\big(m_5\big)-Ci\big(u_3\big)\Big\}+j\cos\big[k(2H+d)\big]\Big\{Si\big(m_5\big)-Si\big(u_3\big)\Big\}\Big] \quad (2.41)$$

$$A_{12} = -\frac{2h}{d}\cos(kH)\Big[\cos\big[k(2H+d)\big]\Big\{Ci\big(m_6\big)-Ci\big(u_5\big)\Big\}+\sin\big[k(2H+d)\big]\Big\{Si\big(m_6\big)-Si\big(u_5\big)\Big\}$$
$$-j\sin\big[k(2H+d)\big]\Big\{Ci\big(m_6\big)-Ci\big(u_5\big)\Big\}+j\cos\big[k(2H+d)\big]\Big\{Si\big(m_6\big)-Si\big(u_5\big)\Big\}\Big] \quad (2.42)$$

when

$$u_2 = k\left[d-\sqrt{(H+h)^2+d^2}\right]$$

$$u_3 = k\left[(H+d)-\sqrt{(H+h)^2+(H+d)^2}\right]$$

$$u_4 = k\left[d-\sqrt{h^2+d^2}\right]$$

$$u_5 = k\left[(H+d)-\sqrt{h^2+(H+d)^2}\right]$$

$$v_0 = k\left[\sqrt{(H-h)^2+(H+d)^2}+(H+d)\right]$$

$$v_1 = k\left[\sqrt{(H-h)^2+d^2}+d\right]$$

$$v_2 = k\left[\sqrt{(H+h)^2+d^2}+d\right]$$

$$v_3 = k\left[\sqrt{(H+h)^2+(H+d)^2}+(H+d)\right]$$

$$v_4 = k\left[\sqrt{h^2+d^2}+d\right]$$

$$v_5 = k\left[\sqrt{h^2+(H+d)^2}+(H+d)\right]$$

$$m_1 = k\left[\sqrt{(H-h)^2+(2H+d)^2}+(2H+d)\right]$$

$$m_2 = k\left[\sqrt{(H+h)^2+(2H+d)^2}+(2H+d)\right]$$

$$m_3 = k\left[\sqrt{h^2+(2H+d)^2}+(2H+d)\right]$$

$$m_4 = k\left[(2H+d)-\sqrt{(H-h)^2+(2H+d)^2}\right]$$

$$m_5 = k\left[(2H+d)-\sqrt{(H+h)^2+(2H+d)^2}\right].$$

Consequently, mutual impedance of perpendicular dipole antennas in lossless medium can be calculated from the closed-form expressions of the 12 terms composition as shown in follow:

$$Z_{21} = \sum_{i=1}^{N} A_i \tag{2.43}$$

To verify the closed-form expressions, the obtained mutual resistance and mutual reactance, which are varied with the distance, are compared with those from commercial electromagnetic simulation program as illustrated in Fig. 2.8 and Fig. 2.9. Let both antennas are half-wavelength long and the height h of the secondary antenna, which is aligned parallel to y-axis, from the center-feed of the primary antenna aligned on the z-axis is 0.125λ. Note that both mutual resistance and mutual reactance from the closed-form expressions are in good agreement with those from simulation program.

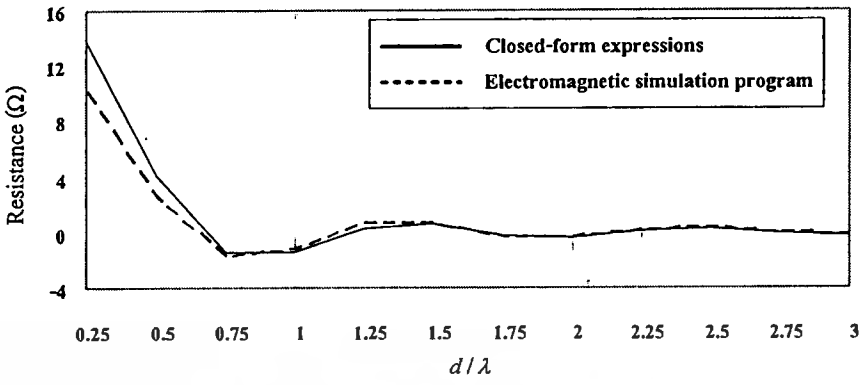

Figure 2.8 Comparison of mutual resistance from closed-form expressions and simulation program.

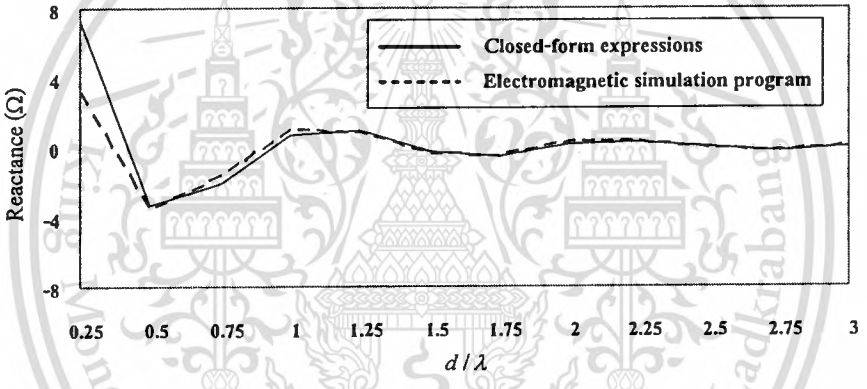

Figure 2.9 Comparison of mutual reactance from closed-form expressions and simulation program.

According to the closed-form expressions, Effect of the varied distance parameter d on mutual impedance is studied and illustrated in Fig. 2.10. The mutual resistance and the mutual reactance decrease as the distance d/λ increases. The more increasing of the distance, the mutual resistance and the mutual reactance are close to zero.

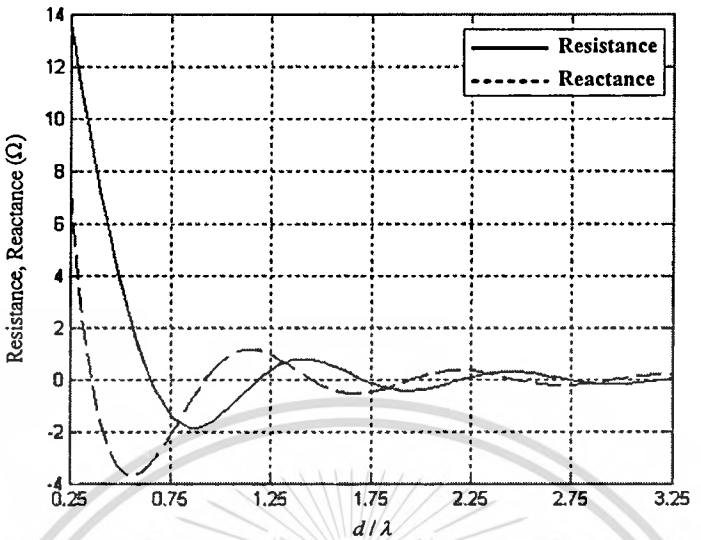

Figure 2.10 Effect of the distance d on mutual impedance.

Effects of the varied height h of the secondary antenna on mutual resistance and mutual reactance are respectively shown in Fig. 2.11 and Fig. 2.12. It can be noticed in Fig. 2.9 that the mutual resistances increase as the increasing of height when the distances are in the range of 0.2λ-0.6λ and they at all heights obviously decrease to zero as the distances more increase. Figure 2.10 shows that the mutual reactances increase when the heights increase in the range of distances equal 0.2λ-0.4λ. Like the mutual resistances, the reactances clearly decrease to zero as the distances more increase. Moreover, the study of the height h effect on the mutual impedance reveals that the mutual impedance is equal to zero at the height is zero.

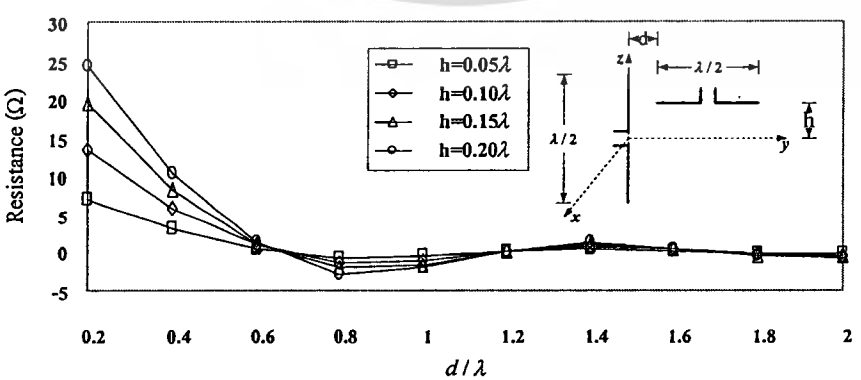

Figure 2.11 Effect of the height h on mutual resistance.

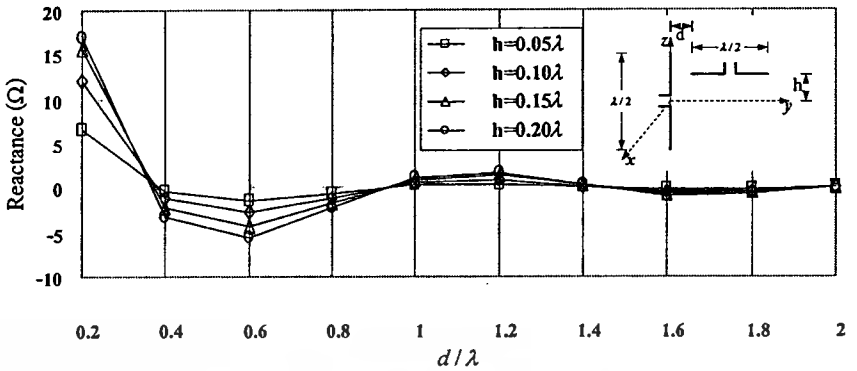

Figure 2.12 Effect of the height h on mutual reactance.

2.3.4 Mutual Impedance Analysis of Perpendicular Dipole Antennas in Lossy Medium

Unlike the lossless medium, the propagation constant k in lossy medium is comprised of the attenuation constant α and the phase constant β as shown in

$$k = \alpha + j\beta = \sqrt{j\omega\mu(\sigma + j\omega\varepsilon)} = \sqrt{-\omega^2\mu\varepsilon + j\omega\mu\sigma} \tag{2.44}$$

where ε and μ are respectively the complex permittivity and the complex permeability. Both of them equal

$$\alpha = \omega\sqrt{\mu\varepsilon}\left\{\frac{1}{2}\left[\sqrt{1+\left(\frac{\sigma}{\omega\varepsilon}\right)^2}-1\right]\right\}^{1/2} \text{ Np/m} \tag{2.45}$$

$$\beta = \omega\sqrt{\mu\varepsilon}\left\{\frac{1}{2}\left[\sqrt{1+\left(\frac{\sigma}{\omega\varepsilon}\right)^2}+1\right]\right\}^{1/2} \text{ rad/m.} \tag{2.46}$$

According to equation (2.25), substitute the propagation constant k with the relation in equations (2.44)-(2.46) and integrate by means of the same procedure in the previous subsection, then gets

$$A_1 = -\left(\frac{h-H}{d}\right)\times\left[\exp(d\beta)\times\{\cos(d\alpha)-j\sin(d\alpha)\}\times\{\{Ci(u_0)-Ci(u_1)\}+j\{Si(u_0)-Si(u_1)\}\}\right] \tag{2.47}$$

$$A_2 = -\left(\frac{h+H}{d}\right)\times\left[\exp(d\beta)\times\{\cos(d\alpha)-j\sin(d\alpha)\}\times\{\{Ci(u_3)-Ci(u_2)\}+j\{Si(u_3)-Si(u_2)\}\}\right] \quad (2.48)$$

$$A_3 = \frac{2h}{d}\times\frac{1}{2}\left[\cos(H\alpha)\times\{\exp(H\beta)+\exp(-H\beta)\}-j\sin(H\alpha)\times\{\exp(H\beta)-\exp(-H\beta)\}\right]\times\left[\exp(d\beta)\times\{\cos(d\alpha)-j\sin(d\alpha)\}\right]$$
$$\times\left[\{Ci(u_5)-Ci(u_4)\}+j\{Si(u_5)-Si(u_4)\}\right] \quad (2.49)$$

$$A_4 = -\left(\frac{h-H}{d}\right)\times\left[\exp(-d\beta)\times\{\cos(d\alpha)+j\sin(d\alpha)\}\times\{\{Ci(v_0)-Ci(v_1)\}-j\{Si(v_0)-Si(v_1)\}\}\right] \quad (2.50)$$

$$A_5 = -\left(\frac{h+H}{d}\right)\times\left[\exp(-d\beta)\times\{\cos(d\alpha)+j\sin(d\alpha)\}\times\{\{Ci(v_3)-Ci(v_2)\}-j\{Si(v_3)-Si(v_2)\}\}\right] \quad (2.51)$$

$$A_6 = \frac{2h}{d}\times\frac{1}{2}\left[\cos(H\alpha)\times\{\exp(H\beta)+\exp(-H\beta)\}-j\sin(H\alpha)\times\{\exp(H\beta)-\exp(-H\beta)\}\right]\times\left[\exp(-d\beta)\times\{\cos(d\alpha)+j\sin(d\alpha)\}\right]$$
$$\times\left[\{Ci(v_5)-Ci(v_4)\}-j\{Si(v_5)-Si(v_4)\}\right] \quad (2.52)$$

$$A_7 = \left(\frac{h-H}{d}\right)\times\{\exp(-2H\beta)\times\exp(-d\beta)\}\times\{\cos(2H\alpha)+j\sin(2H\alpha)\}\times\{\cos(d\alpha)+j\sin(d\alpha)\}$$
$$\times\left[\{Ci(m_1)-Ci(v_0)\}-j\{Si(m_1)-Si(v_0)\}\right] \quad (2.53)$$

$$A_8 = \left(\frac{h+H}{d}\right)\times\{\exp(-2H\beta)\times\exp(-d\beta)\}\times\{\cos(2H\alpha)+j\sin(2H\alpha)\}\times\{\cos(d\alpha)+j\sin(d\alpha)\}$$
$$\times\left[\{Ci(m_2)-Ci(v_3)\}-j\{Si(m_2)-Si(v_3)\}\right] \quad (2.54)$$

$$A_9 = -\frac{2h}{d}\times\frac{1}{2}\left[\cos(H\alpha)\times\{\exp(H\beta)+\exp(-H\beta)\}-j\sin(H\alpha)\times\{\exp(H\beta)-\exp(-H\beta)\}\right]$$
$$\times\{\exp(-2H\beta)\times\exp(-d\beta)\}\times\{\cos(2H\alpha)+j\sin(2H\alpha)\}\times\{\cos(d\alpha)+j\sin(d\alpha)\}$$
$$\times\left[\{Ci(m_3)-Ci(v_5)\}-j\{Si(m_3)-Si(v_5)\}\right] \quad (2.55)$$

$$A_{10} = \left(\frac{h-H}{d}\right)\times\{\exp(2H\beta)\times\exp(d\beta)\}\times\{\cos(2H\alpha)-j\sin(2H\alpha)\}\times\{\cos(d\alpha)-j\sin(d\alpha)\}$$
$$\times\left[\{Ci(m_4)-Ci(u_0)\}+j\{Si(m_4)-Si(u_0)\}\right] \quad (2.56)$$

$$A_{11}=\left(\frac{h+H}{d}\right)\times\left\{\exp(2H\beta)\times\exp(d\beta)\right\}\times\left\{\cos(2H\alpha)-j\sin(2H\alpha)\right\}\times\left\{\cos(d\alpha)-j\sin(d\alpha)\right\}$$
$$\times\left[\left\{Ci(m_5)-Ci(u_3)\right\}+j\left\{Si(m_5)-Si(u_3)\right\}\right] \quad (2.57)$$

$$A_{12}=-\frac{2h}{d}\times\frac{1}{2}\left[\cos(H\alpha)\times\left\{\exp(H\beta)+\exp(-H\beta)\right\}-j\sin(H\alpha)\times\left\{\exp(H\beta)-\exp(-H\beta)\right\}\right]$$
$$\times\left\{\exp(2H\beta)\times\exp(d\beta)\right\}\times\left\{\cos(2H\alpha)-j\sin(2H\alpha)\right\}\times\left\{\cos(d\alpha)-j\sin(d\alpha)\right\}$$
$$\times\left[\left\{Ci(m_6)-Ci(u_5)\right\}+j\left\{Si(m_6)-Si(u_5)\right\}\right] \quad (2.58)$$

and their angular variables are the same as shown in lossless medium.

2.4 Dielectric Property Determination Using Mutual Coupling Magnitudes

Mutual impedance of the perpendicular configuration of dipole antenna obtained from the combination of the 12 terms derived expressions and the modified mutual impedance of parallel configuration are transformed to S-parameter. The transformed mutual impedance is called mutual coupling. The mutual coupling magnitudes of both configurations, exploited as a solution for the dielectric property determination of a material, are calculated with respect to the dielectric constant and the dielectric loss factor variation. The calculated mutual couplings are drawn in the form of a surface curve. This surface curve is used to determine the dielectric property by plotting the mutual coupling magnitudes of both configurations from measurement. The mutual coupling magnitudes of perpendicular configuration are plotted on the solid lines by the black triangle symbol whereas the dash lines are for the parallel polarization plotted by the white dot symbol. Then reading off the values of the dielectric constant, x-axis, and the dielectric loss factor, y-axis, at the cross points between these two symbols. For instance, at the point denoted by ✸ in Fig. 2.13, the magnitudes of mutual coupling from the measurement in the case of perpendicular and parallel configurations are respectively 0.013 and 0.152. Plotting these values on the surface curve, the cross point provides the dielectric constant and the dielectric loss factor which are 2.852 and 0.30, respectively. The essence of this cross point is that only one sufficient condition or one cross point between the lines in the surface curve of each polarization is needed to determine the complex permittivity of the

material under test [30]. Note that the medium in derivation is assumed to be homogeneous. The inhomogeneous variation of the material will result the erroneous of ε' and ε''.

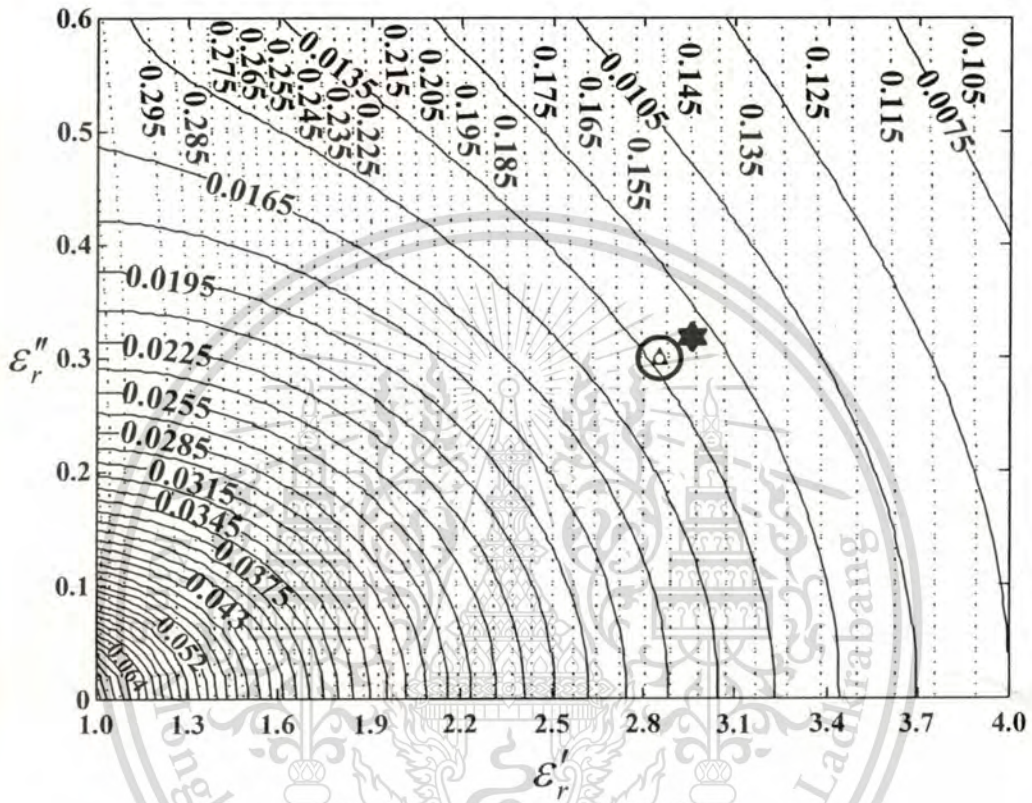

Figure 2.13 Surface curve of mutual coupling magnitudes used in dielectric property determination at d = 2 mm (———: perpendicular configuration, ---------: parallel configuration).

According to the surface curve of mutual coupling magnitudes ($|S_{21}|$), it is achieved by transforming the expressions of mutual impedance (Z_{21}) in lossy medium, which the antennas in the calculation are wire dipole antennas and the medium is assumed to be homogeneous. However, the antenna to be employed as the moisture content sensor of paddy concerns the suitable for practical use. Thus, the switchable antenna selected to use in this dissertation is a printed dipole antenna. The difference of mutual coupling magnitude between wire dipole and printed dipole antennas is

considered and illustrated in Table. 2. Note that the deviations of mutual coupling magnitudes obtained from the printed antenna compared with those from the wire antenna in parallel and perpendicular configurations are respectively in the range of 10.97% - 20.59% and 11.11%-28.57%.

Table 2. Comparison of mutual coupling magnitudes from wire dipole and printed dipole antennas

Dielectric properties		**Mutual coupling magnitudes**					
		Parallel configuration			**Perpendicular configuration**		
ε_r'	ε_r''	**Wire antenna**	**Printed antenna**	**Deviation (%)**	**Wire antenna**	**Printed antenna**	**Deviation (%)**
1	0	0.310	0.276	10.97	0.072	0.064	11.11
1.5	0.1	0.275	0.244	11.27	0.041	0.036	12.19
2	0.2	0.219	0.192	12.34	0.023	0.019	17.39
2.5	0.3	0.174	0.148	14.94	0.016	0.013	18.75
3	0.4	0.142	0.123	13.38	0.011	0.009	18.18
3.5	0.5	0.120	0.098	18.33	0.008	0.006	25.00
4	0.6	0.102	0.081	20.59	0.007	0.005	28.57

2.5 Summary

In this chapter, the brief literatures review of the dielectric properties determination techniques are detailed, the advantages and disadvantages of each technique are also listed, and the reason that leads to present the novel technique is

described. The presented technique utilizes only the magnitude of mutual coupling of perpendicular and parallel configurations dipole antenna in characterizing the dielectric properties. In order to obtain the mutual coupling magnitudes ($|S_{21}|$), an analysis of mutual impedance (Z_{21}) related to the dielectric constants (ε_r') and the dielectric loss factors (ε_r'') variation is transformed and expressed especially in the case of perpendicular configuration. The step-by-step analysis, which is firstly derived in the condition of lossless medium, is exhaustively carried and then the results obtained from closed-form expressions are compared with those from the electromagnetic simulation program to investigate the accuracy. It is obviously evidence that they are in good agreement. Finally, the closed-form expressions are modified for the lossy medium condition and employed in the surface curves which perform as the solution for the dielectric properties determination. To verify the presented technique, the design of switch-configuration dipole antenna used in the experiment will be exhibited in the next chapter.

CHAPTER 3

DESIGN OF A PRINTED SWITCH-CONFIGURATION DIPOLE ANTENNA

3.1 Introduction

In this chapter, design of a switch-configuration dipole antenna exploited in the dielectric properties determination is described. The configuration of designed antenna comprises of four cross elements, which two of them are arranged in parallel configuration and the others are in perpendicular configuration, and is constructed on a single printed circuit board (PCB) that makes it compact and easy to use. The step-by-step design firstly starts with the design of an only one dipole antenna structure to investigate the current distribution and S_{11}, and get the proper dimension by a commercial electromagnetic simulation program [44]. With the obtained proper dimension, it is utilized to design the switch-configuration dipole antenna which two single-pole double-throw (SPDT) switches are incorporated with four cross elements to select the polarization between parallel and perpendicular configurations. Finally, losses caused by parasitic elements and SPDT switches are compensated to enhance the antenna performance by means of co-simulation [45].

3.2 One Dipole Antenna Design

An antenna structure that will be used as switch-configuration dipole antennas is firstly designed and constructed on a low cost FR-4 PCB which is 1.6 mm thick and the dielectric constant and the loss tangent of the substrate are respectively 4.36 and 0.01178. The designed antenna has a balanced uniplanar transition structure, coplanar strips (CPS), which ideally supports signal propagation with low common mode noise, as feeding lines. A 180-degree phase delay between two branches microstrip lines of balun is needed to realize efficient transition between CPS and microstrip lines [46]-[48] since the propagation mode in coupled microstrips is dominantly odd mode which can easily be transferred to CPS mode after the ground plane is truncated [49], [50]. These antennas

operate at a frequency of 2.45 GHz. The structure on the top metallization consists of a 50 Ω microstrip feed line, a 35.4 Ω quarter-wave impedance transformer followed by a symmetric T-junction, a microstrip-to-coplanar stripline balun, and a dipole antenna whereas the metallization at the bottom plane is a truncated microstrip ground as shown in Fig. 3.1.

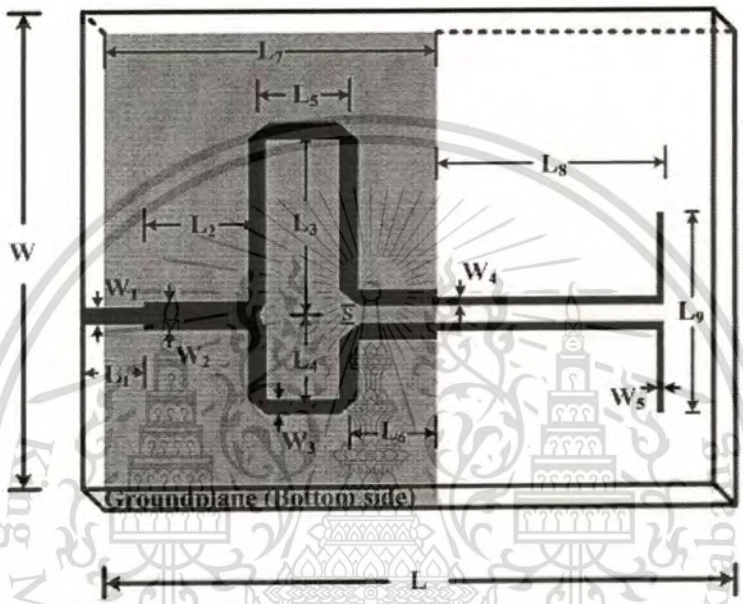

Figure 3.1 Structure of designed antenna.

To provide the antenna with the best performance, its structure is carefully designed each parts. One of the most important fragments is balun whose role is to balance the distributed current from the excitation port to the dipole antenna. It consists of two equally 50 Ω microstrip lines, but the length of both lines does not equal that one of which is $0.75\,\lambda_d$ long whereas the other is $0.25\,\lambda_d$ long as illustrated in Fig. 3.2.

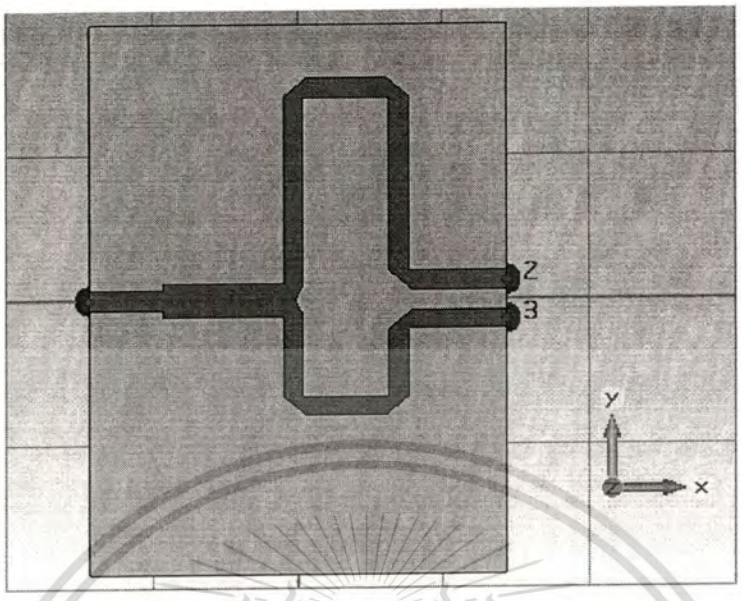

Figure 3.2 Simulation of balun configuration [44].

Figure 3.2 shows the simulated configuration of balun which is connected to a 35.4 Ω quarter-wave impedance transformer and a 50 Ω microstrip line. In the simulation, port 1 is defined to be an excitation port; port 2 and port 3 are ports for investigating output of balun which are respectively connected to the $0.75\,\lambda_d$ and $0.25\,\lambda_d$ branches.

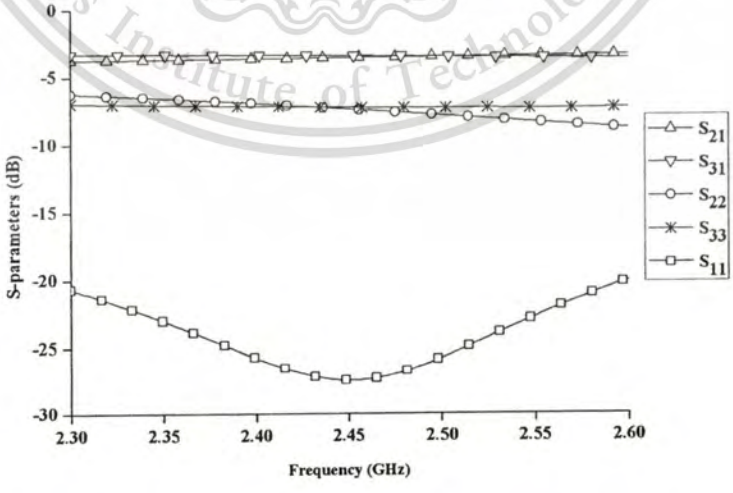

Figure 3.3 Simulated S-parameters of balun.

The simulated S-parameters of balun are illustrated in Fig. 3.3. At the frequency of 2.45 GHz, note that S_{11} at the excitation port equals -27.48 dB, and at the output ports S_{22} and S_{33} are respectively -7.41 dB, -7.29 dB. The transmission at the output ports, S_{21} and S_{31}, are -3.62 dB and -3.49 dB, respectively. It is obviously seen that S_{21} and S_{31} almost equal. Furthermore, the current density in Fig. 3.4 shows that the current on this structure uniformly distributes, thus it can be conclude that the designed balun balances the output power well.

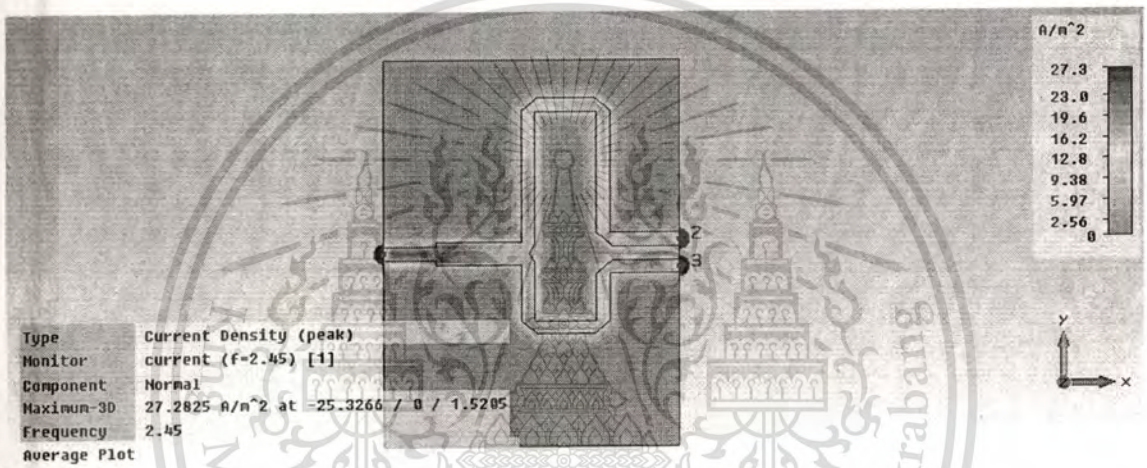

Figure 3.4 Current density of the simulated balun [44].

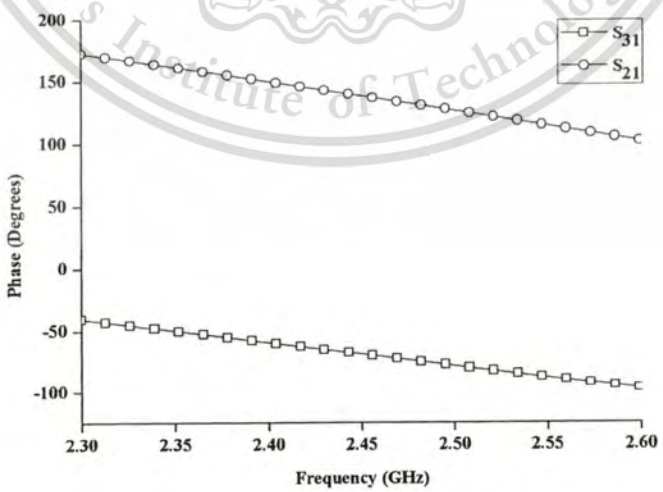

Figure 3.5 Simulated output phase of balun.

To realize the output ports of balun performing in the odd mode, the phase difference of both ports should be equal to 180 degrees. Note that the simulated phase difference between S_{21} and S_{31} at the frequency of 2.45 GHz is almost 180 degrees as illustrated in Fig. 3.5.

After obtaining the proper dimension of balun, it is connected with the CPS fragment which acts as the transition to transfer signals and match impedance between balun and elements of dipole antenna. Then the whole structure of a one dipole antenna is simulated. The impedance and the length of CPS are respectively 70 Ω and $\lambda_d/4$ where λ_d is the wavelength in the substrate. All dimensions of the designed antenna are listed in Table 3 and the simulated S_{11} using an electromagnetic simulation program [44] is shown in Fig. 3.6. These dimensions will be exploited in the design of the switched-polarization dipole antennas in next section.

Table 3. Dimensions of a one dipole antenna

Parameters	Dimension (mm)
W	75.85
W_1	2.69
W_2	4.64
W_3	2.69
W_4	1.41
W_5	2.69
L	100.00
L_1	10.00
L_2	17.89
L_3	29.30
L_4	14.65
L_5	14.65
L_6	14.65
L_7	57.18
L_8	36.27
L_9	31.99
S	2.69

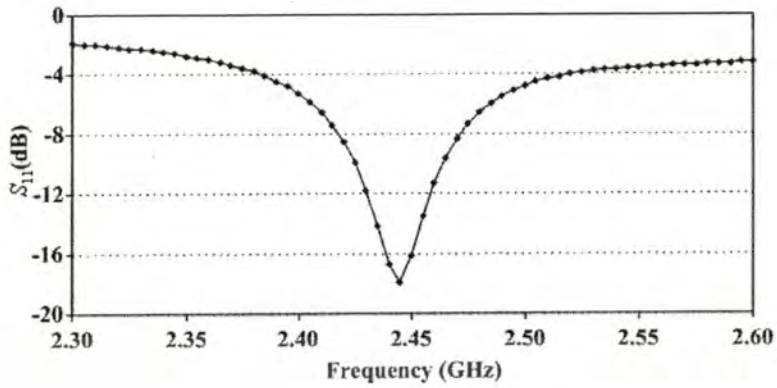

(b)

Figure 3.6 Simulated S_{11} of a one dipole antenna.

3.3 Switch-Configuration Dipole Antenna Structure

The structure of the switch-configuration dipole antennas exploits the dimensions of the design in the previous section, as shown in Fig. 3.7. On the top side of the PCB, there is a dipole antenna with a feed transmission line and four cross elements that perform as the transmitting and the receiving antennas, respectively. For the receiving antenna, the feed transmission line is on the bottom side which is connected to two mounted SPDT switches. Each switch controls an L-shape coupled element in the direction of parallel or perpendicular configuration. The first switch is attached to the upper and the right elements of the four cross elements while the lower and the left elements are connected to the other ones. In the case of parallel configuration, the upper and lower elements are selected to switch on while the right and left elements are operating in the perpendicular configuration case. These two configurations are set at the same feed point of which the distance between the transmitting antenna and the left element of the four cross elements is 2 mm. For parallel configuration, the distance is equal to the sum of the perpendicular configuration distance and the length of the left element of the four cross elements.

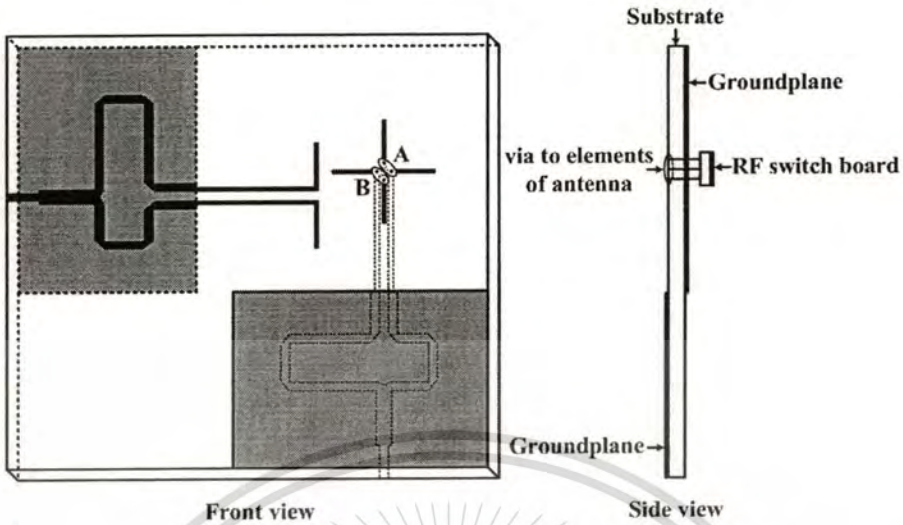

Figure 3.7 Switch-configuration dipole antenna structure (A: via to RF switch 1, B: via to RF switch 2).

3.4 Loss Compensation

The RF switches and parasitic elements performing in different configuration cause losses in practice. Thus, loss compensation is essential to be analyzed by a co-simulation [45]. This analysis is needed to compensate for the degraded receiving signal since the mutual coupling magnitude of each configuration, used in determining the dielectric properties as a solution on surface curves, is calculated in the case of pure configuration. The simulations will be classified into two categories, parallel and perpendicular configurations. Each category performs simulation of input port S_{11} and output port S_{22}. It covers three cases: pure configuration, parasitic elements effect, and combination of parasitic elements and rf switches effect as illustrated in Fig. 3.8, Fig. 3.9, and Fig. 3.10, respectively.

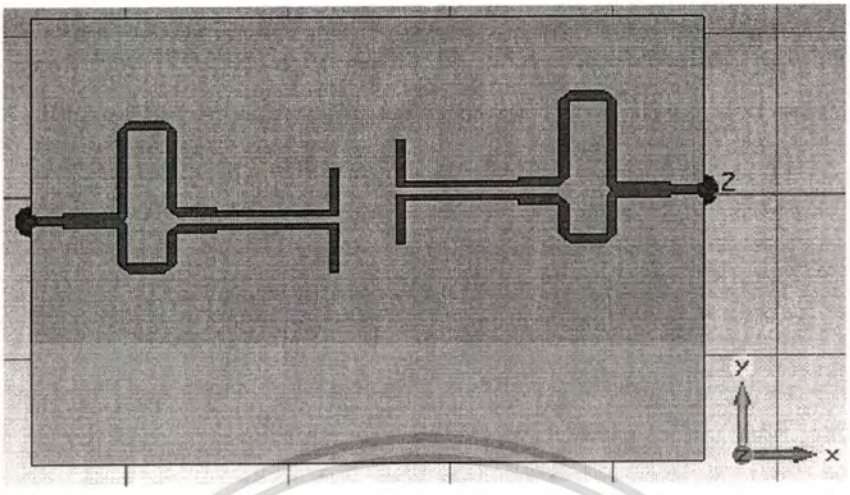

(a)

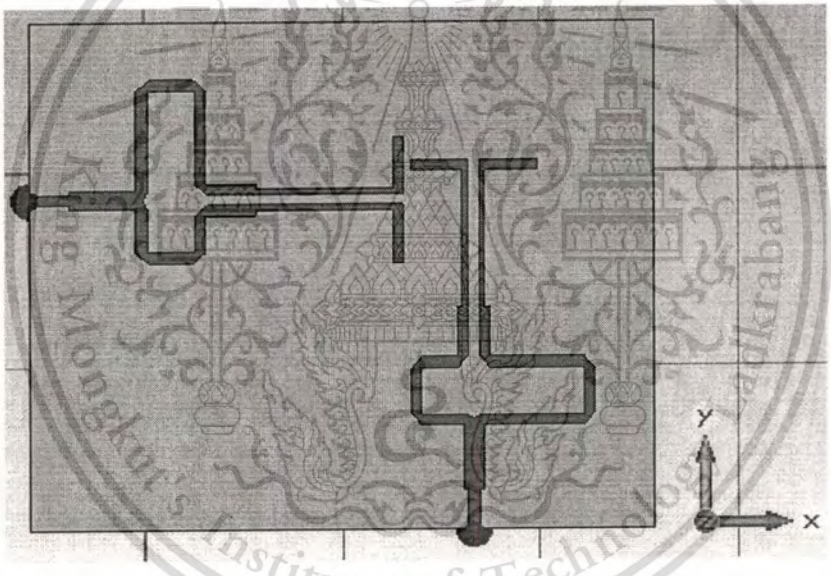

(b)

Figure 3.8 Simulation of loss compensation in pure configuration case (a) parallel configuration, (b) perpendicular configuration [44].

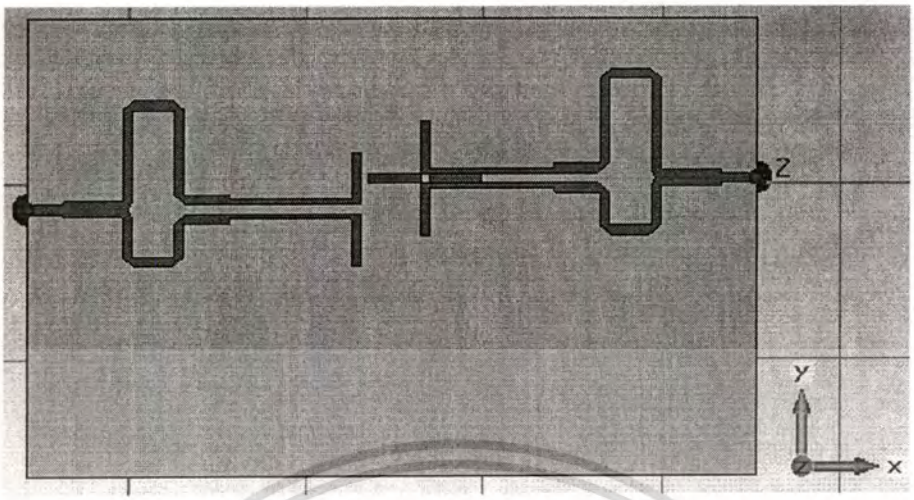

(a)

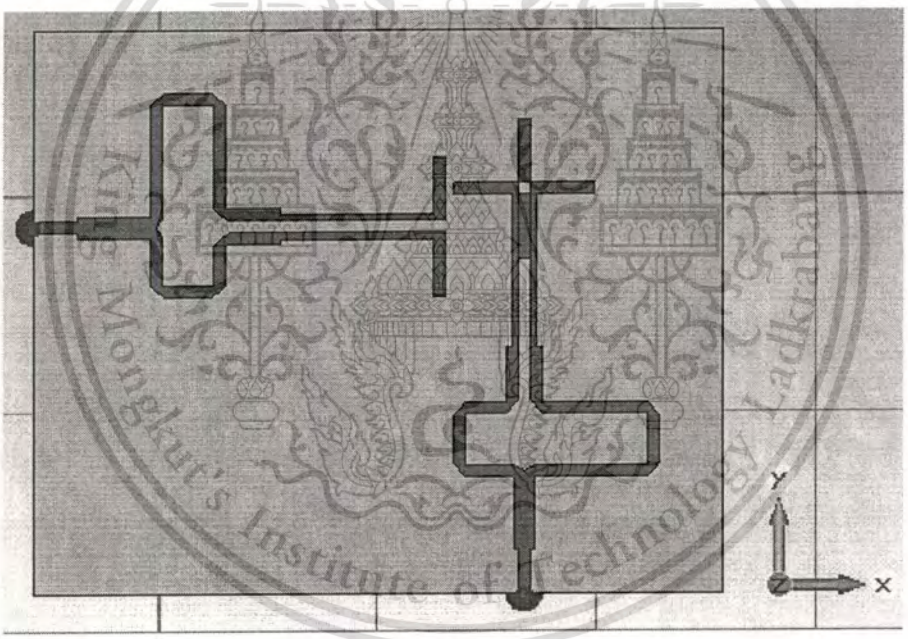

(b)

Figure 3.9 Simulation of loss compensation in parasitic elements effect case (a) parallel configuration with perpendicular elements, (b) perpendicular configuration with parallel elements [44].

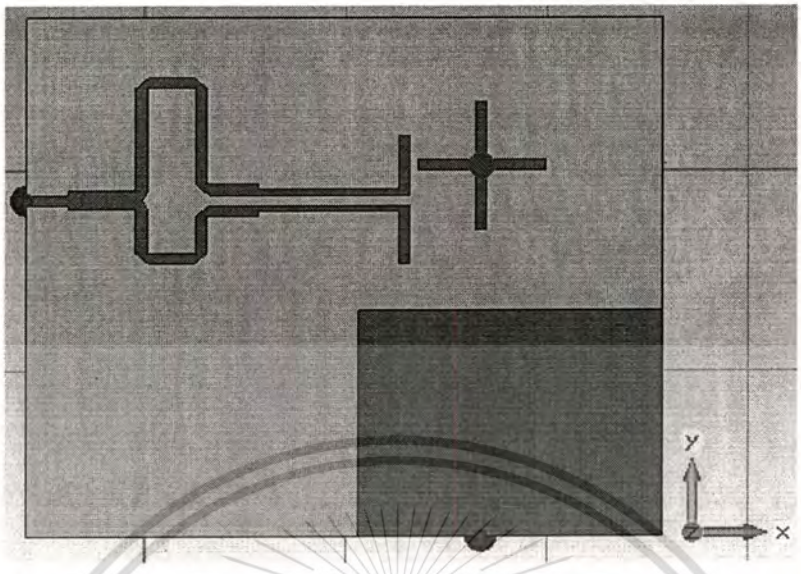

Figure 3.10 Simulation of loss compensation in combination of parasitic elements and rf switches effect case [44].

The simulated S_{11} and S_{22} of parallel configuration are shown in Fig. 3.11(a) and Fig. 3.11(b), respectively. The results at 2.45 GHz show that both S_{11} and S_{22} are about -19 dB. When two parasitic elements of perpendicular configuration are added, they slightly shift the operating frequency to a lower frequency and increase S_{11} and S_{22} to -12.54 dB and -18.17 dB, respectively. In addition, the effect of rf switches [51] integrated with parasitic elements of the other configuration causes S_{11} and S_{22} to become higher, to -10.32 dB and -15.44 dB, respectively.

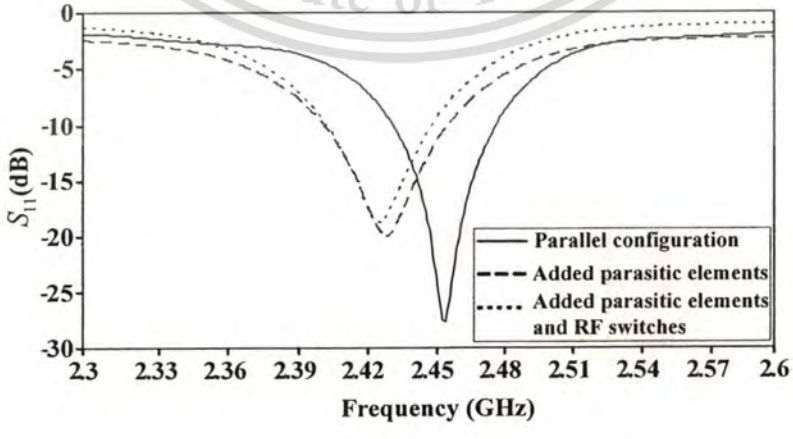

(a)

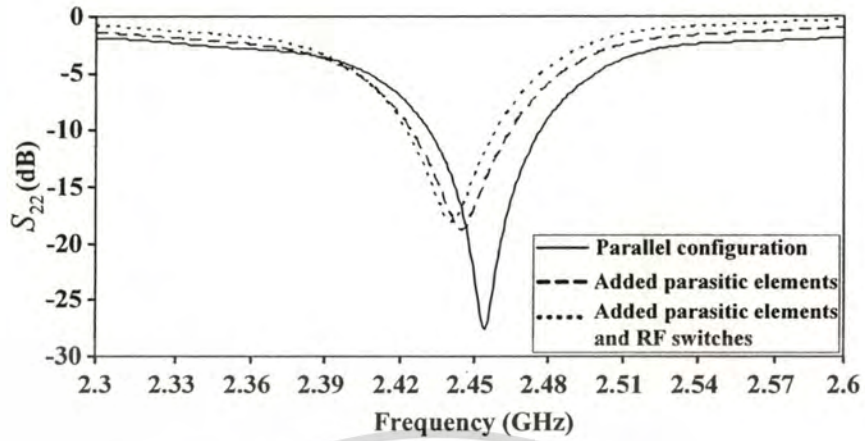

(b)

Figure 3.11 S_{11} and S_{22} of parallel configuration (a) S_{11}, (b) S_{22}.

The simulated S_{11} and S_{22} for perpendicular configuration are illustrated in Fig. 3.12(a) and Fig. 3.12(b), respectively. In the pure configuration case, S_{11} is -11.46 dB and S_{22} is -23.86 dB. They are insignificantly affected by the parasitic elements of parallel configuration, yielding S_{11} at -11.96 dB and S_{22} at -22.33 dB. However, they become higher at both ports when the effect of rf switches is simulated, yielding the values of -10.17 dB and -19.15 dB at the input and output ports, respectively.

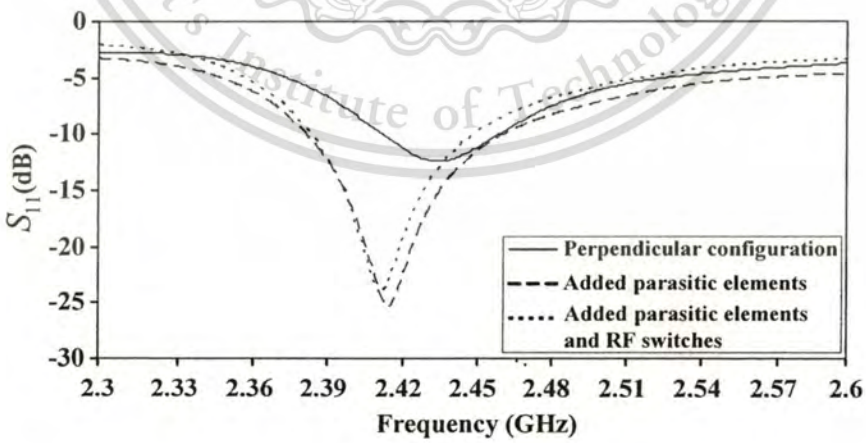

(a)

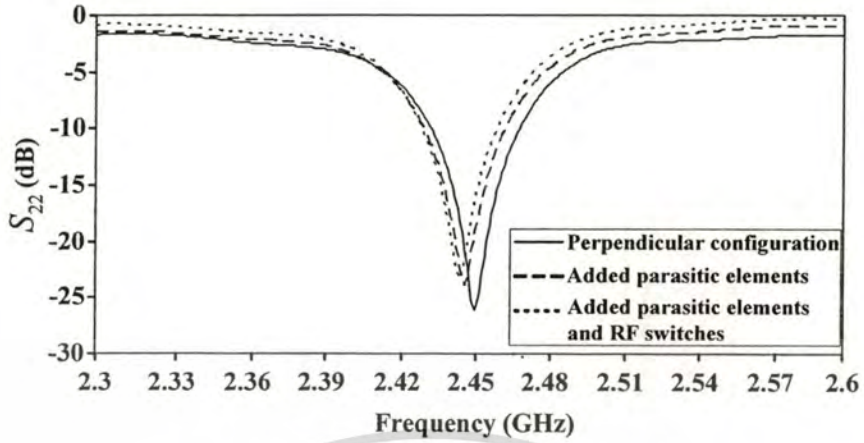

(b)

Figure 3.12 S_{11} and S_{22} of perpendicular configuration (a) S_{11}, (b) S_{22}.

Although both parasitic elements and rf switches diminished S_{11} and S_{22}, all ports are still matched. However, they do affect the coupling signal, as shown in Fig 3.13(a) and Fig. 3.13(b). The coupled signals are illustrated in the form of mutual coupling magnitude. The mutual coupling magnitude in the pure parallel configuration case is 0.067, but it increases to 0.269 due to the effect of the two parasitic elements. Nevertheless, the effect of added rf switches decreases the mutual coupling magnitude to 0.240.

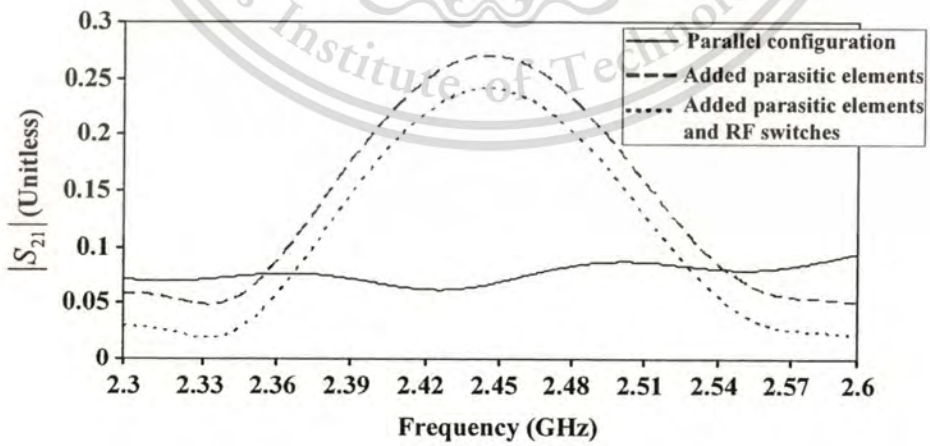

(a)

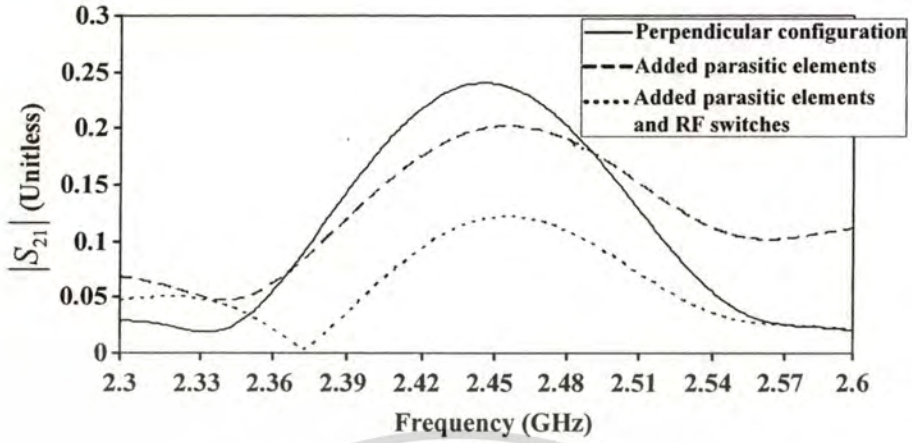

(b)

Figure 3.13 Effect of parasitic elements and rf switches on mutual coupling magnitude (a) parallel configuration, (b) perpendicular configuration.

For the pure perpendicular configuration case, the mutual coupling magnitude is 0.200 and it decreases to 0.120 by adding two parasitic elements of parallel configuration, while adding rf switches further reduce it to 0.107. Subsequently, these analyzed results are exploited to compensate for all the losses in the designed switch-configuration dipole antennas. It helps supplement the efficiency of the antennas. Furthermore, these results are used in calibration, discussed in the next subsection.

3.5 Fabricated Switch-Configuration Dipole Antenna

With the proper dimension obtained from the design and the best performance by compensating all losses, the switch-configuration dipole antenna is fabricated on a FR-4 substrate whose dielectric constant and loss tangent are respectively 4.36 and 0.00178. The whole dimension of this structure is 130 mm x 158 mm as illustrated in Fig. 3.14.

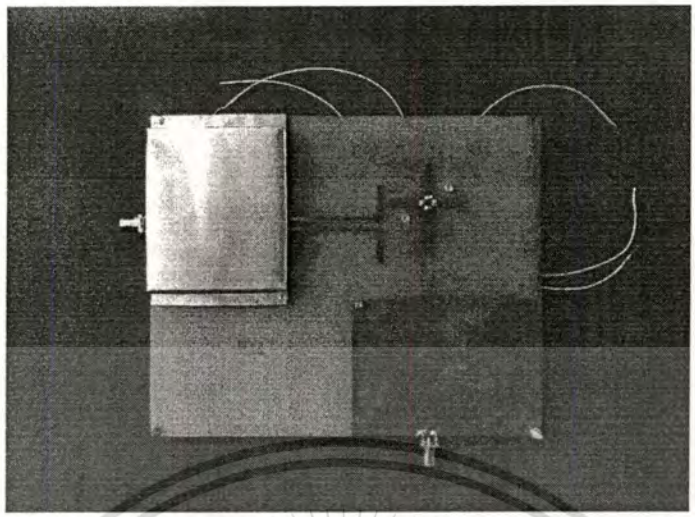

(a)

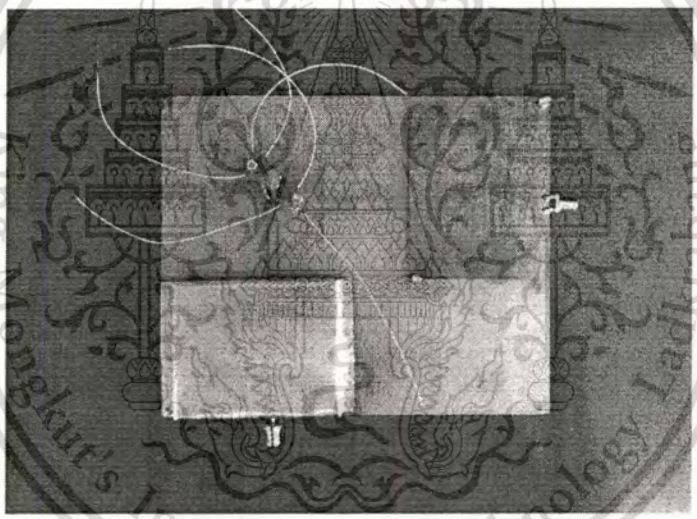

(b)

Figure 3.14 Fabricated switch-configuration dipole antenna (a) top side, (b) bottom side.

Figure 3.14 shows the fabricated antenna whose top side has a transmitting dipole antenna with a feed transmission line and four cross elements of the receiving antennas. While a feed transmission line of the receiving antennas connected to two mounted SPDT switches is on the bottom side. The switches are controlled by +5 DC biasing voltage.

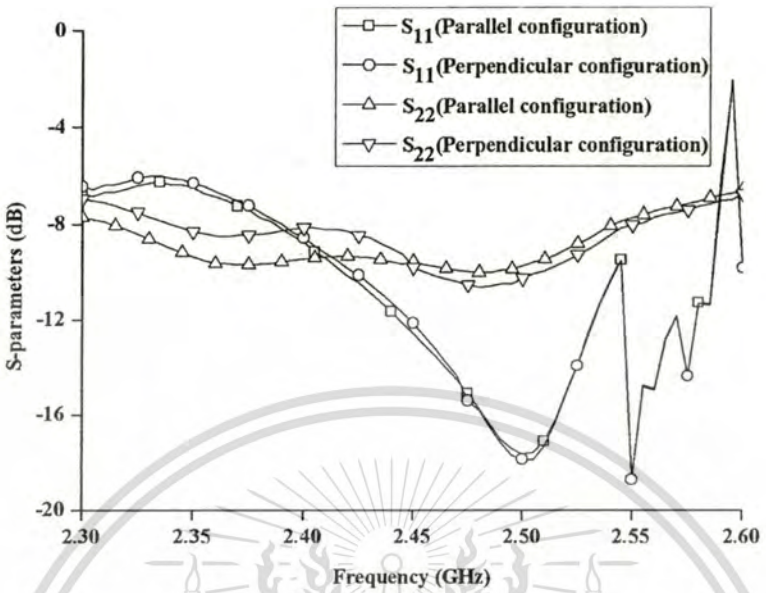

Figure 3.15 Measured return loss of the switch-configuration dipole antenna.

The fabricated antenna is investigated on return loss and mutual coupling in both configuration cases to consider its performance. The measured return loss at the input S_{11} and output S_{22} ports is shown in Fig. 3.15. At the frequency of 2.45 GHz, note that both S_{11} and S_{22} are respectively -12 dB and -9 dB which are almost identical in the perpendicular and parallel configurations. The mutual coupling of both configuration cases is measured and illustrated in Fig. 3.16. For the parallel configuration, the mutual coupling is equal to -16 dB whereas it is -18 dB in the case of perpendicular configuration.

Note that all investigations of the fabricated antenna are measured with the condition of free space in an anechoic chamber in order to get results for use in calibrating in the dielectric properties determination which will be described in next chapter.

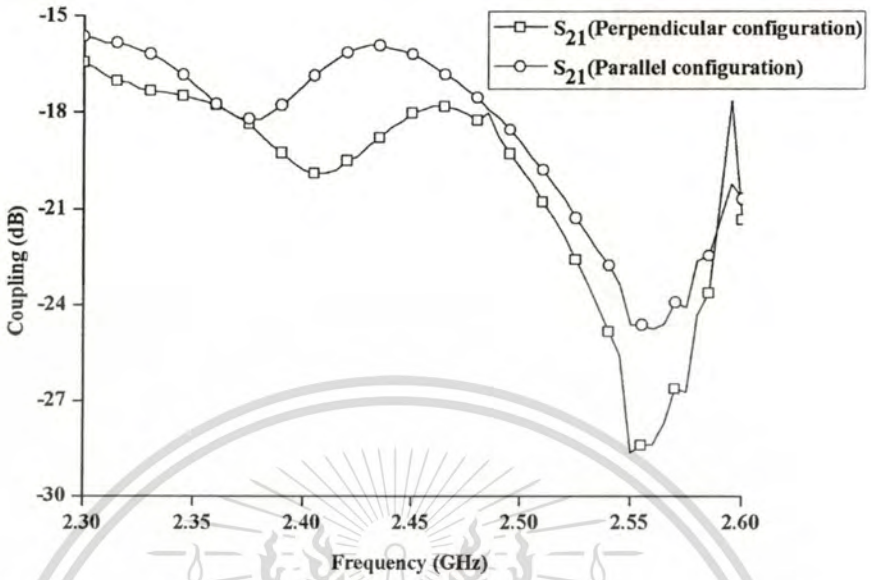

Figure 3.16 Measured mutual coupling of the switch-configuration dipole antenna.

3.6 Summary

In this chapter, the switch-configuration dipole antenna to use for the dielectric properties determination in the next chapter are designed and fabricated. To obtain the best performance, it is carefully considered step-by-step: initial step of only one dipole antenna structure design, switch-configuration antenna design step, and final step of losses compensation. The achieved structure with maximal performance is then fabricated and investigated. It is considered by means of S_{11} and mutual coupling measurement in both parallel and perpendicular configurations.

CHAPTER 4

THE USE OF A SWITCH-CONFIGURATION DIPOLE ANTENNA IN THE DIELECTRIC PROPERTIES DETERMINATION

4.1 Introduction

The designed and fabricated switch-configuration dipole antenna on a single PCB obtained from the previous chapter is employed to use in the dielectric properties determination. In the experiments, the material under test is paddy which the percentage of moisture content is varied. The obtained dielectric properties are correlated with the moisture content from a standard method of American Society of Agricultural and Biological Engineers (ASAE). In order to show the accuracy of the proposed sensor, the results are compared with those from the conventional method, the transmission line technique in the previous work [13]. Furthermore, the error compensation is considered since the surface curves of mutual coupling magnitudes used as the solution to characterize the dielectric properties is derived in the condition of infinite medium, but the container size used in this experiment is finite. Finally, the feasibility of applying this sensor in a closed-loop drying system is validated by setting up a simple model system of the experiments.

4.2 Dielectric Properties of Varied Moisture Content Paddy

To demonstrate the determination of dielectric properties by using the designed switched-configuration dipole antennas sensor and the surface curve of mutual coupling magnitude, experiments are set up by connecting these antennas to an HP8530A network analyzer and inserting them into the medium of material under test to measure the magnitude of mutual coupling from parallel and perpendicular configurations as shown in Fig. 4.1(a). The SPDT switches are controlled by an external switching controller with +5 DC biasing voltage as illustrated in Fig. 4.1(b). Material under test is paddy contained in

a 40 cm × 65 cm × 30 cm plastic container that the ideal size should be greater than 10 λ at the operating frequency in order to cancel multiple reflection phenomena. The paddy is prepared by varying the percentage of its moisture content in the range of 11% to 22% moisture content, wet basis. The measurement is done on ten samples repeatedly taken from each location at 27 °C for each configuration and then averaged to acquire accurate results. The averaged mutual coupling magnitude is firstly compensated for losses due to parasitic elements and RF switches in order to transform them to reflect the pure configuration as mentioned in the previous subsection.

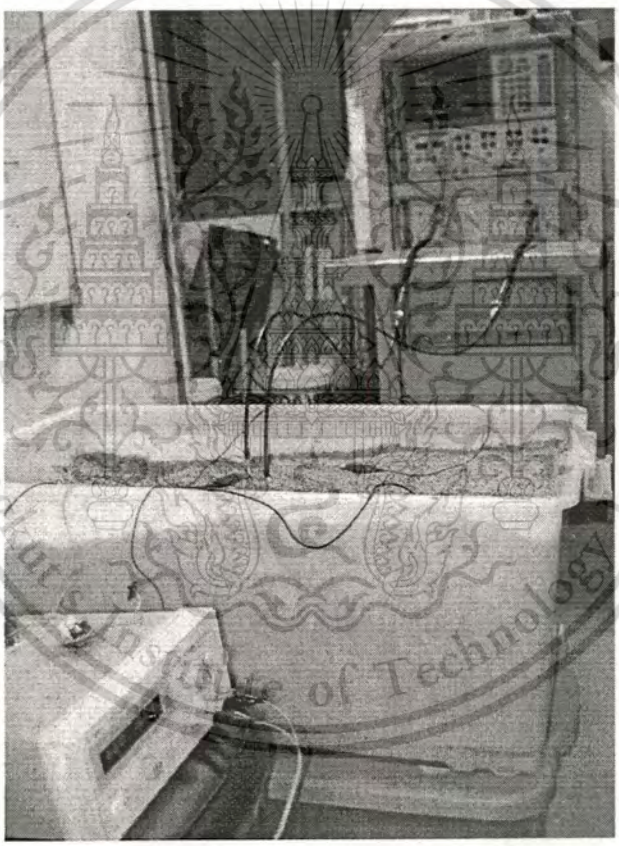

(a)

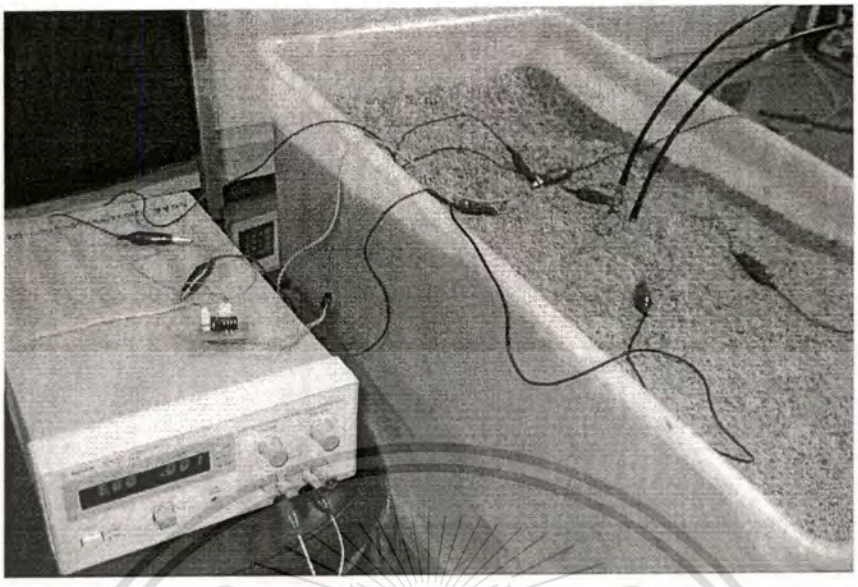

(b)

Figure 4.1 Setup measurements of varied moisture content paddy: (a) whole setup, (b) control of SPDT switches.

It is necessary to compensate since the loss causes the measured mutual coupling of both configurations to be lower than actual values. The lower mutual coupling magnitude provides the higher dielectric constant and the lower dielectric loss factor. Consequently, the measured moisture content is higher than expected. The compensating factors are 1.871 for perpendicular configuration and 0.279 for parallel configuration. Then the compensated magnitudes are calibrated with another factor, a ratio of the measured value of the air obtained from the free-space measurement with the same setup conditions and the derived value. The measured mutual coupling magnitudes of the air for parallel and perpendicular configurations are 0.053 and 0.200, whereas the corresponding derived values are 0.283 and 0.073, respectively. Therefore, the calibration factors for parallel and perpendicular configurations are 5.351 and 0.069, respectively. These factors are multiplied by the compensating mutual coupling magnitudes before being plotted on the surface curves as shown in Fig. 4.2.

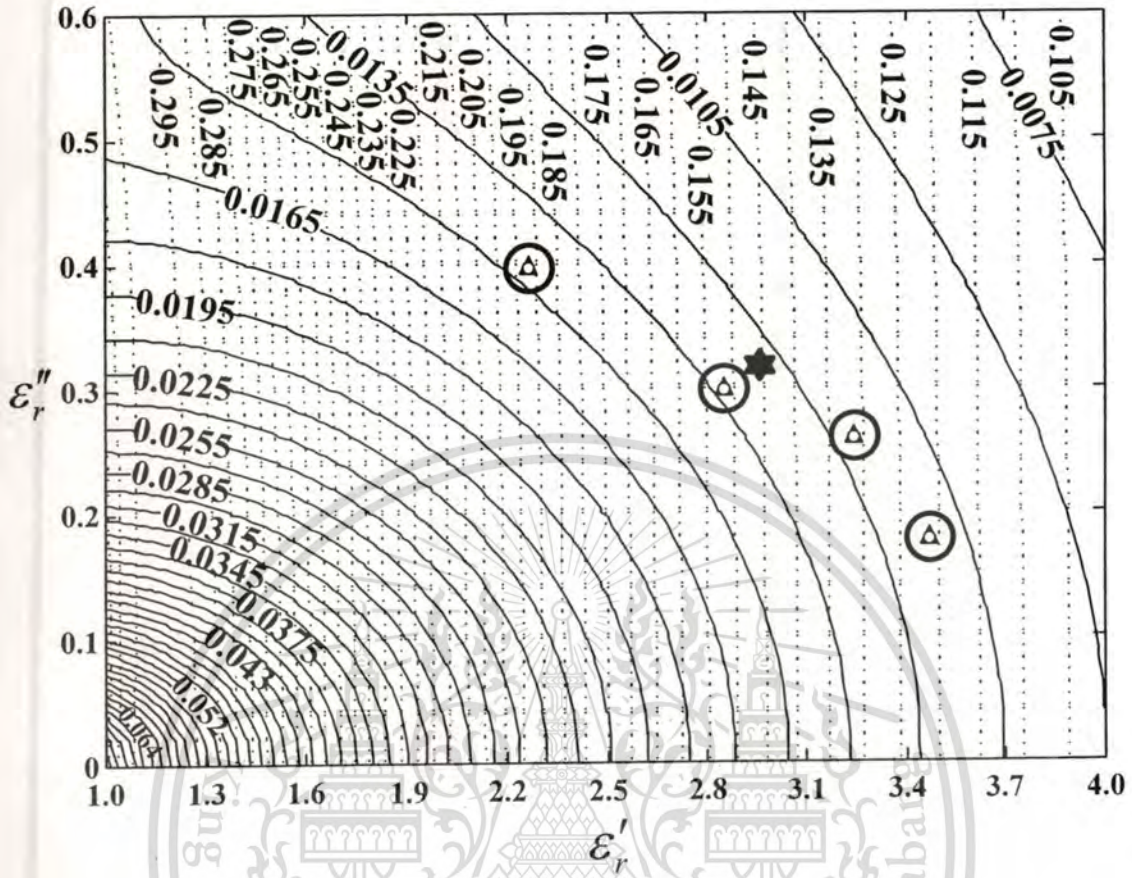

Figure 4.2 Surface curve of mutual coupling magnitudes used in dielectric properties determination of varied moisture content paddy at d = 2 mm (———: perpendicular polarization, ---------: parallel polarization).

Figure 4.2 shows that the dielectric constant and the dielectric loss factor varied in the range of $1<\varepsilon_r'<4$ and $0<\varepsilon_r''<0.6$, respectively. Dashed lines represent mutual coupling magnitudes of parallel configuration, whereas solid lines represent those of perpendicular configuration. The parallel configuration values are plotted in white dots whereas the perpendicular configuration values are plotted in black triangles. Four levels of moisture content are used in the experiments, varying from 11 to 20. The dielectric properties of the paddy at each moisture content level is read directly off the cross point of the mutual coupling magnitude lines of parallel and perpendicular configurations.

Table 4. Dielectric properties of paddy at various moisture contents

Moisture content (%)	Dielectric constant			Dielectric loss factor		
	Presented technique	Reference [32]	Reference [13]	Presented technique	Reference [32]	Reference [13]
11.27	2.278 ± 0.082	2.360	2.320 ± 0.040	0.400 ± 0.140	0.260	0.200 ± 0.060
14.09	2.852 ± 0.182	2.670	2.600 ± 0.070	0.300 ± 0.040	0.340	0.280 ± 0.060
17.85	3.243 ± 0.193	3.050	2.980 ± 0.070	0.265 ± 0.255	0.520	0.340 ± 0.180
20.66	3.478 ± 0.028	3.450	3.110 ± 0.340	0.177 ± 0.363	0.540	0.370 ± 0.170

The achievable values and the standard deviations of the dielectric constant and the dielectric loss factor are shown in Table 4. Generally, moisture content can be presented as an integer, however, we show it in two decimal places as the practical sensor in the market. These values are compared with the values from conventional transmission measurement technique [13] and the method of utilizing coupled-dipole antennas [32]. The correlation of the achievable results with the gold standard measurement results [13] are illustrated in Fig. 4.3.

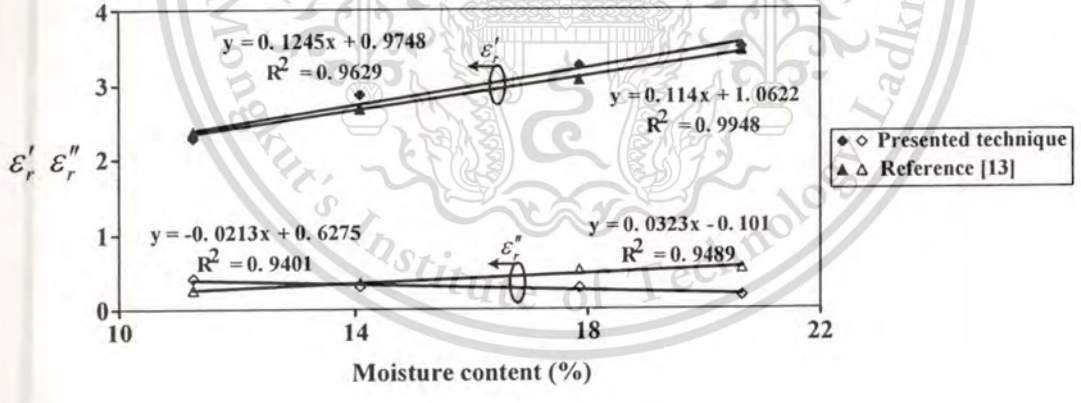

Figure 4.3 Dielectric properties of varied moisture content paddy.

According to Table 4 and Fig. 4.3, they inform us that the dielectric constants obtained by our technique are almost identical to those in [32], [13] at 11% and 14% of moisture content. They were more accurate than those in [32] when compared to [13] at moisture content of 17% and 20%. On the other hand, the dielectric loss factors obtained in [32]

compared to [13] are more exact than those from our technique at all moisture content levels. Compared to the transmission measurement technique that measured both the magnitude and phase shift in [13], the deviation of the dielectric loss values in our technique might be related to the fact that we measured only the magnitude. In addition, our technique is a quasi-free space technique of which deviation is inherent [52], [53].

It should be noted that the surface curve used in determining the dielectric constant and the dielectric loss factor of the mutual coupling magnitude obtained from measurement is derived in the homogeneous medium condition. If the bulk of paddy is large, it may cause the inhomogeneous distribution of moisture content. The inhomogeneous distribution may possibly give the erroneous results. Thus, we measured 10 times repeatedly at different positions within the container. The obtained results are averaged to lessen the deviation.

4.3 Error Compensation

According to the moisture content measurement, there are slight deviations of both the dielectric constants and the dielectric loss factors between the presented technique and results from [32], [13]. It must be compensated since the solution exploited in the dielectric properties characterization is derived for an infinite medium condition whereas the container size used in this experiment is finite. The penetration depths of the paddy with respect to moisture content at 2.45 GHz are in the range of 4.36-6.50 cm. Although this chosen container size is about tenfold that of the penetration depth, large enough to minimize the internal multiple reflections, there remains the scattering effect which cannot be neglected. Consequently, the cause of this error must be analyzed for compensation and correction. In addition to this analysis, the electric field is assumed to be plane wave which is transmitted from the transmitting antenna to 6 plastic container walls and reflected to the receiving antenna as shown with the tracing rays in Fig. 4.4. The directions of scattering from four side walls are illustrated in the top view. The width, length, and height of the considered container are respectively 40, 65, and 30 cm. The scattered rays to the cover and the bottom side are shown in the side view. Both antennas are separated by a distance R.

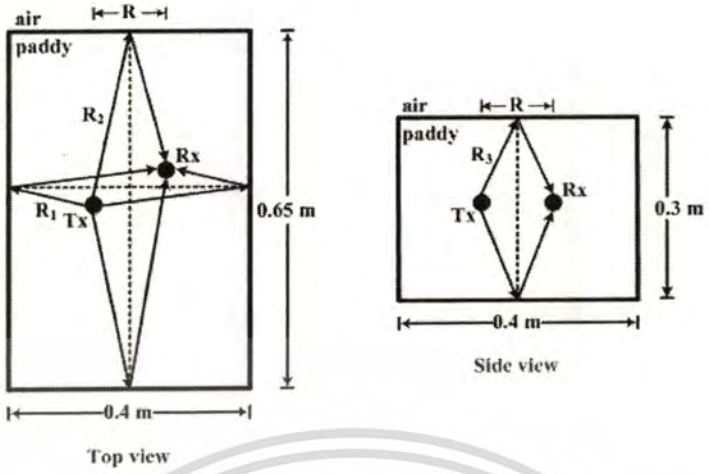

Figure 4.4 Ray tracing of scattered wave in a container.

The incident and reflected waves are E_i and $\Gamma\angle\phi$, respectively. Thus, the scattering fields E_s of all directions can be expressed as

$$E_s = E_i\{2(\exp(-jkR_1)+\exp(-jkR_2)+\exp(-jkR_3))+\Gamma\angle\phi(2\exp(-jkR_2) +2\exp(-jkR_3)+\exp(-jk(R_1+R))+\exp(-jk(R_1-R)))\} \quad (4.1)$$

where Γ and ϕ are the reflection coefficient and phase, respectively. The reflection coefficient for each moisture content of paddy is obtained from

$$\Gamma = \frac{\eta_2 - \eta_1}{\eta_2 + \eta_1} \quad (4.2)$$

where η_1 and η_2 denote the intrinsic impedance of paddy and air, respectively.

The scattered waves are calculated in accordance with the size of the container used in the experiment. The magnitude of mutual coupling is investigated. In addition, an analysis is done to examine the optimal size of the container that provides minimum scattering effect. The size of the container is analyzed by increasing and decreasing all dimensions in two steps. Each step is equal to 10 cm. The sizes of container are set to $60\times85\times50$ cm^3 (+20 cm), $50\times75\times40$ cm^3 (+10 cm), $30\times55\times20$ cm^3 (-10 cm), and

$20 \times 45 \times 10$ cm^3 (-20 cm). The investigated mutual coupling magnitudes of both configurations due to the scattering effect are shown in Fig. 4.5.

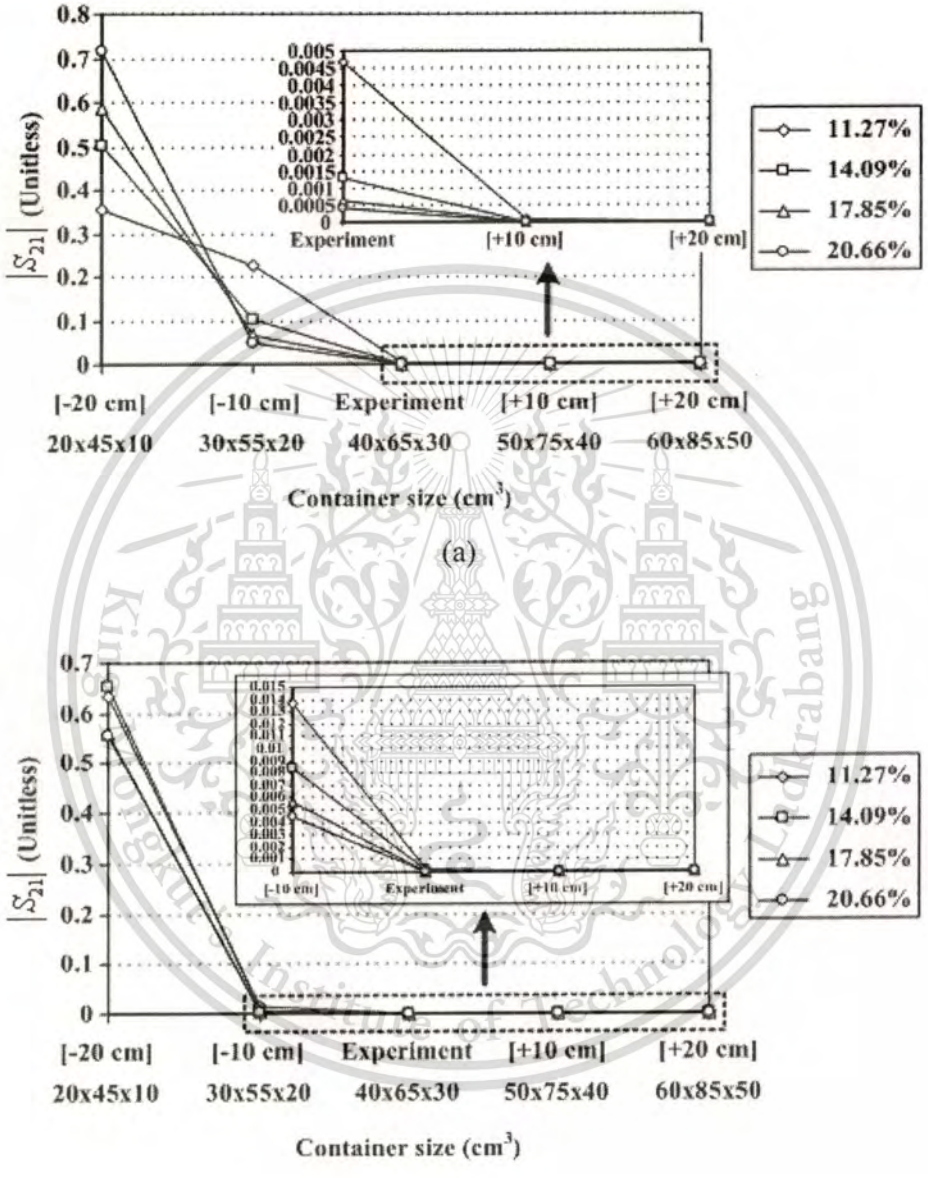

Figure 4.5 Effect of scattered wave on mutual coupling magnitude, (a) perpendicular configuration, (b) parallel configuration.

The results for perpendicular configuration are in the range of 0.0004-0.005, whereas those for parallel configuration are in the range of 0.00004-0.0003. For the container size examination, it can be observed that the mutual coupling magnitudes of both configurations decrease as the container size get larger at all moisture contents. Hence, the acquired mutual coupling magnitudes of both configurations are compensated for the scattering effect. The compensated mutual coupling magnitudes are plotted on the surface curve solution illustrated in Fig. 4.6.

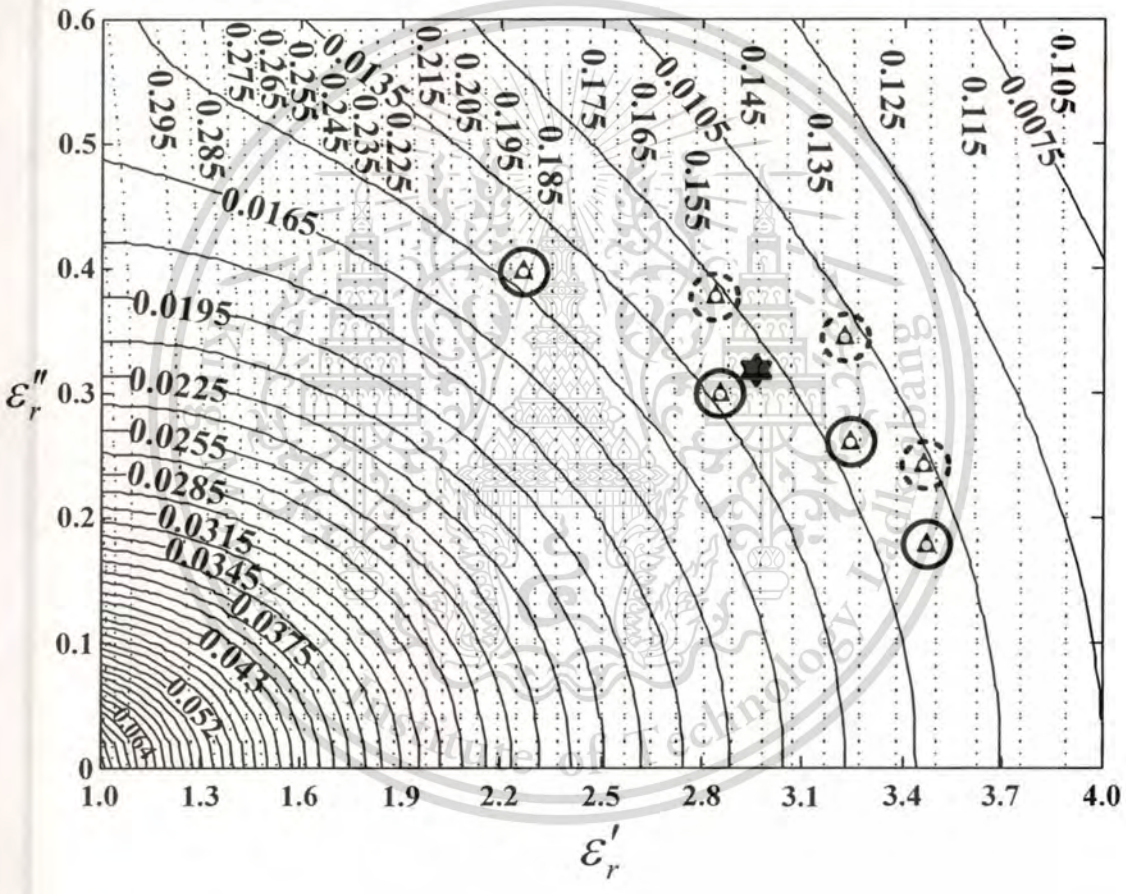

Figure 4.6 Surface curve of mutual coupling magnitudes used in dielectric properties determination at $d = 2$ mm (○ : experimental results, ◌ : compensated results, ——— : perpendicular polarization, --------- : parallel polarization).

Table 5. Comparison of the dielectric properties between compensated results, experimental results, and [13]

Moisture content (%)	Dielectric constant			Dielectric loss factor		
	Error compensated	Experiment	Reference [13]	Error compensated	Experiment	Reference [13]
11.27	-	2.278 ± 0.082	2.360	-	0.400 ± 0.140	0.260
14.09	2.845 ± 0.175	2.852 ± 0.182	2.670	0.380 ± 0.040	0.300 ± 0.040	0.340
17.85	3.235 ± 0.185	3.243 ± 0.193	3.050	0.345 ± 0.175	0.265 ± 0.255	0.520
20.66	3.475 ± 0.025	3.478 ± 0.028	3.450	0.245 ± 0.295	0.177 ± 0.363	0.540

The dielectric constant and the dielectric loss factor for each moisture content level, directly read off the surface curve solution, and the standard deviations are listed in Table 5. It is noticed that the compensated dielectric constants at moisture contents of 14.09%, 17.85% and 20.66% are slightly different compared to the experimental results, but the compensated dielectric loss factors is increased compared to those in [13]. In the case of 11.27% moisture content paddy, the dielectric properties cannot be provided by the surface curve solution since there is no cross point between the compensated mutual coupling magnitudes of both configurations. Nevertheless, the error compensation procedure which compensates for the scattering fields from the container walls has yielded more accurate dielectric property readings.

4.4 *In-situ* Moisture Content Monitoring

To validate the feasibility of applying this sensor in a closed-loop drying system, a simple model system is set up as shown in Fig. 4.7. In this system, there are four bins of paddy: heater bin, monitoring bin, storage bin, and initial bin. The procedure starts by filling the paddy into the initial bin and measuring its moisture content. When the moisture content is higher than 14%, the paddy will be conveyed to the heater bin and heated with a 1000-W heat blower. The heated paddy will be released into the monitoring bin and its moisture content measured every hour. If the moisture content is lower than 14%, the paddy will be released into the storage bin to preserve. On the other hand, the paddy will be released into the initial bin and conveyed to the heater bin when the

moisture content is higher than 14%. The drying system will be operating continuously, and the sensors in each bin will be monitoring all the time.

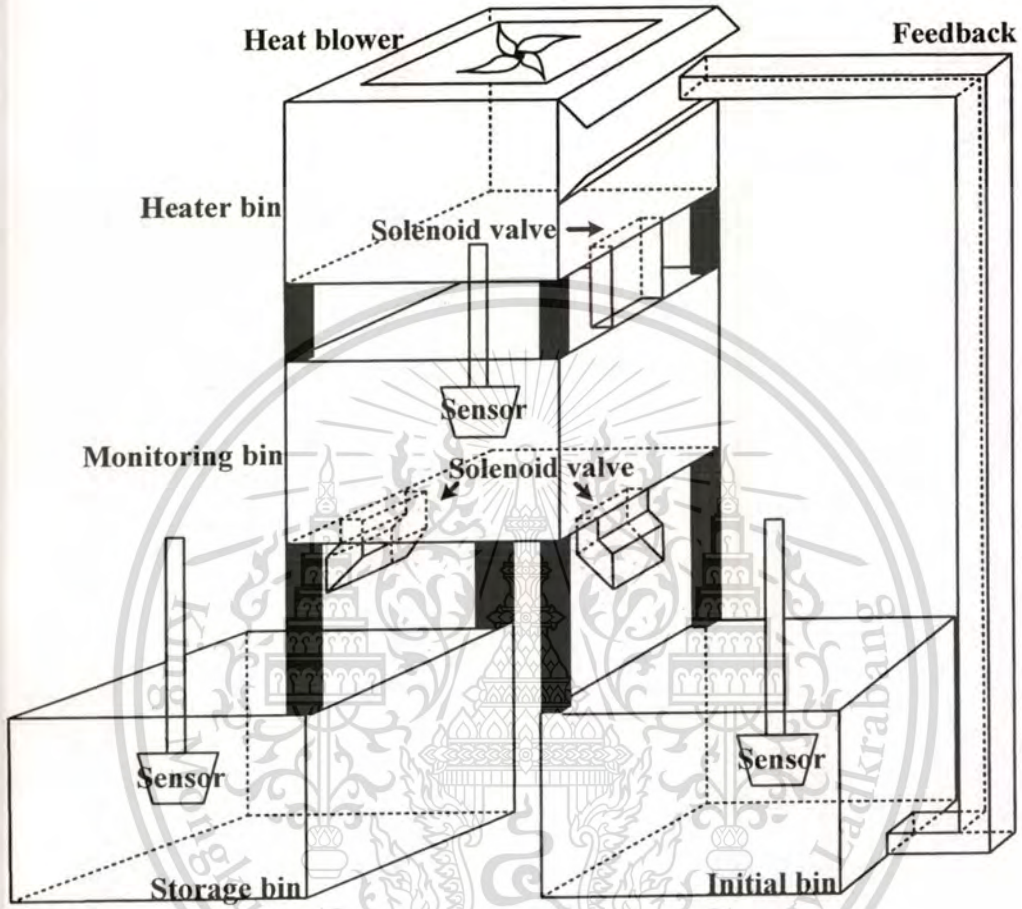

Figure 4.7 *In-situ* moisture content monitoring setup for a closed-loop drying system.

A practical sensor is illustrated in Fig. 4.8. The transmitting antenna connects with a frequency synthesizer. The receiving antenna, whose cross elements are attached to two SPDT switches, connects with a power detector. There is a controller which controls the performance of the synthesizer, the detector, and the RF switches, and a liquid crystal display screen displays the measured voltage of the mutual coupling magnitude. Moreover, there is an additional function of wireless monitoring that is built into the controller and display component. It is very useful for monitoring moisture in a mill. The moisture content of the paddy is monitored all the time and the measured results wirelessly sent outside for easy access by workers or the owner.

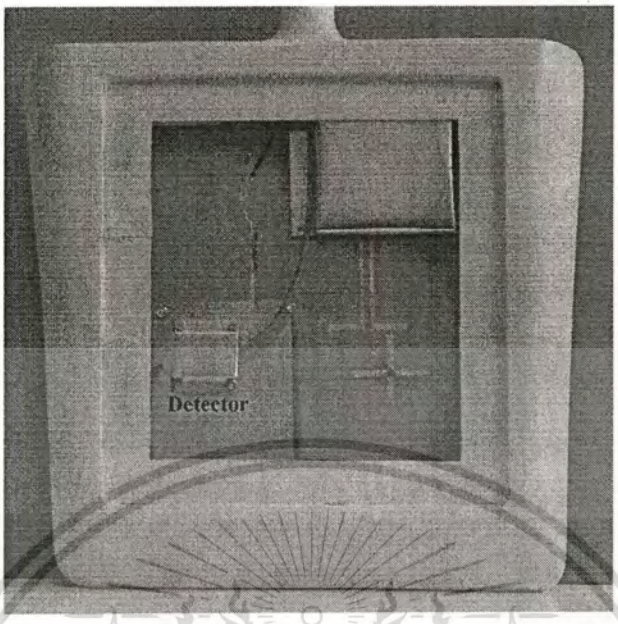

(a)

(b)

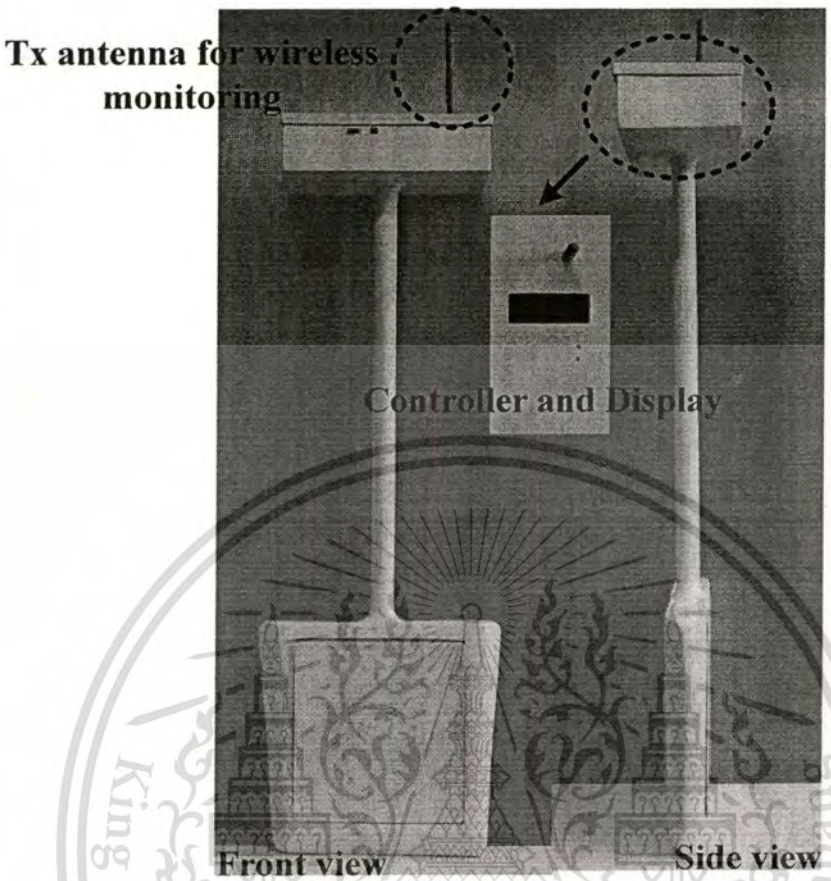

(c)

Figure 4.8 Sensor covered with radome for practical use, (a) front side, (b) bottom side, (c) overall structure.

The correlation between voltage and moisture content is investigated. The moisture content is obtained from a standard method of ASAE [12] that equipments used in the experiments are illustrated in Fig. 4.9. The procedure of this method is listed as follow:

1). Fill 10 g of paddy in heat resistant glass with cover plate. In this experiments, thirty samples are required.
2). Weigh these samples by an electronic balance with the accuracy of 0.0001 g before heating.
3). Heat them in an oven at 130°C for 19 h.

4). Cool them in a desiccator and weigh.

5). Repeatedly heat them for 6 h and weigh.

6). Stop this process when the weight change is less than 0.005 g.

Thus, the moisture content can be calculated from the ratio of the lost weight to the weight before heating.

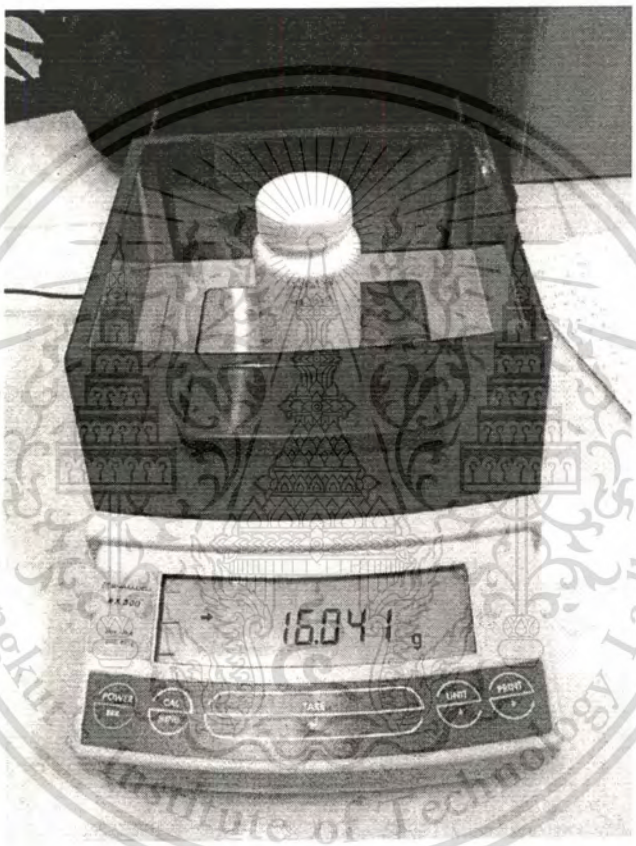

(a)

(b)

(c)

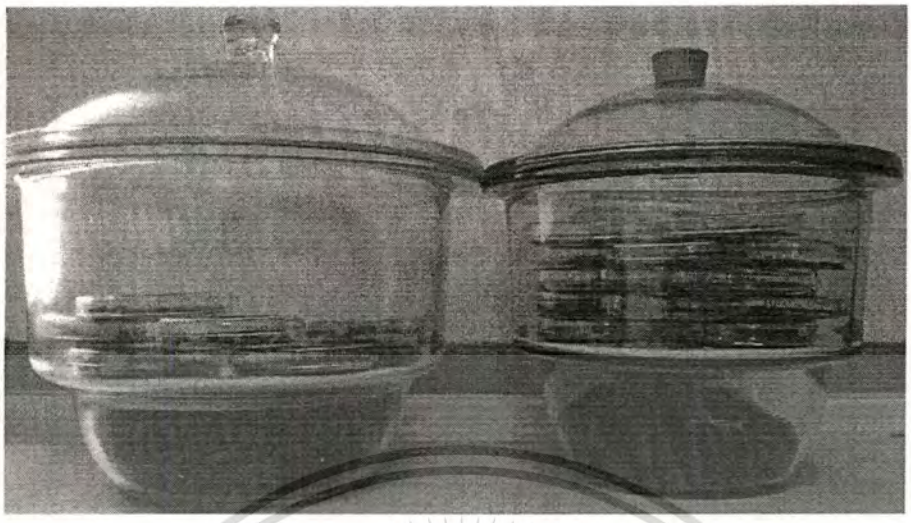

(d)

Figure 4.9 Equipments used in moisture content determination by standard method of ASAE, (a) electronic balance, (b) oven, (c) thermocouple, (d) desiccators.

The voltage correlated with the moisture content of both configurations is illustrated in Fig. 4.10. The voltages of both configurations decrease when the moisture content becomes higher. The voltages of both configurations, in Fig. 4.10, are linearly curve fitted to show the resolution of measurement. The standard deviations of the voltages are shown in Table 5.

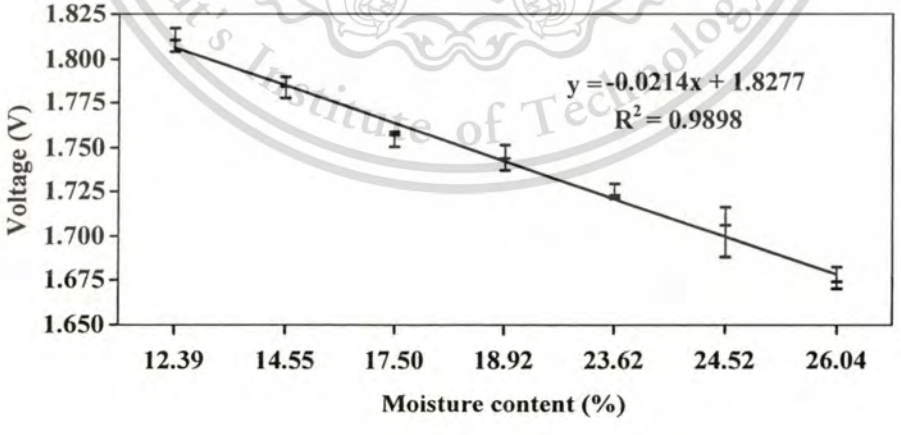

(a)

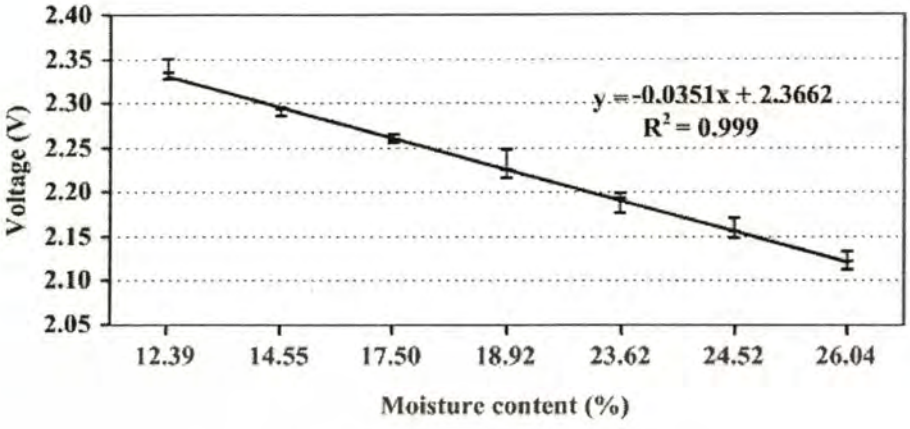

(b)

Figure 4.10 Voltage versus varied moisture content paddy, (a) perpendicular configuration, (b) parallel configuration.

Table 6. Variation of moisture content from the measured voltage

Moisture content (%)	Measured voltage (V)		Variation of moisture content (%)	
	Perpendicular case	Parallel case	Minimum	Maximum
12.39	1.810 ± 0.005	2.335 ± 0.008	12.05	12.50
14.55	1.783 ± 0.004	2.293 ± 0.004	14.53	14.76
17.50	1.756 ± 0.003	2.259 ± 0.003	17.47	17.64
18.92	1.743 ± 0.005	2.226 ± 0.008	18.70	19.16
23.62	1.722 ± 0.003	2.193 ± 0.009	23.31	23.83
24.52	1.706 ± 0.011	2.156 ± 0.008	23.70	25.19
26.04	1.674 ± 0.004	2.121 ± 0.006	25.85	26.20

The variation of moisture content can be provided by the deviated voltage that correlated with equation in Fig. 4.10. In Table 6, since the standard deviations of the measured voltages in both configurations are not equal, the highest deviation of moisture content is chosen to correlate with the equation. For instance, at the moisture content of 12.39%, the standard deviation of measured voltage in parallel configuration is higher than the one in perpendicular configuration. Hence, we used the value from parallel configuration to correlate with the equation in Fig. 4.10(b). On the other hand, the equation in Fig. 4.10(a) is chosen due to the higher standard deviation of measured voltage in perpendicular configuration. The moisture content in this case varied from 12.05% to 12.50%. From

Table 5, it is obvious that the low standard deviations exhibit the relatively high accuracy of the sensor. Note that, in this experiment, the measured voltages are not compensated, so they are lower than the actual values. The compensated voltage provides the lower moisture content.

The voltage is clearly identified for each moisture content level so that it can be used as a criterion for characterizing the moisture content in a closed-loop drying system. The results of moisture content monitoring in a closed-loop system are shown in Fig. 4.11. The x-axis is the time used in drying system, whereas the y-axis is the voltage of measured mutual coupling. It reveals that the moisture content of the paddy starts out more than 26.04%. It takes about 13 h to reduce moisture content to 12.39%. As having been demonstrated in this experiment, it is expected that this presented sensor will perform effectively in *in-situ* monitoring applications with the benefits of low cost, low profile, low time consumption and real time monitoring.

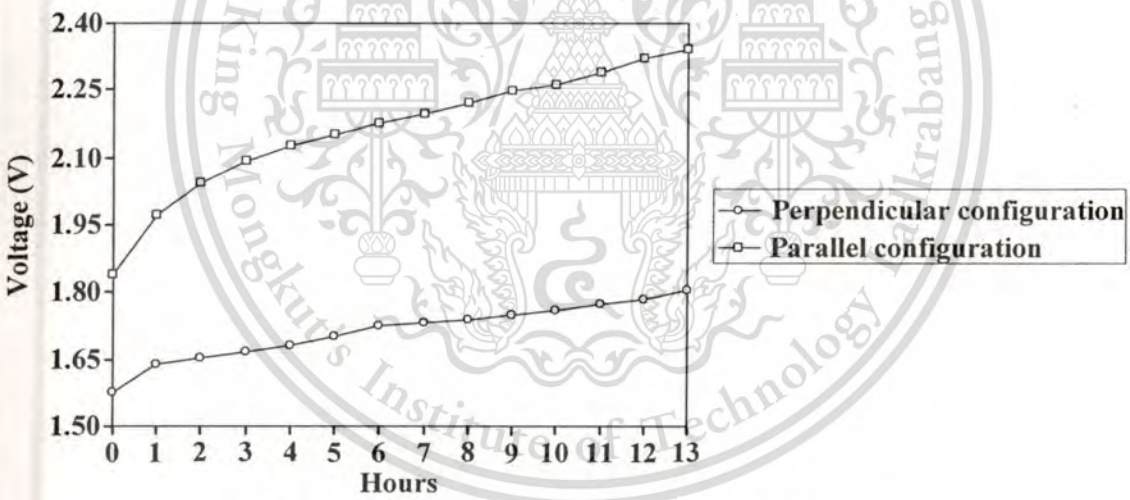

Figure 4.11 Voltage versus moisture content over time.

The effect of temperature changes on the performance of the sensor can be considered. An increasing of temperature will increase the dielectric constant [13] and affect the dielectric loss factor of the antenna substrate [54]. It shifts the resonant frequency to higher frequency. The RF switches have insignificant insertion loss when the temperature increases from +25°C to +85°C [51]. The detector is able to work in the

temperature range of -40°C to +85°C [55]. For the frequency synthesizer, the increase of temperature may cause the voltage-controlled oscillator to produce a lower oscillation frequency at the same tuning voltage [56]. It degrades the output power, but it can still perform in the temperature range of -40°C to +85°C. Consequently, the effect of temperature changes degrades the performance of the sensor that reduces the mutual coupling magnitude in the measurement, whereas it increases the dielectric constant and the dielectric loss factor of paddy. The higher dielectric properties cause the measured moisture content to be higher than the actual values. Thus, the system spends longer time and consumes more energy which results in higher drying cost. The detail of the effect of temperature changes remains for further study.

4.5 Summary

The validation of applying a switch-configuration dipole antenna as the sensor for moisture content of paddy is presented. In the experiments, the measured dielectric properties of paddy with various moisture contents indicate that, the dielectric constant are comparable to those in the published literature, but there are deviations in the values of the dielectric loss factors. Thus, the error is analyzed and compensation is made to correct the results. The analysis also shows that the size of the container which is 40 × 65 × 30 cm^3 is sufficient in practical exploitation with the presented solution. Furthermore, an experiment to correlate voltage with moisture content from a standard method of ASAE is done in order to use as a criterion for characterizing the moisture content in a closed-loop drying system. For a closed-loop drying system, a model system is set up to validate the feasibility of this sensor application. The results indicate that this sensor performs well, with the benefits of low cost, low time consumption, *in-situ* monitoring, and real-time monitoring.

CHAPTER 5

A PATTERN RECONFIGURABLE ANTENNA ON SUBSTRATE INTEGRATED WAVEGUIDE BY APPLYING A SWITCHABLE ANTENNA

5.1 Introduction

According to aforementioned in the previous chapter, the use of a switch-polarization dipole antenna as a moisture content sensor of paddy, with the same concept of switch polarization, it is also able to further develop the cross-element structure at higher frequencies, 24 GHz for other applications, i.e., an industrial sensor such as Doppler sensor for automotive and security systems and a switch-beam antenna for wireless communications. In this chapter, the cross-element structure employs a slot antenna since its structure is the complement to a dipole antenna. Its attractive characteristics are low profile, conformable with planar structure, and easy integration with planar circuits. The cross-element slot antenna is designed by means of the combination of a pattern reconfigurable and a substrate integrated waveguide (SIW) techniques in order to develop an antenna whose size is compact and its performance is able to switch or reconfigure its radiation patterns.

5.2 Substrate Integrated Waveguide (SIW)

Slot antenna is one of the most interesting antennas whose attractive characteristics found in a number of application systems that require low profile, conformable with planar structure, and easy integration with planar circuits. However, its major drawback concerns the bidirectional radiation pattern since slot is always etched at metal plate that is able to freely radiate both sides. To eliminate the backside radiation, a metal reflector or a shallow cavity is applied. A simple short-end waveguide is usually served as backed cavity in slot antenna, which the optimal distance from slot to the reflector or the cavity bottom is roughly equal to one-quarter wavelength [57]. A slot

antenna or longitudinal slot array antennas on a broad wall of a rectangular waveguide is a classic antenna which is generally used in radar or satellite tracking applications [58], and is sometimes for microwave applications [59]. Rectangular waveguide plays an important role in realizing high performance RF passive components because of its high Q-factor and high power capacity. However, the disadvantages of conventional waveguide are large sizes and usually require a precisely complex transition in integration with planar structures that cause a difficult to achieve at millimeter-wave frequencies. Recently, a promising candidate called substrate integrated waveguide (SIW) is introduced and investigated. The structure of SIW exhibits the same propagation characteristics as conventional metallic rectangular waveguides, including the pattern of field distribution and the dispersion characteristics. Moreover, it still preserves the advantages of conventional metallic rectangular waveguides, i.e., high Q-factor and high power handling capability. The main significant advantages of SIW technique are the capability of integration with all components on the same substrate such as passive microwave circuits [60]-[65], active components [66]-[68], and antennas [69]-[72], since this technology can prevent losses due to transmission and radiation of planar transmission lines, i.e., microstrip and coplanar waveguides.

SIW technique was firstly proposed in the name of post wall waveguide [69], or called laminate waveguide [73], then it has been extensively developed [74], [75]. The concept of SIW is to make an equivalent waveguide by adopting a periodic via-hole structure to realize bilateral edge walls in a substrate of PCB as illustrated in Fig. 5.1.

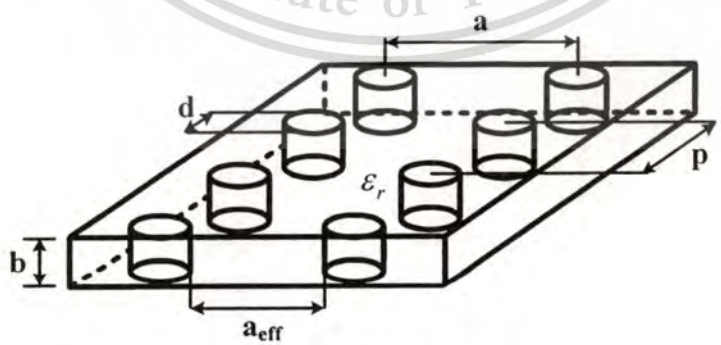

Figure 5.1 SIW structure.

In Fig. 5.1, a represents the distance between parallel arrays of via holes, b is the height of a substrate, d is the diameter of each via, and p is the distance between sequential via holes. To realize propagation performance of SIW as a conventional rectangular waveguide, each metallic via is essentially needed to arrange as close as possible to prevent radiation leakage. Practical modes in SIW only specifically coincide with a set of $TE_{n,0}$ modes of conventional rectangular waveguides whose dispersion characteristic was studied using the boundary integral-resonant mode expansion (BI-RME) method combined with the Froquet's theorem to estimate the first two dominant modes [76]. While $TM_{n,0}$ modes are not supported due to strong radiation of the presence of gaps between metal vias that affects the transverse magnetic fields which determine the longitudinal surface currents [77]. In particular, the cut-off frequency of the fundamental mode of $TE_{1,0}$ is given by

$$f_c(TE_{10}) = \frac{c_0}{2\sqrt{\varepsilon_r}} \times \left(a - \frac{d^2}{0.95 \times p} \right)^{-1}. \tag{5.1}$$

Empirical relation between the dimensions of SIW and the effective width a_{eff} of conventional rectangular waveguide that provides the same propagation characteristics is shown in

$$a_{eff} = a - 1.08\frac{d^2}{p} + 0.1\frac{d^2}{a}. \tag{5.2}$$

The best conditions which attenuation constant and radiation leakage between successive vias are little enough to be neglected are $d/p \geq 0.5$ and $d/\lambda_0 \leq 0.1$, where λ_0 denotes free space wavelength.

According to equation 5.1 and equation 5.2, a SIW structure is designed to operate at the frequency of 24 GHz on the Rogers (RT 5880) Duroid substrate whose dielectric constant and loss tangent are respectively 2.2 and 0.0009. The substrate thickness h is equal to 1.6 mm. The cut-off frequency of the fundamental mode $TE_{1,0}$ is assumed at the frequency of 21 GHz whereas the diameter of each via d and the distance

between sequential via holes p are assumed to equal 1 and 2 mm, respectively. Thus, the width a and the effective width a_{eff} of equivalent rectangular waveguide are respectively 5.3 and 4.78 mm. The obtained dimensions of via and spacing between each successive vias are employed to model and simulate in the commercial electromagnetic simulation program [44] as shown in Fig. 5.2.

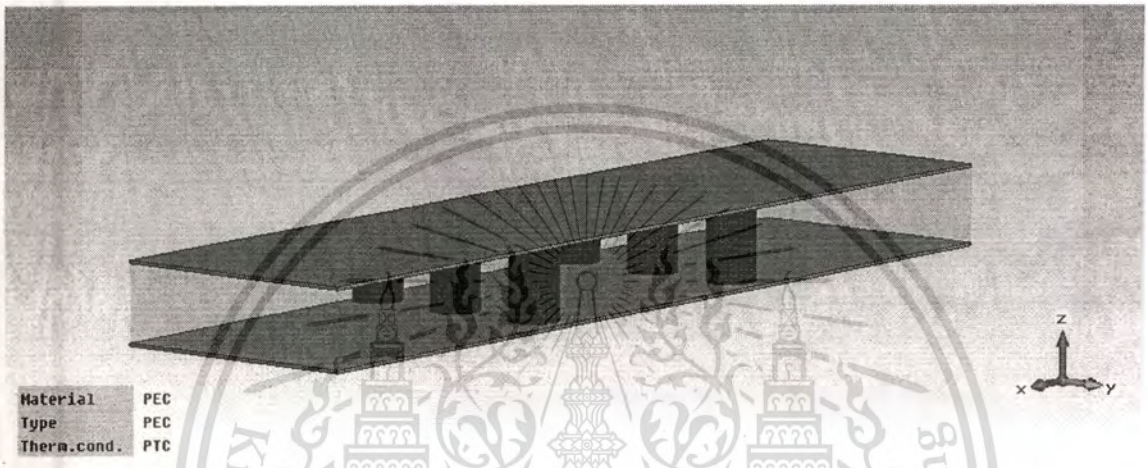

Figure 5.2 Simulation of SIW structure.

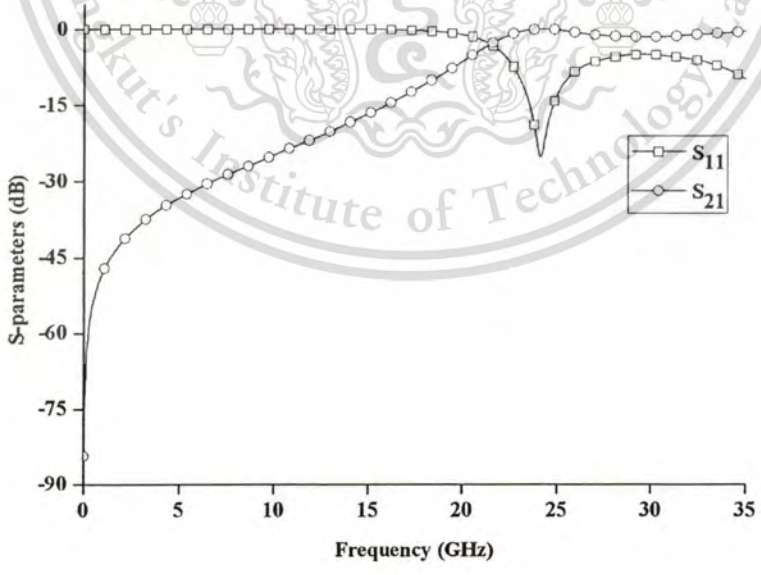

Figure 5.3 Simulated s-parameters of SIW structure.

In Figure 5.3, the simulated S_{21} are illustrated to indicate that the cut-off frequency is about 21 GHz whereas S_{11} are lower than -10 dB for the frequencies higher than 21 GHz, especially lowest at the frequency of 24 GHz. In addition, the current distribution is plotted in Fig. 5.4 to show the density level inside the SIW structure of which the maximum density is at the center and there is slightly leakage between each successive via, since the distance between each via is not close enough to prevent the leakage that is caused by the constraint of in-house PCB fabrication. However, it is obviously noticed that the leakage level is quite low enough to be neglected. Thus, the dimensions of SIW structure are obtained to employ in the pattern reconfigurable design in the next subsection.

Figure 5.4 Current distribution inside SIW structure.

5.3 Pattern Reconfigurable Antenna

A reconfigurable antenna, whose role benefits to future wireless applications, is considered as one of the most significant antennas, since the capability of independently altering its operating functions such as frequencies, impedance bandwidth, polarizations, and radiation patterns for specific requirements without changing the overall dimensions. The concept of reconfigurable antenna was originally published in [78], and was exceedingly progressed in [79]. Normally, it is categorized into three groups: resonant frequency [80]-[87], polarization [88]-[96], and radiation pattern [97]-[104], but the third of which has much been paid attention because of its capability of noise avoidance by

steering beam toward the direction of desired signal, while the resonant frequency remains unchanged [105], [106]. To transform a fixed operating antenna to a reconfigurable antenna requires a suitable design of conversion methodology, which the existence methods majorly concern with two constituents: total radiating structure and matching network that the first of which is considered in this dissertation. The tuning techniques to switch radiation patterns are also necessary that can be classified into the following three groups: mechanical actuation, tunable materials, and integrated electronic devices. The technique of using integrated electronic devices employs active devices such as PIN diodes [107]-[110], MEM switches [111], [112], or transistors [113] to integrate with antennas and make either a conduction path or a break in the conduction path of RF current. In order to select the type of switch, it fundamentally depends on switching speed, power handling capability, impedance characteristics, bias network, activation condition, package, and cost. The pin diode is an attractive choice to apply in the system that requires electronically tunable device, low profile, light weight, and highly agile mobility due to its fast switching time and relatively high current handling capability.

5.3.1 Design of Antenna Structure

The structure of designed antenna composes of a radiation component and a feed excitation component: the configuration of the radiating section is like a cross-element slot antenna with rounded parasitic slot elements constructed on the ground plane, whereas the feed excitation section is on the opposite side as illustrated in Fig. 5.5. For the feeding part, a 50-ohm grounded coplanar waveguide followed a 50-ohm microstrip is adopted as the feeding element to excite the cross-element slot antenna. The advantage of feeding by means of coupling technique, which the radiating element and the feeding element are not on the same side, is effectively capable of isolating the radiation generated by the feed network.

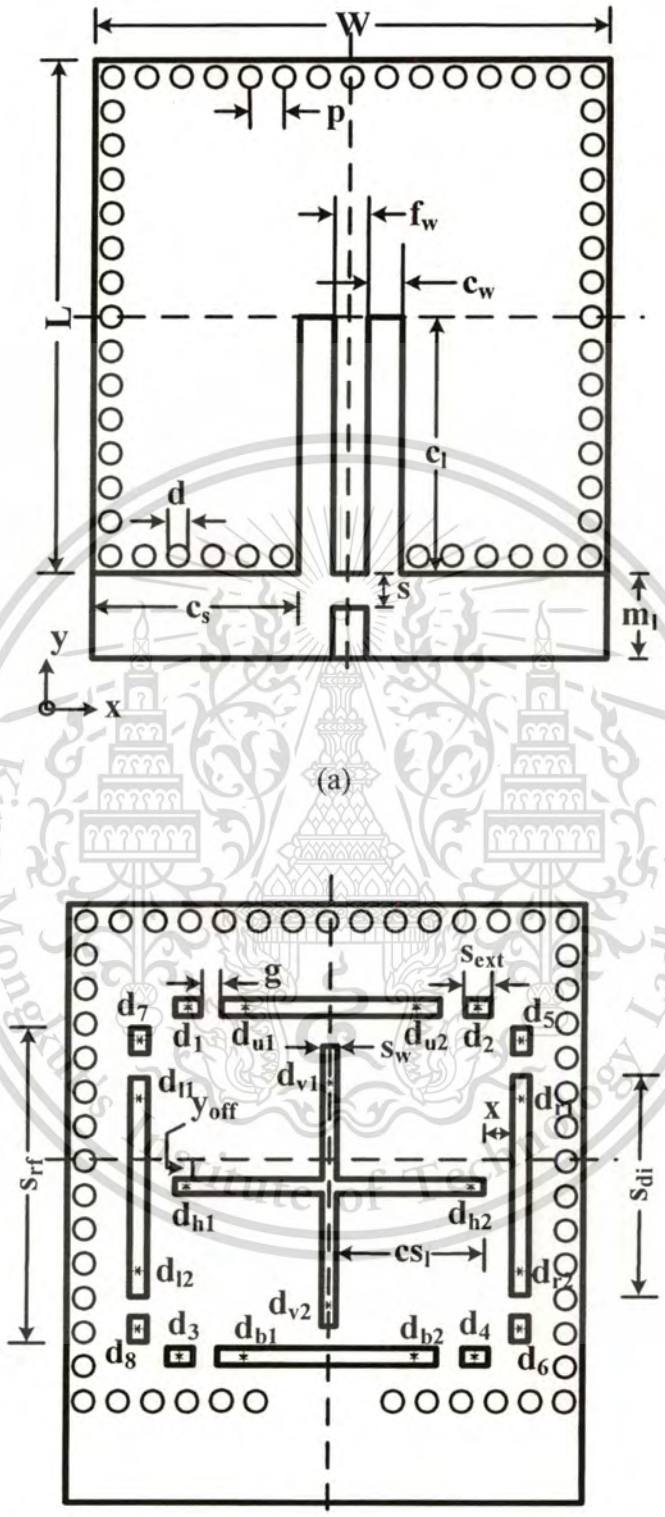

Figure 5.5 Antenna configuration (a) feed excitation section, (b) radiating section.

This antenna is designed based on the structure of a Yagi-Uda antenna which was proposed in literature [114], but its radiation pattern was able to point only one direction. An interesting work was recently proposed [115] however its radiation patterns were only switched between two directions. Thus, this work is designed to enhance the performance of switching radiation patterns between four directions rounded its structure. According to aforementioned, this structure acts like a Yagi-Uda antenna that the cross-element slot performs as the driven element while the parasitic slots functions between the director or the reflector element by setting the state "ON" or "OFF" of PIN diodes. In order to switch polarizations between x or y, it depends on the state selection of each pair of four PIN diodes etched on the cross-element which two of them are on vertical slot and the others are on horizontal slot. While setting the state of PIN diodes etched on parasitic slots is steering the beam direction between $+x$ or $-x$, and $+y$ or $-y$. For example, when selecting the state of PIN diodes d_{h1} and d_{h2} to be "ON", and both PIN diodes on the left parasitic slots d_7 and d_8 are switched the state "ON" while both PIN diodes on the right parasitic slots d_5 and d_6 are "OFF", the left and right parasitic slots respectively behave as the director and the reflector, then the radiation pattern directs to $+x$ as illustrated in Fig. 5.6.

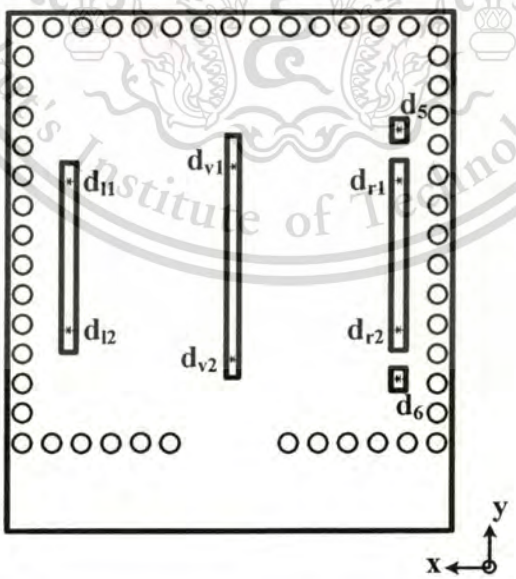

Figure 5.6 Antenna configuration in reconfiguring radiation pattern to $+x$ direction.

On the contrary, when the state of PIN diodes d_{h1} and d_{h2} remain "ON", and both PIN diodes on the left parasitic slots d_7 and d_8 are switched the state "OFF" while both PIN diodes on the right parasitic slots d_5 and d_6 are "ON", the left and right parasitic slots respectively behave as the reflector and the director, then the radiation pattern directs to $-x$ as illustrated in Fig. 5.7.

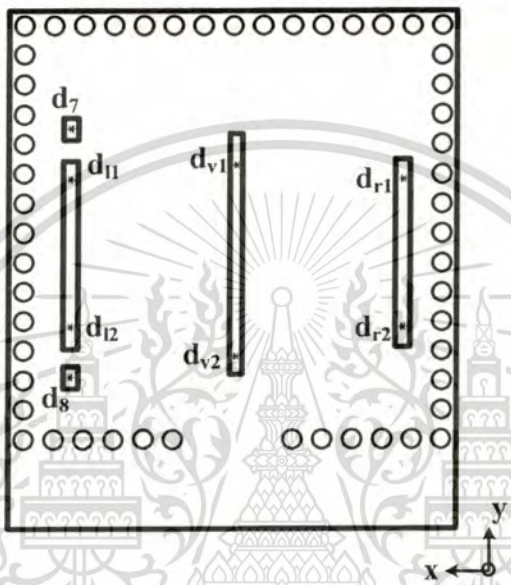

Figure 5.7 Antenna configuration in reconfiguring radiation pattern to $-x$ direction.

In addition to steer the radiation patterns to y directions: $+y$ and $-y$, the two switches etched on vertical slot of the cross-element slot d_{v1} and d_{v2} are set the state "ON". While two pairs of PIN diodes etched on parasitic slots that one of them d_1 and d_2 and the others d_3 and d_4 are respectively on the upper and the lower slots, are employed to select the beam directions between $+y$ and $-y$. For example, when the state of PIN diodes d_1 and d_2 are switched the state "ON", and both PIN diodes d_3 and d_4 are "OFF", the upper and lower parasitic slots respectively behave as the director and the reflector, then the radiation pattern directs to $+y$ as illustrated in Fig. 5.8. On the other hand, the radiation pattern will directs to $-y$, when the state of PIN diodes d_1 and d_2 are switched the state "OFF", and both PIN diodes d_3 and d_4 are "ON" that makes the upper and lower

parasitic slots respectively behave as the reflector and the director as illustrated in Fig. 5.9.

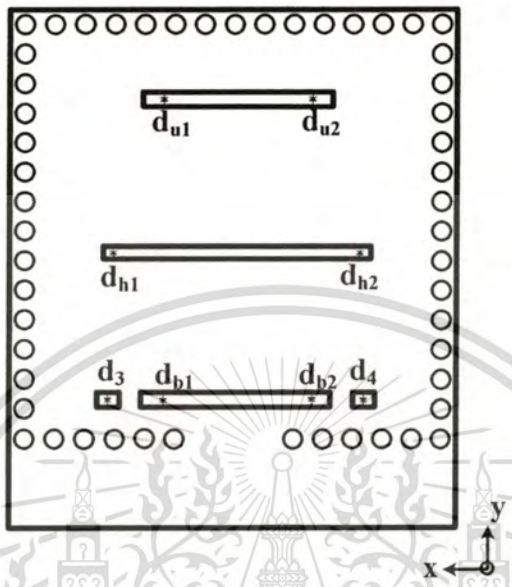

Figure 5.8 Antenna configuration in reconfiguring radiation pattern to $+y$ direction.

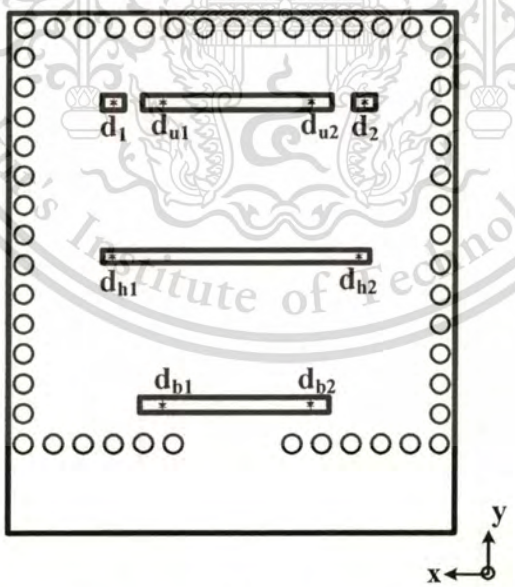

Figure 5.9 Antenna configuration in reconfiguring radiation pattern to $-y$ direction.

Details of the states of all PIN diodes in steering the radiation patterns to each direction and all dimensions of the designed antenna are respectively listed in Table 7 and Table 8.

Table 7. States of all PIN diodes in steering the radiation patterns

PIN diodes	Beam direction			
	$+x$	$-x$	$+y$	$-y$
d_{v1}	OFF	OFF	ON	ON
d_{v2}	OFF	OFF	ON	ON
d_{h1}	ON	ON	OFF	OFF
d_{h2}	ON	ON	OFF	OFF
d_{u1}	ON	ON	OFF	OFF
d_{u2}	ON	ON	OFF	OFF
d_{b1}	ON	ON	OFF	OFF
d_{b2}	ON	ON	OFF	OFF
d_{l1}	OFF	OFF	ON	ON
d_{l2}	OFF	OFF	ON	ON
d_{r1}	OFF	OFF	ON	ON
d_{r2}	OFF	OFF	ON	ON
d_1	ON	ON	ON	OFF
d_2	ON	ON	ON	OFF
d_3	ON	ON	OFF	ON
d_4	ON	ON	OFF	ON
d_5	OFF	ON	ON	ON
d_6	OFF	ON	ON	ON
d_7	ON	OFF	ON	ON
d_8	ON	OFF	ON	ON

Table 8. Dimensions of a switch-polarization slot antenna

Parameters	Dimension (mm)
W	26.88
L	26.88
d	1.00
p	2.00
f_w	0.55
c_w	0.65
c_s	12.52
c_l	13.97
m_l	3.73
s	1.00
g	0.20
x	1.05
s_w	0.40
c_{sl}	2.85
y_{off}	0.30
s_{di}	5.11
s_{rf}	6.51
s_{ext}	0.50

5.3.2 Biasing Circuit of PIN Diodes

PIN diode whose performances of low profile, light weight, and highly agile mobility is selected to use for achieving the reconfigurable radiation patterns. To switch opening or closing the connection, a series circuit is chosen due to the simple configuration. The equivalent circuits of PIN diode in cases of forward bias "ON" and reverse bias "OFF" are illustrated in Fig. 5.10. While the biasing circuit that consists of PIN diode, dc block capacitor, and RF choke inductor is shown in Fig. 5.11.

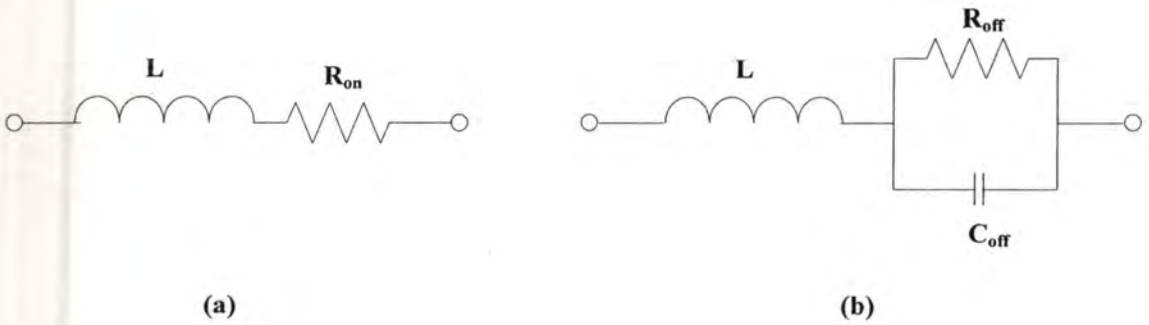

Figure 5.10 Equivalent circuits of PIN diode (a) ON state, (b) OFF state.

The values of the equivalent RLC elements model inside PIN diode package are provided from [116], and detailed that a resistor in case of the diode "ON" state, R_{on}, equals 5 Ω. It, R_{off} is 10 kΩ in case of the diode "OFF" state. The inductor for both states of diodes, L, is equal to 0.5 nH. The capacitor at the diode "OFF" state, C_{off}, equals 0.02 pF.

According to the biasing circuit of PIN diode, two DC block capacitors which perform as the isolator between RF components and DC ones are equal to 220 pF. Since the calculated value from $X_C = -j(1/\omega c)$ equals $-j\,0.03$ Ω that stands for a condition of near short circuit which the RF signal is able to pass through with little reflection. The RF choke inductors, which isolate the RF signal that flows into the DC source, employs a quarter-wavelength microstrip line with very narrow width. In order to set the state "ON" of PIN diode, the forward bias voltage and current are respectively equal to 1.36 V and 10 mA.

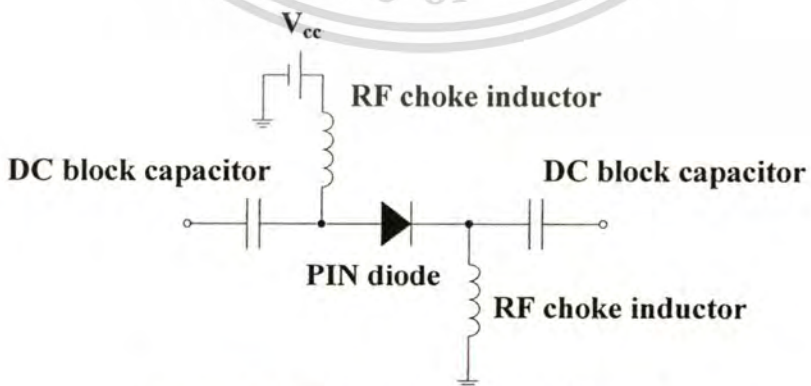

Figure 5.11 Biasing circuit of PIN diode.

5.4 Performance of The Designed Antenna

The S_{11}, radiation patterns, and gain of the designed antenna are carried out from the simulation for all directions: $+x$, $-x$, $+y$, and $-y$. The configuration of the designed antenna is modified by means of setting "ON" and "OFF" states of two groups of PIN diodes: ones are etched on the cross slot geometry and the others are on parasitic slots around the cross slot that the former results in polarization diversity between x and y, while the latter results in switching direction between $+x$ or $-x$ and $+y$ or $-y$. Then, the antenna is fabricated on a Rogers (RT 5880) Duroid substrate whose dielectric constant and loss tangent are respectively 2.2 and 0.0009 to validate the designed pattern reconfigurable antenna. The whole dimension of the antenna is 28.00 mm x 30.00 mm x 1.5 mm as illustrated in Fig. 5. 12.

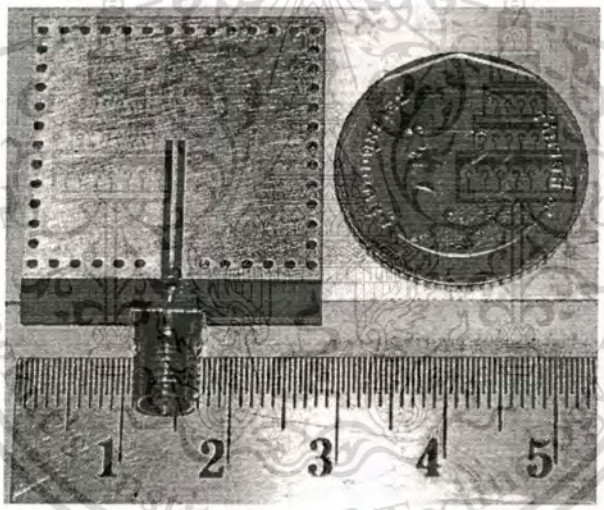

(a)

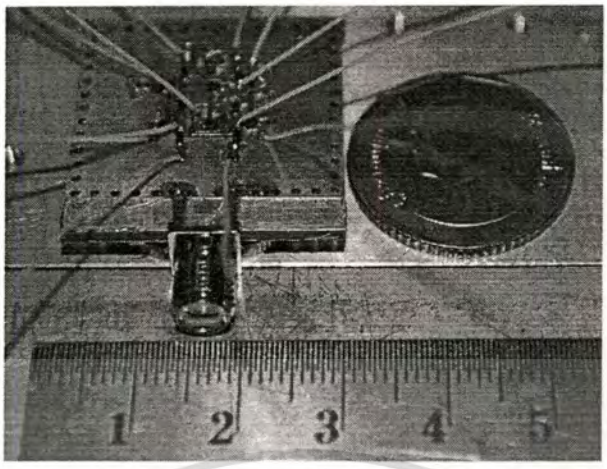

(b)

Figure 5.12 Fabricated pattern reconfigurable antenna (a) Top side, (b) Bottom side.

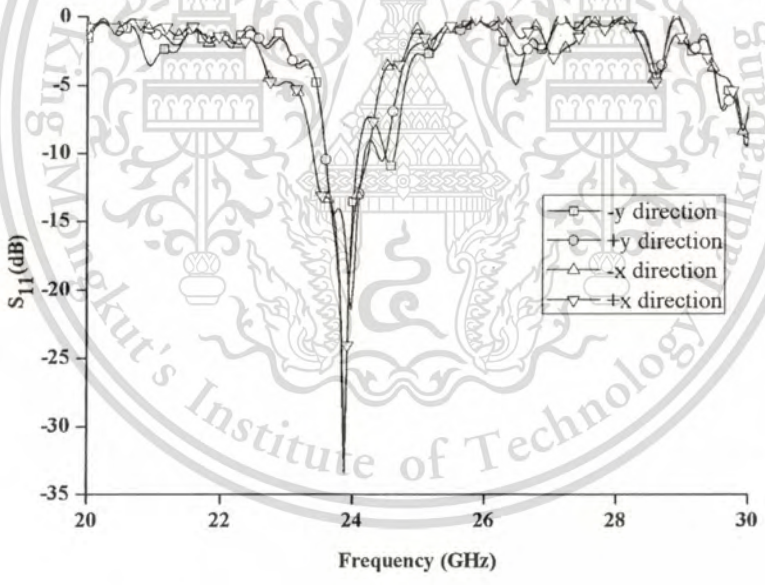

Figure 5.13 Simulated S_{11} of all directions.

The simulated S_{11} for all directions of the designed antenna are illustrated in Fig. 5.13. Note that S_{11} of the directions $+x$ and $-x$ are nearly identical whereas they are slightly different for $+y$ and $-y$ directions. For the x directions, S_{11} is equal to -15.18

dB in $+x$ direction and it is -15.21 dB in $-x$ direction. The impedance bandwidth is 810 MHz (23.40 GHz - 24.21 GHz). In the directions of $+y$ and $-y$, S_{11} are respectively equal to -19.96 and -13.55 dB. The impedance bandwidth equals 570 MHz (23.58 GHz – 24.15 GHz) and 480 MHz (23.58 GHz – 24.06 GHz) for $+y$ and $-y$ directions, respectively. While the S_{11} of all directions are measured and shown in Fig. 5.14. At the frequency of 24 GHz, S_{11} of the directions $+x$ and $-x$ are nearly identical which are equal to -11.3 dB and -10.8 dB, respectively. For $+y$ and $-y$ directions, S_{11} are respectively equal to -15.92 dB and -10.30 dB. Obviously seen that, the resonant frequencies of $+x$, $-x$, and $-y$ directions slightly shift to higher frequency while it slightly shifts to lower frequency when switch to $+y$ direction. The impedance bandwidths of all directions are wider than those from simulation.

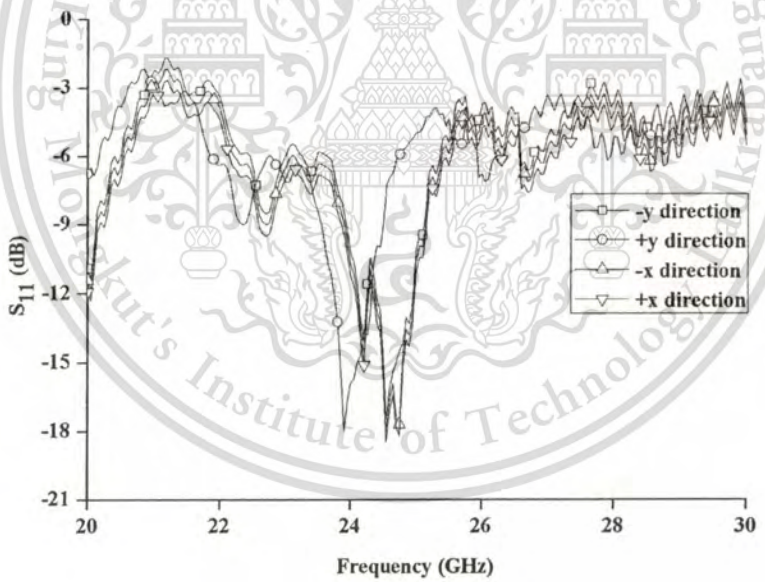

Figure 5.14 Measured S_{11} of all directions.

In order to validate the performance of the designed antenna in reconfiguring the radiation patterns, experiments is set up by connecting the antenna to an HP8530A network analyzer. The PIN diodes are controlled by +1.2 dc biasing voltage and 10 mA current. The experiment set up is illustrated in Fig. 5.15. The simulated and measured radiation patterns in E-plane (xy-plane) and H-plane (xz-plane and yz-plane) of all directions are compared and illustrated in Fig. 5.16-5.19.

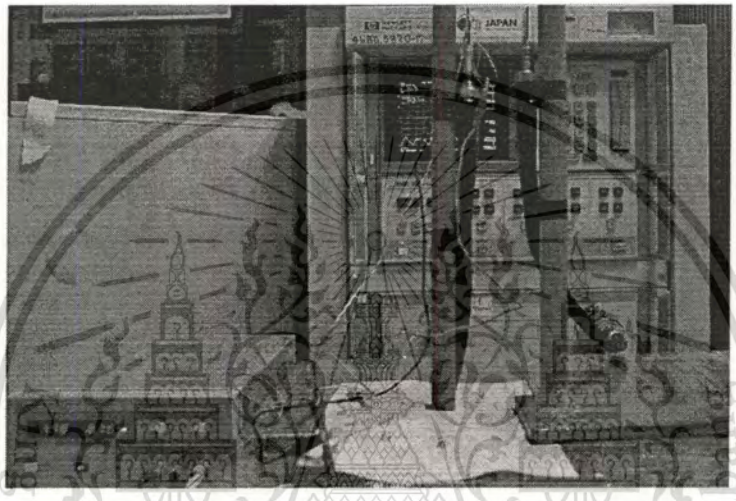

Figure 5.15 Setup of radiation pattern measurement.

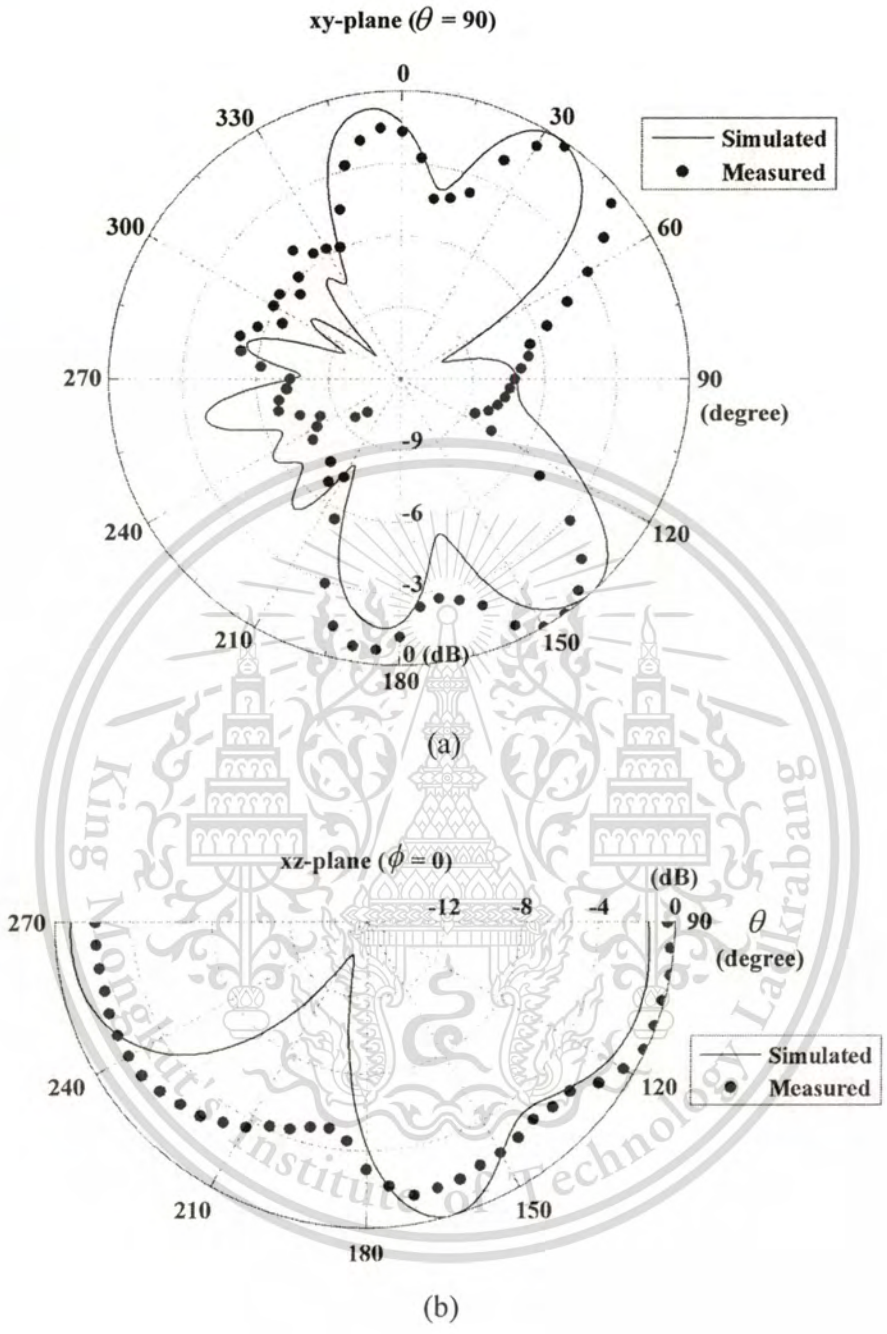

Figure 5.16 Radiation pattern in $+x$ direction (a) E-plane, (b) H-plane.

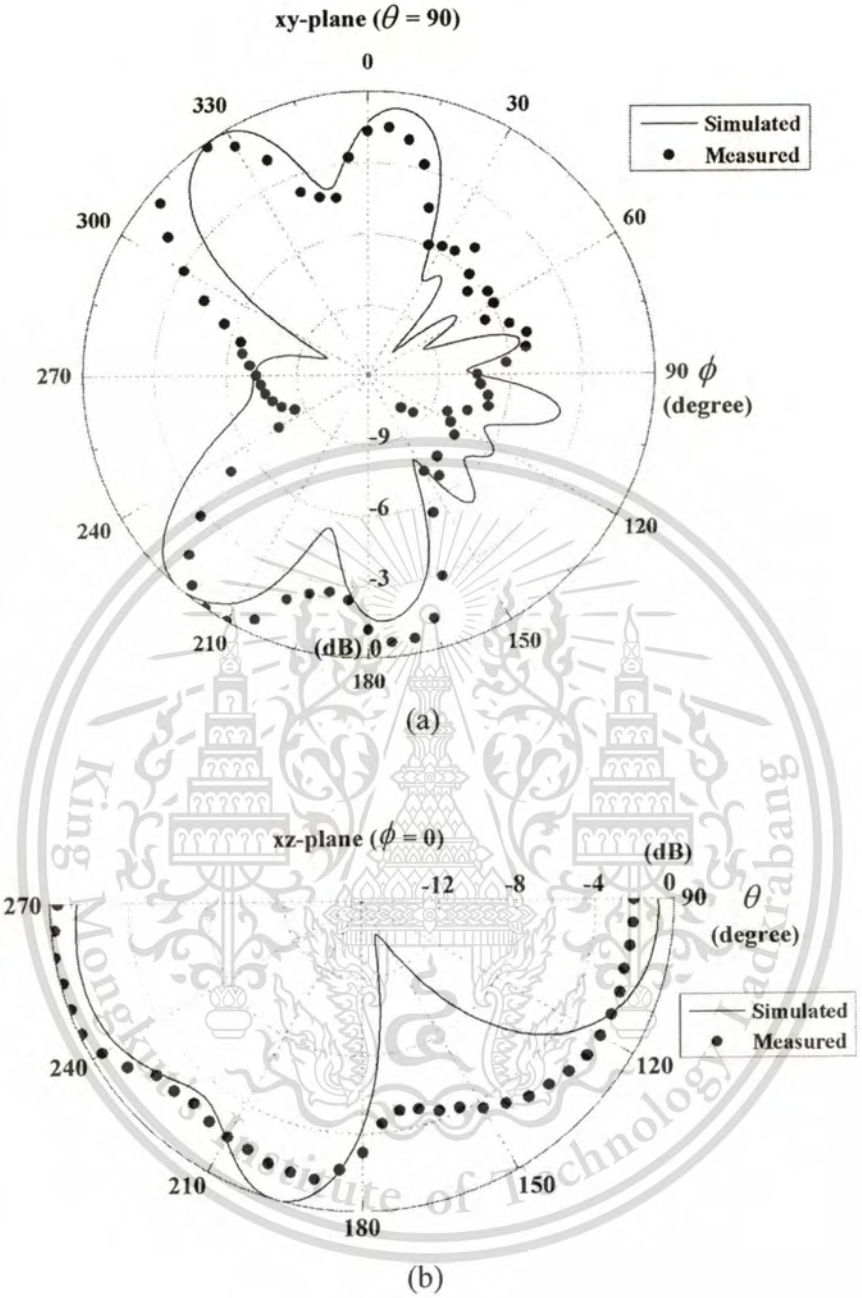

Figure 5.17 Radiation pattern in $-x$ direction (a) E-plane, (b) H-plane.

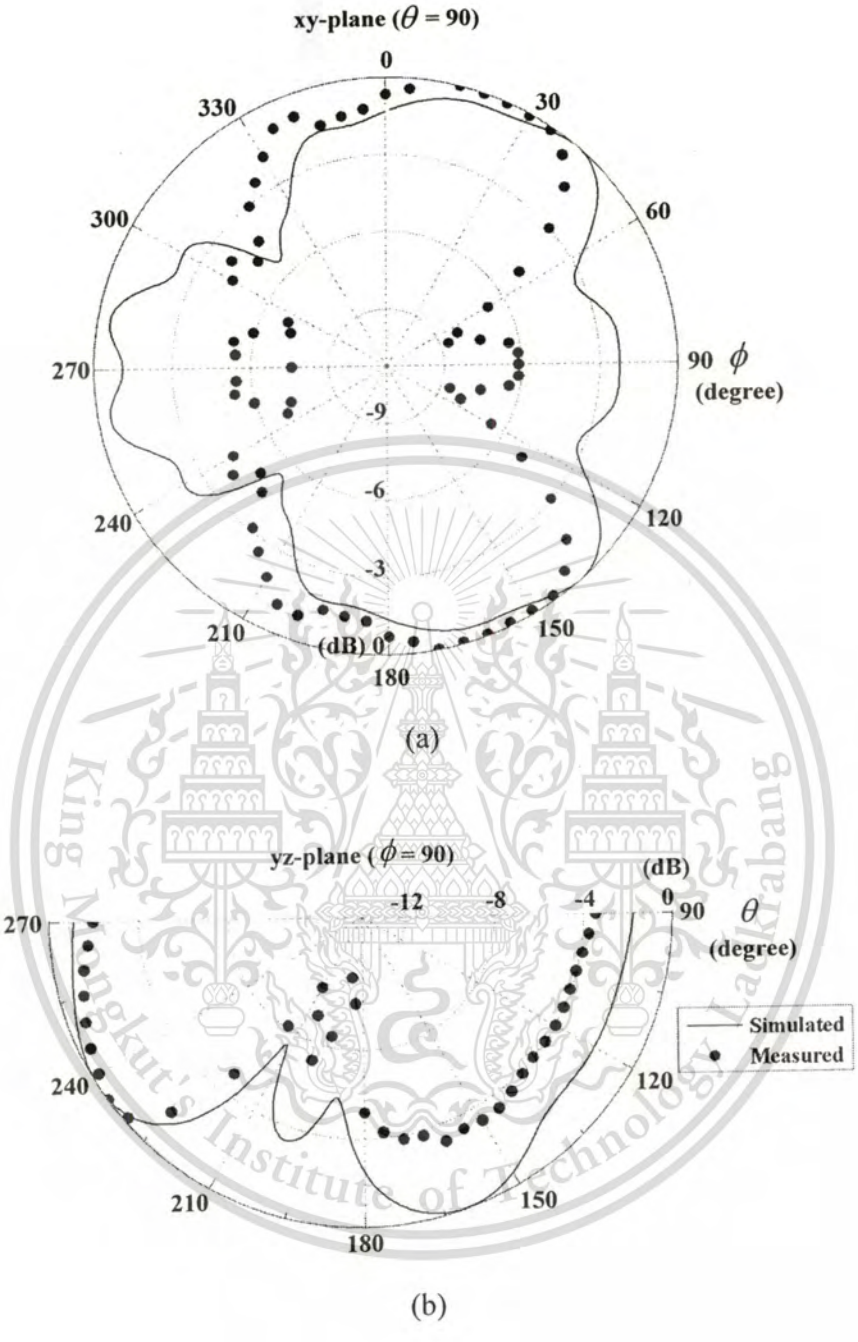

Figure 5.18 Radiation pattern in $+y$ direction (a) E-plane, (b) H-plane.

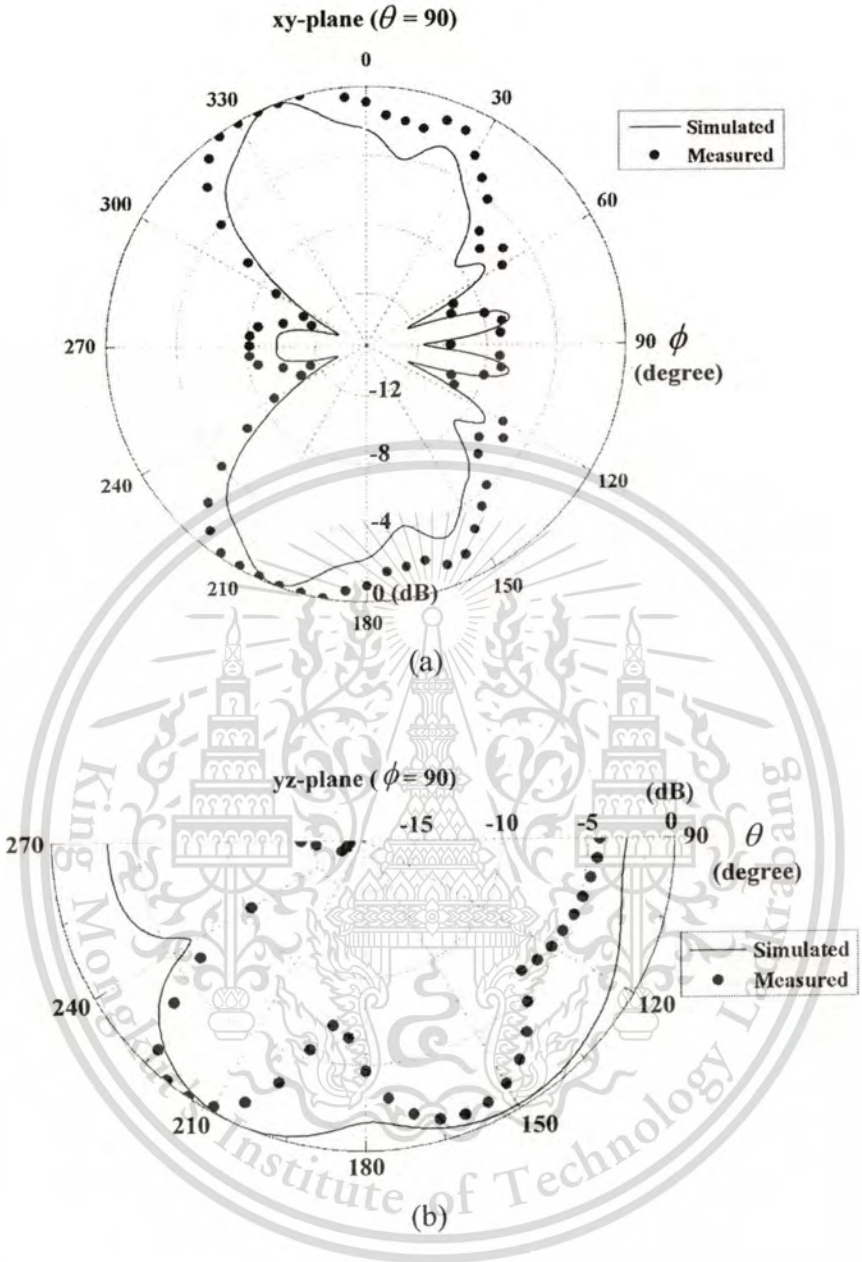

Figure 5.19 Radiation pattern in $-y$ direction (a) E-plane, (b) H-plane.

Obviously seen that the simulated and measured radiation patterns in directions of $+x$ and $-x$ have quite a bit back radiations due to leakage of the slot acting as the reflector. While the main beams are not quite good since the distance between the driven slot and the slot acting as the reflector is no close enough. For the direction of $+y$, there is much back radiation since the leakage in the slot acting as the reflector which have the

excitation line passes through on the opposite side. Thus, it makes this geometry have two aperture coupled: one is the driven slot and another one is the slot acting as the reflector. In switching to the direction of $-y$, the main beam is quite directional, but there still have back radiation. However, the measured results are comparable to those obtained from the simulation. They confirm that the designed antenna is able to function in reconfigurable the radiation patterns, but the back radiation problem should be improved to enhance the performance of this antenna which remains for the further study. The simulated gain of the directions $+x$, $-x$, $+y$, and $-y$ are respectively equal to 2.4, 2.3, 1.3, and 2.2.

5.4 Summary

Further developed of the switchable antenna for a pattern reconfigurable antenna to operate at the frequency of 24 GHz is presented. The designed antenna is constructed on a single PCB by employing the SIW technique which the feeding and the radiating segments are on the opposite side. The geometry consists of a cross slot rounded with parasitic slots that all slots have PIN diodes etched on to reconfigure the radiation patterns by setting the state of PIN diodes. At the cross slot configuration, the PIN diodes performs in diverting polarization between x and y, whereas the PIN diodes on parasitic slots function in switching direction between $+x$ or $-x$ and $+y$ or $-y$. This antenna is designed in the commercial electromagnetic simulation program, fabricated, and measured to verify its performance: S_{11}, radiation patterns, and gain. The measured S_{11} shows that the resonant frequencies slightly shift from the frequency of 24 GHz, but they are in good agreement with those simulated values in all cases of direction. While the measured radiation patterns confirm that the designed antenna is able to function in reconfiguring the radiation patterns to 4 directions around its geometry, but there are quite a bit back radiation due to the leakage of electric field.

CHAPTER 6

CONCLUSION AND REMARK FOR FUTURE STUDIES

6.1 Conclusion

The use of switchable antenna is presented in this dissertation via the agricultural application and the development of the antenna with the performance of reconfiguring its radiation patterns by means of substrate integrated waveguide (SIW) technique. For the application in agriculture, it is employed as a moisture content sensor of paddy in the closed-loop drying system. Three new aspects concerning with this developed sensor are presented: a new-closed form calculation of mutual impedance of perpendicular configuration dipole antenna, a design of antenna structure, and an investigation to enhance the performance of sensor. Moreover, the novel technique to characterize the dielectric property of a material that detects only the magnitude of mutual coupling and exploiting the configuration switching between parallel and perpendicular configurations instead of measuring phase, is also presented. In the experiments, the obtained dielectric properties are compared with the results from the work in literature and found that the dielectric constants are comparable to the reference values, but there are significant differences in the values of the dielectric loss factors since the structure of presented sensor is not a closed boundary like the transmission line technique used in reference. Therefore, error compensation is conducted to correct the results. Then, the feasibility of applying it with a closed-loop drying system is validated by setting up a simple model system. It shows good performance for *in-situ* and real-time monitoring.

In addition, the antenna whose configuration is like the cross geometry as of the sensor is further developed by means of SIW technique to construct it on a single printed circuit board (PCB). Each element of the cross geometry is attached with PIN diodes to function in reconfiguring radiation patterns to 4 directions around its structure. To reconfigure the radiation patterns, the parasitic elements around the cross geometry are also attached with PIN diodes to switch the function between the director and the

reflector like the Yagi-Uda antenna. With the advantage of reconfiguring radiation patterns, this designed antenna has the potential to be a candidate in industrial applications such as sensors for automotive or security and communication systems.

6.2 Remark for Future Studies

According to the experiment of applying a switch-configuration antenna for the moisture content sensor of paddy in a closed-loop drying system, the results show that it efficiently performs and is expected to use for *in-situ* and real-time monitoring. However, the effect of temperature that may cause the uncertainty in measurement is not studied and detailed in this dissertation. Thus, it should be further studied to enhance the accuracy of this sensor. Moreover, the non-uniform distribution of moisture content occurs in a huge amount of paddy in the rice mill. To solve this problem, the sensor may be developed by exploiting an array of the switch-configuration antenna to measure at many depths.

For the antenna developed for industrial applications, the radiation patterns are not quite good due to the leakage between the successive via. This problem is caused by the limitation of in-house PCB fabrication which the leakage can be prevented by increasing the distance between the successive via. Furthermore, the limitation of distance between the parasitic slot performing as the director and the parasitic element of cross slot also affects the radiation pattern. Thus, it can be solved and developed in the future studies by using the technique of meander line to shorten this distance.

REFERENCES

[1] A. P. Mossman, "A review of basic concepts in rice drying research," *Crit. Rev. Food Sci. Nutrition*, vol. 25, no. 1, pp. 49-70, 1986.

[2] S. Soponronnarit, "Fluidised-bed paddy drying," *Sci. Asia*, vol. 25, pp. 51-56, 1999.

[3] N. Sunthonvit, G. Srzednicki, and J. Caske, "Effects of high-temperature drying on the flavor components in Thai fragrant rice," *Dry. Technol.*, vol. 23, no. 7, pp.1407-1418, 2005.

[4] C. Taechapairoj, S. Prachawarakorn, and S. Soponronnarit, "Characteristics of rice dried in superheated-steam fluidized-bed," *Dry. Technol.*, vol. 22, no. 4, pp. 719-743, 2004.

[5] S. Prachawarakorn, N. Poomsa-ad, and S. Soponronnarit, "Quality maintenance and economy with high-temperature paddy-drying process," *J. Stored Products Res.*, vol. 41, no. 3, pp. 333-351, 2005.

[6] E. I. Goksu, G. Summu, and A. Esin, "Effect of microwave fluidized bed drying of Macaroni beads," *J. Food Eng.*, vol. 66, no. 4, pp. 463-468, Feb. 2005.

[7] G. Roussy, S. Jassm, and J-M Thiebaut, "Modeling of a fluidized bed irradiated by a single or a multimode electric microwave field distribution," *J. Microw. Power Electromagn. Energy*, vol. 30, no. 3, pp. 178-187, 1995.

[8] W. Radajewski, P. Jolly, and G. Y.Abawi, "Grain drying in a continuous flow drier supplemented with a microwave heating system," *J. Agric. Eng. Res.*, vol. 41, no. 3, pp.211-225, Nov. 1988.

[9] C. Sangdao, S. Songsermpong, and M. Krairiksh, "A continuous fluidized bed microwave paddy drying system using applicators with perpendicular Slots on a concentric cylindrical cavity," *Dry. Technol.*, vol. 29, no. 1, pp. 35-46, 2010.

[10] J-W. Baik, S. Pyo, T-H Lee, and Y-S. Kim, "Switchable printed Yagi-Uda antenna with pattern reconfiguration," *ETRI J.*, vol. 31, no. 3, pp. 318-320, Jun. 2009.

[11] P. Heide, M. Vossiek, M. Nalezinski, L. Oréans, R. Schuber, and M. Kunert, "24 GHz short-range microwave sensors for industrial and vehicular applications," *Workshop on Short Range Radar*, Jul. 1999.

[12] *Moisture measurements – Unground Grain and Seeds*, ASAE Std. S352.2, 1997.

[13] S. O. Nelson, S. Trabelsi, and A. W. Kraszewski, "RF sensing of grain and seed moisture content," *IEEE sensors. J.*, vol. 1, no. 2, pp. 119-126, Aug. 2001.

[14] L. J. Briggs, "An electrical resistance method for the rapid determination of the moisture content of grain," Bureau Plant Ind., U. S. Dept. Arg., Washington, DC, CA, 1908.

[15] E. F. Burton and A. Pitt, "A new method for the rapid estimation for moisture in wheat," *Can. J. Res.*, vol. 1, pp. 155-162, 1929.

[16] C. V. K. Kandala, C. L. Butts, and S. O. Nelson, "Capacitance sensor for nondestructive measurement of moisture content in nuts and grain," *IEEE Trans. Instrum. Meas.*, vol. 56, pp. 1809-1813, Oct. 2007.

[17] A. V. Hippel, "*Dielectric materials and applications*," The technology press of MIT and John Wiley & Sons, New York, 1954.

[18] L. F. Chen, C. K. Ong, C. P. Neo, V. V. Vardan, and V. K. Vardan, "*Microwave electronics: measurement and material characterization*," John Wiley & Sons, New York, 2004.

[19] M. A. Stuchly and S. S. Stuchly, "Coaxial line reflection methods for measuring dielectric properties of biological substances at radio and microwave frequencies–A review," *IEEE Trans. Instrum. Meas.*, vol. IM-29, pp. 176-183, Sep. 1980.

[20] K. J. Bois, L. Handjojo, A. Benally, K. Mubarak, and R. Zoughi, "Dielectric plug-loaded two-port transmission line measurement technique for dielectric property characterization of granular and liquid materials," *IEEE Trans. Instrum. Meas.*, vol. 48, no. 6, pp. 1141-1148, Dec. 1999.

[21] *Basics of measuring the dielectric properties of materials*, Application note, Agilent technologies.

[22] P. J. Shull, *Nondestructive Evaluation: Theory, Techniques, and Applications*. New York: Marcel Dekker, 2002.

[23] D. K. Ghodgaonkar, V. V. Varadan, and V. K. Varadan, "A free-space method for measurement of dielectric constants and loss tangents at microwave frequencies," *IEEE Tran. Instrum. Meas.*, vol. 37, no. 3, pp. 789-793, May 1989.

[24] M. S. Venkatesh and G. S. V. Raghavan, "An overview of dielectric properties measuring techniques," *Can. Biosyst. Eng.*, vol. 47, pp. 7.15-7.30, 2005.

[25] G. Bindu, A. Lonappan, V. Thomas, C. K. Aananda, and K. T. Mathew, "Dielectric studies of corn syrup for application in microwave breast imaging," *Progr. Electromagn. Res.*, vol. 59, pp. 175-186, 2006.

[26] K. J. Bois, A. Benally, P. S. Nowak, and R. Zoughi, "Cure-state monitoring and water-to-cement ratio determination of fresh Portland cement based materials using near field microwave techniques," *IEEE Trans. Instrum. Meas.*, vol. 47, no. 3, pp. 628-637, Jun. 1998.

[27] K. J. Bois, A. Benally, and R. Zoughi, "Microwave near-field reflection property analysis of concrete for material content determination," *IEEE Trans. Instrum. Meas.*, vol. 49, no. 1, pp. 49-55, Feb. 2000.

[28] K. Mubarak, K. J. Bois, and R. Zoughi, "A simple, robust and on-site microwave technique for determining water-to-cement (w/c) ratio of fresh Portland cement-based materials," *IEEE Trans. Instrum. Meas.*, vol. 50, no. 5, pp. 1255-1263, Oct. 2001.

[29] R. Zoughi, *Microwave Non-Destructive Testing and Evaluation*. Netherlands: Kluwer Academic Publishers, 2000.

[30] Z. Ma and S. Okamura, "Permittivity determination using amplitudes of transmission and reflection coefficients at microwave frequency," *IEEE Trans. Microw. Theory Tech.*, vol. 47, no. 5, pp. 546-550, May 1999.

[31] S. N. Kharkovsky, F. Akay, U. C. Hasar, and C. D. Atis, "Measurement and monitoring of microwave reflection and transmission properties of cement-based specimens," *IEEE Trans. Instrum. Meas.*, vol. 51, no. 6, pp. 546-550, Dec. 2002.

[32] J. Mearnchu, T. Limpiti, D. Torrungrueng, P. Akkaraekthalin, and M. Krairiksh, "A handheld moisture content sensor using coupled-dipole antennas," *Latin Amer. Appl. Res.*, vol. 40, no. 3, pp. 199-206, 2010.

[33] T. Limpiti and M. Krairiksh, "Complex permittivity determination by measuring magnitude of mutual coupling between co and cross polarized dipoles," in *Proc. Asia-Pacific Microw. Conf.*, pp. 2031-2034, Dec. 2007.

[34] T. Limpiti and M. Krairiksh, "Dielectric property determination using magnitude of mutual coupling by switched-polarization dipoles," in *Proc. IEEE Int. Conf. Antennas Syst.*, pp. 157-1-157-4, Dec. 2009.

[35] T. Limpiti and M. Krairiksh, "*In situ* moisture content monitoring sensor detecting mutual coupling magnitude between parallel and perpendicular dipole antennas," *IEEE Trans. Instrum. Meas.*, vol. 61, no. 8, pp. 2230-2241, Aug. 2012.

[36] H. E. King, "Mutual impedance of unequal length antenna in echelon," *IRE Trans. Antennas Propag.*, vol. AP-5, no. 3, pp. 306-313, Jul. 1957.

[37] H. C. Baker and A. H. Lagrone, "Digital computation of the mutual impedance between thin dipoles," *IRE Trans. Antennas Propag.*, vol. AP-10, no. 2, pp. 172-178, Mar. 1962.

[38] J. H. Richmond and N. H. Geary, "Mutual impedance of nonplanar-skew sinusoidal dipoles," *IEEE Trans. Antennas Propag.*, vol. AP-23, no. 3, pp. 412-414, May 1975.

[39] K. Lui, C. A. Balanis, and G. C. Barber, "Exact mutual impedance between sinusoidal electrical and magnetic dipoles," *IEEE Trans. Antennas Propag.*, vol. 39, no. 5, pp. 684-686, May 1991.

[40] C. A. Balanis, *Antenna Theory: Analysis and Design*. New York: Wiley, 1982.

[41] K. F. Lee, *Principles of Antenna Theory*. John Wiley & Sons, 1984.

[42] T. Limpiti and M. Krairiksh, "Closed-form expressions of mutual impedance between perpendicular thin dipoles," in *Proc. ECTI-CON 2007*, pp. 951-954, May 2007.

[43] IE3D, Zealand Software Inc.

[44] CST Microwave Studio, 2008.

[45] Advanced Design System Fundamentals, Part Number E8900-90329-ADS 1.5 (4/01).

[46] Y. Qian and T. Itoh, "A broadband uniplanar microstrip-to-CPS transition," in *Proc. Asia Pacific Microw. Conf. Dig.*, pp. 609-612, Dec. 1997.

[47] N. Kaneda, Y. Qian, and T. Itoh, "A novel Yagi-Uda dipole array fed by a microstrip-to-CPS transition," in *Proc. APMC*, pp. 1413-1416, Dec. 1998.

[48] N. Kaneda, W. R. Deal, Y. Qian, R. Waterhouse, and T. Itoh, "A broadband planar quasi-Yagi antenna," *IEEE Trans. Antennas Propag.*, vol. 50, no. 8, pp. 1158-1160, Aug. 2002.

[49] N. I. Dib, R. N. Simons, and L. P. B. Katehi, "New uniplanar transition for circuit and antenna applications," *IEEE Trans. Microw. Theory Tech.*, vo. 43, no. 12, pp. 2868-2873, Dec. 1995.

[50] L. Zhu and K. Wu, "Model-based characterization of CPS-fed printed dipole for innovative design of uniplanar integrated antenna," *IEEE Microw. Guided Wave Lett.*, vol. 9, no. 9, pp. 342-344, Sep. 1999.

[51] Hittite Microw. Corp., Datasheet HMC336MS8G/336MS8GE, GaAS MMIC SPDT Non-Reflective Positive Control Switch, DC-6 GHz.

[52] F. Sagnard, F. Bentabet, and C. Vignant, "*In situ* measurements of the complex permittivity of materials using reflection ellipsometry in the microwave band: theory (part I)," *IEEE Trans. Instrum. Meas.*, vol. 54, no. 3, pp. 1266-1273, Jun. 2005.

[53] F. Sagnard, F. Bentabet, and C. Vignant, "*In situ* measurements of the complex permittivity of materials using reflection ellipsometry in the microwave band: experiments (part II)," *IEEE Trans. Instrum. Meas.*, vol. 54, no. 3, pp. 1274-1282, Jun. 2005.

[54] P. Kabacik and M. E. Bialkowski, "The temperature dependence of substrate parameters and their effect on microstrip antenna performance," *IEEE Trans. Antennas Propag.*, vol. 47, no. 6, pp. 1042-1049, Jun. 1999.

[55] Datasheet "Maxim Innovation Delivered," MAX4003, 100 MHz to 2500 MHz, 45 dB RF Detector in a UCSP.

[56] Nat. Semicond., LMX2336/LMX2347, PLLatinum Frequency Synthesizer for RF Personal Communications, Datasheet.

[57] G. Q. Luo, Z. F. Hu, L. X. Dong, and L. L. Sun, "Planar slot antenna backed by substrate integrated waveguide cavity," *IEEE Antennas Wireless Propag. Lett.*, vol. 7, pp. 236-239, 2008.

[58] J. L. Volakis, *Antenna Engineering Handbook, 4th Edition*. McGraw-Hill, 2007.

[59] T. Limpiti, C. Sangdao, and M. Krairiksh, "Feasibility study of soil dehydration using microwave," in *Proc. Thailand-Japan Microwave (TJMW 2012)*, Aug. 2012.

[60] D. Deslandes and K. Wu, "Single-substrate integration technique of planar circuits and waveguide filters," *IEEE Trans. Microw. Theory Tech*, vol. 51, no. 1, pp. 593-596, Feb. 2003.

[61] X. Xu, G. Bosisio, and K. Wu, "A new six-port junction based on substrate integrated waveguide technology," *IEEE Trans. Microw. Theory Tech.*, vol. 53, no. 7, pp. 2267-2273, Jul. 2005.

[62] H. J. Tang, W. Hong, Z. C. Hao, J. X. Chen, and K. Wu, "Optimal design of compact millimeter-wave SIW circular cavity filters," *Electron. Lett.*, vol. 41, no. 19, pp. 1068-1069, Sep. 2005.

[63] D. Stephens, P. R. Young, and I. D. Robertson, "Millimeter-wave substrate integrated waveguides and filters in photoimageable thick-film technology," *IEEE Trans. Microw. Theory Tech.*, vol. 53, no. 2, pp. 3832-3838, Dec. 2005.

[64] J. X. Chen, W. Hong, Z. C. Hao, H. Li, and K. Wu, "Development of a low cost microwave mixer using a broad-band substrate integrated waveguide (SIW) coupler," *IEEE Microw. Wirel. Compon. Lett.*, vol. 16, no. 2, pp. 84-86, Feb. 2006.

[65] K. Wu, "Towards system-on-substrate approach for future millimeter-wave and photonic wireless applications," in *Proc. Asia-Pacific Microw. Conf.*, pp. 1895-1900, Dec. 2006.

[66] Y. Cassivi and K. Wu, "Low cost microwave oscillator using substrate integrated waveguide cavity," *IEEE Microw. Wirel. Compon. Lett.*, vol. 13, no. 2, pp. 48-50, Feb. 2003.

[67] C. Zhong, J. Xu, Z. Yu, and Y. Zhu, "Ka-band substrate integrated waveguide Gunn Oscillator," IEEE Microw. Wirel. Compon. Lett., vol. 18, no. 7, pp. 461-463, Jul. 2008.

[68] M. Abdolhamidi and M. Shahabadi, "X-band substrate integrated waveguide amplifier," *IEEE Microw. Wirel. Compon. Lett.*, vol. 18, no. 12, pp. 815-817, Dec. 2008.

[69] J. Hirokawa and M. Ando, "Single-layer feed waveguide consisting of posts for plane TEM wave excitation in parallel plates," *IEEE Trans. Antennas Propag.*, vol. 46, no. 5, pp. 625-630, May 1998.

[70] J. Hirokawa and M. Ando, "Efficiency of 76-GHz post-wall waveguide-fed parallel-plate slot arrays," *IEEE Trans. Antennas Propag.*, vol. 48, no. 11, pp. 1742-1745, Nov. 2000.

[71] L. Yan, W. Hong, G. Hua, J. Chen, K. Wu, and T. J. Cui, "Simulation and experiment on SIW slot array antenna," *IEEE Microw. Wirel. Compon. Lett.*, vol. 14, no. 9, pp. 446-448, Sep. 2004.

[72] D. Deslandes and K. Wu, "Substrate integrated waveguide leaky-wave antenna: concept and design considerations," in *Proc. Asia-Pacific Microw. Conf.*, Dec. 2005.

[73] H. Uchimura, T. Takenoshita, and M. Fujii, "Development of a "Laminated Waveguide"," *IEEE Trans. Microw. Theory Tech.*, vol. 46, no. 12, pp. 2438-2443, Dec. 1998.

[74] F. Xu and K. Wu, "Guided-wave and leakage characteristics of substrate integrated waveguide," *IEEE Trans. Microw. Theory Tech.*, vol. 53, no. 1, pp. 66-73, Jan. 2005.

[75] G. Q. Luo, W. Hong, Q. H. Lai, K. Wu, and L. L. Sun, "Design and experimental verification of thin frequency selective surface with quasi-elliptic bandpass response," *IEEE Trans. Microw. Theory Tech.*, vol. 55, no. 12, pp. 2481-2487, Dec. 2007.

[76] Y. Cassivi, L. Perregrini, P. Arcioni, M. Bressan, K. Wu, and G. Conciauro, "Dispersion characteristics of substrate integrated rectangular waveguide," *IEEE Microw. Wirel. Compon. Lett.*, vol. 12, no. 9, pp. 333-335, Sep. 2002.

[77] M. Bozzi, A. Georgiadis, and K. Wu, "Review of substrate-integrated waveguide circuits and antennas," *IET Microw. Antennas Propag.*, vol. 5, no. 8, pp. 909-920, Jun. 2011.

[78] D. H. Schaubert, F. G. Farrar, S. T. Hayes, and A. R. Sindoris, "Frequency-agile polarization diverse microstrip antennas and frequency scanned arrays," *US Patent 4,367,474, to the United States of America as represented by the Secretary of the Army*, Washington D.C.1983.

[79] J. K. Smith, "Reconfigurable program (RECAP)," *DARRA*, 1999.

[80] S. Yang, C. Zhang, H. Pan, A. Fathy, and V. Nair, "Frequency-reconfigurable antennas for multiradio wireless platforms," *IEEE Microw. Mag.*, vol. 10, pp. 66-83, Feb. 2009.

[81] A-F. Sheta and S. F. Mahmoud, "A widely tunable compact patch antenna," *IEEE Antennas Wirel. Propag. Lett.*, vol. 7, pp. 40-42, 2008.

[82] A. C. K. Mak, C. R. Rowell, R. D. Murch, and C-L. Mak, "Reconfigurable multiband antenna designs for wireless communication devices," *IEEE Trans. Antennas Propag.*, vol. 55, no. 7, pp. 1919-1928, Jul. 2007.

[83] M. Ali, A. T. M. Sayem, and V. K. Kunda, "A reconfigurable stacked microstrip patch antenna for satellite and terrestrial links," *IEEE Trans. Vehicular Tech.*, vol. 56, no. 2, pp. 426-435, Mar. 2007.

[84] S. V. Shynu, G. Augustin, C. K. Aanandan, P. Mohanan, and K. Vasudevan, "C-shaped slot loaded reconfigurable microstrip antenna," *Electron. Lett.*, vol. 42, no. 6, pp. 316-318, Mar. 2006.

[85] N. Behdad and K. Sarabandi, "Dual-band reconfigurable antenna with a very wide tunability range," *IEEE Trans. Antennas Propag.*, vol. 54, no. 2, pp. 409-416, Feb. 2006.

[86] G. H. Huff and J. T. Bernhard, "Frequency reconfigurable CPW-fed hybrid folded slot/slot dipole antenna," in *Proc. IEEE/ACES Int. Conf. Wirel. Comm. Appl. Comp. Electromag.*, pp. 574-577, Apr. 2005.

[87] S. Kawasaki and T. Itoh, "A slot antenna with electronically tunable length," in *Proc. IEEE/URSI Int. Symp. Antennas Propag.*, vol. 1, pp. 130-133, Jun. 1991.

[88] X-X. Yang, B-C. Shao, F. Yang, A. Z. Elsherbeni, and B. Gong, "A polarization reconfigurable patch antenna with loop slots on the ground plane," *IEEE Antennas Wirel. Propag. Lett.*, vol. 11, pp. 69-72, 2012.

[89] R-H. Chen and J-H. Row, "Single-feed microstrip patch antenna with switchable polarization," *IEEE Trans. Antennas Propag.*, vol. 56, no. 4, pp. 922-926, Apr. 2008.

[90] B. Kim, B. Pan, S. Nikolaou, Y-S. Kim, J. Papapolymerou, and M. M. Tentzeris, "A novel single-feed circular microstrip antenna with reconfigurable polarization capability," *IEEE Trans. Antennas Propag.*, vol. 56, no. 3, pp. 630-638, Mar. 2008.

[91] S-H. Hsu and K. Chang, "A novel reconfigurable microstrip antenna with switchable circular polarization," *IEEE Antennas Wirel. Propag. Lett.*, vol. 6, pp. 160-162, 2007.

[92] Y. J. Sung, T. U. Jang, and Y-S. Kim, "A reconfigurable microstrip antenna for switchable polarization," *IEEE Microw. Wirel. Comp. Lett.*, vol. 14, pp. 534-536, Nov. 2004.

[93] M. K. Fries, M. Grani, and R. Vahldieck, "A reconfigurable slot antenna with switchable polarization," *IEEE Microw. Wirel. Comp. Lett.*, vol. 13, pp. 490-492, Nov. 2003.

[94] R. N. Simons, D. Chun, and L. P. B. Katehi, "Polarization reconfigurable patch antenna using microelectromechanical systems (MEMS) actuators," in *Proc. IEEE/URSI Int. Symp. Antennas Propag.*, vol. 2, pp. 6-9, 2002.

[95] F. Yang and Y. Rahmat-Samii, "A reconfigurable patch antenna using switchable slots for circular polarization diversity," *IEEE Microw. Wirel. Comp. Lett.*, vol. 12, no. 3, pp. 96-98, Mar. 2002.

[96] M. Boti, L. Dussopt, and J-M. Laheurte, "Circularly polarized antenna with switchable polarization sense," *Electron. Lett.*, vol. 36, no. 18, pp. 1518-1519, Aug. 2000.

[97] K. Wang, S. Lee, and K. Kim, "Design of symmetric beam pattern reconfigurable antenna," *Electron. Lett.*, vol. 46, no. 23, pp. 1536-1537, Nov. 2010

[98] M. P. Daly and J. T. Bernhard, "Beam steering in pattern reconfigurable arrays using directional modulation," *IEEE Trans. Antennas Propag.*, vol. 58, no. 7, pp. 2259-2265, Jul. 2010.

[99] W. S. Kang, J. A. Park, and Y. J. Yoon, "Simple reconfigurable antenna with radiation pattern," *Electron. Lett.*, vol. 44, no. 3, pp. 182-183, Jan. 2008.

[100] S-H. Chen, J-S. Row, and K-L. Wong, "Reconfigurable square-ring patch antenna with pattern diversity," *IEEE Trans. Antennas Propag.*, vol. 55, no. 2, pp. 472-475, Feb. 2007.

[101] C. W. Jung, M-J. Lee, G. P. Li, and F. D. Flaviis, "Reconfigurable scan-beam single-arm spiral antenna integrated with RF-MEMS switches," *IEEE Trans. Antennas Propag.*, vol. 54, no. 2, pp. 455-463, Feb. 2006.

[102] G. H. Huff and J. T. Bernhard, "Integration of packaged RF MEMS switches with radiation pattern reconfigurable square spiral microstrip antennas," *IEEE Trans. Antennas Propag.*, vol. 54, no. 2, pp. 464-469, Feb. 2006.

[103] S. Zhang, G. H. Huff, G. Cung, and J. T. Bernhard, "Three variations of a pattern-reconfigurable microstrip parasitic array," *Microw. Optic. Tech. Lett.*, vol. 45, no. 5, pp. 369-372, Jun. 2005.

[104] S. Zhang, G. H. Huff, J. Feng, and J. T. Bernhard, "A pattern reconfigurable microstrip parasitic array," *IEEE Trans. Antennas Propag.*, vol. 52, no. 10, pp. 2773-2776, Oct. 2004.

[105] C. A. Balanis, Modern Antenna Handbook. John Wiley & Sons, 2008.

[106] J. T. Bernhard, *Reconfigurable Antennas*. Morgan & Claypool, 2007.

[107] A. Ramadan, M. Al-Jusseini, Y. Tawk, K. Y. Kabalan, and A. El-Hajj, "A novel frequency/pattern-reconfigurable microstrip antenna for WLAN applications," *European Con. Antennas Propag. (EuCAP 2010)*, Apr. 2010.

[108] W. Lee, H. Kim, and Y. J. Yoon, "Reconfigurable slot antenna with wide bandwidth," *IEEE Int. Sym. Antennas Propag. Dig.*, pp. 3063-3066, Jul. 2006.

[109] F. Yang and Y. Rahmat-Samii, "Patch antennas with switchable slots (PASS) in wireless communications: concepts, designs, and application," *IEEE Antennas Propag. Mag.*, vol. 47, no. 2, pp. 13-29, Apr. 2005.

[110] D. Peroulis, K. Sarabandi, and L. P. B. Katehi, "Design of reconfigurable slot antennas," *IEEE Trans. Antennas Propag.*, vol. AP-56, no. 4, pp. 645-654, Feb. 2005.

[111] B. A. Cetiner, G. R. Crusats, L. Jofre, and N. Biyikh, "RF MEMS integrated frequency reconfigurable annular slot antenna," *IEEE Trans. Antennas Propag.*, vol. AP-58, no. 3, pp. 626-632, Mar. 2010.

[112] R. K. Gupta, U. C. Sharma, P. Ayanu, and G. Kumar, "MEMS based reconfigurable dual band antenna," *Microw. Opt. Tech. Lett.*, vol. 50, no. 6, pp. 1570-1575, Jun. 2008.

[113] O. Kivekas, J. Ollikainen, and P. Vainikainen, "Tunable internal antenna for mobile phones," in *Proc. 12th int. JINA*, pp. 53-56, Nov. 2002.

[114] B-S. Ke, Y. Qian, and T. Itoh, "A two-element Yagi-Uda array using tunable slot antenna," in *Proc. Asia-Pacific Microw. Conf.*, Dec. 1997.

[115] T. Limpiti and M. Krairiksh, "Design of a 24 GHz pattern reconfigurable slotted Yagi-Uda antenna on substrate integrated waveguide," in *Proc. ECTI-CON 2013*, May 2013.

[116] Datasheet of "MA4AGBLP912," AlGaAs Beamlead PIN diode, MA-COM, Application Note.

PUBLICATIONS

[1] T. Limpiti and M. Krairiksh, "Design of a 24 GHz Pattern Reconfigurable Slotted Yagi-Uda Antenna on Substrate Integrated Waveguide," in *Proceedings of Electrical Engineering/Electronics, Computer, Telecommunications, and Information Technology Conference (ECTI-CON 2013)*, Krabi, Thailand, May 2013.

[2] T. Limpiti and M. Krairiksh, "*In Situ* Moisture Content Monitoring Sensor Detecting Mutual Coupling Magnitude Between Parallel and Perpendicular Dipole Antennas," *IEEE Transactions on Instrumentation and Measurement*, vol. 61, no. 8, pp. 2230-2241, August 2012.

[3] T. Limpiti, C. Sangdao, and M. Krairiksh, "Feasibility Study of Soil Dehydration Using Microwave," in *Proceedings of Thailand-Japan Microwave 2012*, Chulalongkorn University, Thailand, August 2012.

[4] T. Limpiti and M. Krairiksh, "Dielectric Property Determination Using Magnitude of Mutual Coupling by Switched-Polarization Dipoles," in *Proceedings of 2009 IEEE International Conference on Antennas Propagation and System (INAS 2009)*, Johor Bahru, Johor, Malaysia, December 2009.

AUTHOR BIOGRAPHY

Thunyawat Limpiti was born on November 27, 1982 in Phatthalung, Thailand. He received the B.Eng. and M.Eng. degrees in Telecommunication Engineering from King Mongkut's Institute of Technology Ladkrabang (KMITL), Bangkok, Thailand, in 2005 and 2008, respectively. He received a Ph.D. scholarship from the Thailand Research Fund (TRF) through the Royal Golden Jubilee Ph.D. Program. His research interests are in antenna design for wireless communication, an RF circuit design, and microwave techniques for the dielectric property determination of materials.